2012

Develoment and Application of Chemical Strategies to Study Protein Fatty-Acylation in Eukaryotes

Mingzi Zhang

DEVELOPMENT AND APPLICATION OF CHEMICAL STRATEGIES TO STUDY PROTEIN FATTY-ACYLATION IN EUKARYOTES

A Thesis Presented to the Faculty of

The Rockefeller University

in Partial Fulfillment for the Requirements for

the degree of Doctor of Philosophy

by

Mingzi Zhang

June 2012

DEVELOPMENT AND APPLICATION OF CHEMICAL STRATEGIES TO STUDY PROTEIN FATTY-ACYLATION IN EUKARYOTES

Mingzi Zhang, Ph.D.

The Rockefeller University 2012

Reversible *S*-palmitoylation confers spatiotemporal control of protein function by modulating protein stability, trafficking and activity as well as protein-protein and membrane-protein associations. While it is evident that palmitoylation is regulated *in vivo*, mechanisms that mediate cellular stimuli-driven changes of the lipid modification are not understood. Furthermore, the requirement for substrate specificity among the highly redundant palmitoyl acyltransferases (PATs) remains unresolved.

To study the regulation of PATs and palmitoylomes, I developed bioorthogonal chemical strategies for improved analysis of dynamic palmitoylation in mammalian cells. I showed that alkyne-functionalized fatty acids, in conjunction with azido-fluorophores, provide the most sensitive detection of acylated proteins following Cu^{I}-catalyzed azide-alkyne cycloaddition. Linkage-specific hydrolysis, mutagenesis and inhibitor studies reveal that these alkynyl-fatty acids are incorporated into proteins by endogenous fatty-acylation machinery via native linkages at specific amino acid residues. In addition, shorter and longer chain fatty acids label myristoylated and palmitoylated proteins respectively. Since myristoylation is co-translational and constitutive, I employed both palmitoylation and myristoylation chemical reporters with orthogonal fluorophores to

simultaneously monitor palmitate and protein turnover. Dual pulse-chase analysis of Lck, a tyrosine kinase required for T-cell signaling, revealed accelerated palmitate cycling upon T-cell activation. Pharmacological perturbation of Lck palmitate turnover suggests yet uncharacterized serine hydrolases contribute to dynamic palmitoylation in cells. These significant improvements allow rapid and robust biochemical analysis of palmitoylated proteins without overexpression, facilitating the functional characterization of cellular factors and drugs that modulate protein palmitoylation.

Taking advantage of the sensitive bioorthogonal detection of protein palmitoylation and the simple PAT network in the fission yeast *Schizosaccharomyces pombe*, I provided evidence for regulation of PATs and palmitoylomes *in vivo* at physiological enzyme and substrate concentrations. I showed that the Erf2-Erf4 PAT modulates sexual differentiation, and that upregulation of its expression is required to establish the meiotic palmitoylome. Importantly, I demonstrated that changes in Erf2-Erf4 levels within the physiological range control PAT specificity and result in the differential palmitoylation of its substrates in vegetative and meiotic cells. Underscoring the biological significance of controlling PAT levels, Erf2-Erf4 overproduction in proliferating cells alters the palmitoylome and the subcellular distribution of Rho3, a major meiotic target, stimulating sexual differentiation in the absence of normal physiological cues. From this study, I conclude that PAT substrate specificity depends on enzyme levels and propose the rheostatic control of PAT activity as a mechanism by which cells shape stimuli-induced palmitoylomes. Future questions stemming from this work are also discussed.

To my parents

ACKNOWLEDGEMENTS

First, I would like to thank my advisor Dr. Howard Hang the original members of the Hang lab for their help and support over the past five years, especially Dr. Anuradha Raghavan, whose enthusiasm and cheerfulness, made me decide to rotate and join the lab in the end. We had lots of fun and memorable moments alongside all the stress and pressure associated with a new lab. Many thanks to Dr. Kelvin Tsou, who not only contributed as co-first author in the tandem labeling project, but is also a supportive lab mate. A large part of my work would not have been possible without the strong support and guidance from Dr. Paul Nurse and his lab members including Dr. Felice Kelly, who introduced me to fission yeast and genetics. It was a pleasure working with Dr. Jenny Wu and Dr. Damien Coudreuse, who with their highly creative and logical minds as well as impressive writing abilities, have helped me greatly with the preparation of my manuscript. In addition, I would like to thank my third committee member, Dr. Frederick Cross for his constructive insights and guidance on my projects and career development, and Dr. Maurine Linder for joining the committee as the outside examiner.

My graduate school life would not have been possible without the support of my friends and family. I would also like to thank all my friends, especially Vicki Zheng, Simen Ng, Jeannie Yang and Elizabeth Campbell for their friendship and memories. I am especially grateful to Daphne Chang and Neil Davies, my family away from home. Most importantly, I would like to express my deepest gratitude to my parents for being with me on this long and memorable journey and helping me through the most difficult times.

TABLE OF CONTENTS

LIST OF FIGURES

LIST OF TABLES

LIST OF ABBREVIATIONS

2BP	2-bromopalmitate
ABE	Acyl-biotin exchange
AHA	Azidohomoalanine
APT1/2	Acyl protein thioesterase 1/2
Az, Alk-12, 16	Azido or alkynyl 12 or 16-carbon chain fatty acids
Az, Alk-rho	Azido or alkynyl rhodamine
Az-azo-biotin	Azido-azobenzene-biotin
cAMP	Cyclic adenosine monophosphate
CuAAC	Copper(I)-catalyzed azide-alkyne cycloadditon
DAPI	4, 6-diamidino-2-phenylindole
DHHC-PAT	(Asp-His-His-Cys)-containing palmitoyl acyltransferase
DNA	Deoxyribonucleic acid
ER	Endoplasmic reticulum
Erf2	Effector of Ras function 2
Erf4	Effector of Ras function 4
HA	Hemagglutinin
HD	Huntington disease
HTT	Huntingtin protein
kD	Kilodalton
LAT	Linker for Activation of T-cells
MAFP	Methyl arachidonyl fluorophosphonate
MAPK	Mitogen-activated protein kinase
MAPKK	Mitogen-activated protein kinase kinase
MAPKKK	Mitogen-activated protein kinase kinase kinase
NMT	*N*-Myristoyltransferase
NO	Nitric oxide
OD	Optical density of cultures

PAT	Palmitoyl acyltransferase
PCR	Polymerase chain reaction
PM	Plasma membrane
PMSF	Phenylmethylsulfonyl fluoride
PPT1	Palmitoyl protein thioesterase 1
PSD95	Post-synaptic density protein 95
PTM	Posttranslational modification
PV	Pervanadate
SAPK	Stress-activated protein kinase
SDS-PAGE	Sodium dodecyl sulfate – polyacrylamine gel electrophoresis
s.d.	Standard deviation of the mean
TCR	T-cell receptor
UV	Ultraviolet radiation
XMLR	X-linked mental retardation
YFP	Yellow fluorescent protein

CHAPTER 1

GENERAL INTRODUCTION

Post-translational modifications are important for protein function

Post-translational modifications of proteins (PTMs) are important for building functional complexity of proteomes in living organisms. To date, more than 200 PTMs involving the covalent attachment of metabolites and other proteins, both static and dynamic, have been identified. Together, they increase the diversity of functional groups beyond those in the side chains of the 20-22 proteinogenic amino acids, enabling new chemistry, new recognition patterns for binding partners as well as control of enzyme activity, protein stability and location (Fig. 1.1b). The function and regulation of some of these modifications such as phosphorylation have been extensively studied and characterized. In contrast, our understanding of modifications such as *S*-palmitoylation, the focus of this thesis, is limited.

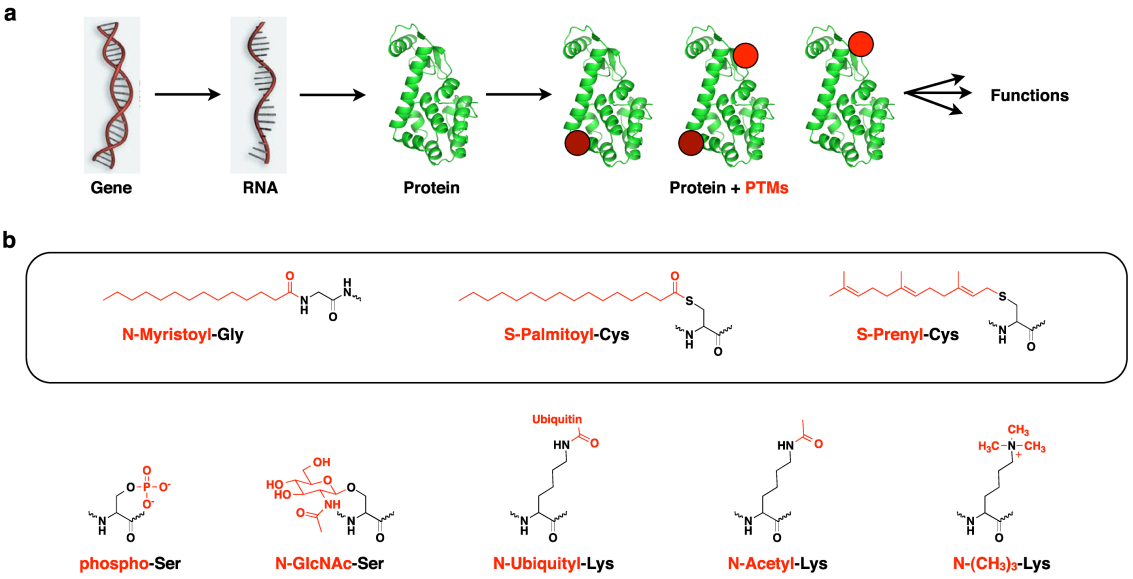

Figure 1.1 | Post-translational modifications (PTMs) are important for protein function. a, Different covalent modifications of proteins, depicted by red circles, generate proteome complexity and diversify protein function. **b,** Examples of PTMs (red) of indicated amino acid side chains. Major forms of protein lipidation are indicated in box.

Protein S-palmitoylation

Lipid modifications, myristoylation, palmitoylation and prenylation (Fig. 1.1b, box), increase protein hydrophobicity, primarily functioning as lipid anchors to stabilize protein-membrane interactions and in some cases directly regulate protein activity as well as protein-protein interactions. These distinct lipid modifications differ not only in chemical linkage, chain length and degree of saturation of the lipids, but also in the associated enzymes, which recognize discrete protein substrates. *S*-Palmitoylation, also known as *S*-acylation, is the only reversible lipid modification - the palmitate turns over faster than the protein itself[1, 2]. Palmitoylation takes place on the thiol side chains of cysteine residues post-translationally via thioester linkages (Fig. 1.2). Although it typically involves attachment of a saturated 16-carbon palmitate group to proteins,

incorporation of longer fatty acids with different degrees of unsaturation have been reported[3-5]. Some proteins, such as the secreted Sonic hedgehog morphogen[6-9], are irreversibly palmitoylated through the formation of an N-terminal amide bond (*N*-palmitoylation) but in this thesis, palmitoylation refers to *S*-palmitoylation. To date, there is no unique consensus site, making it challenging to accurately predict palmitoylated proteins and modification sites.

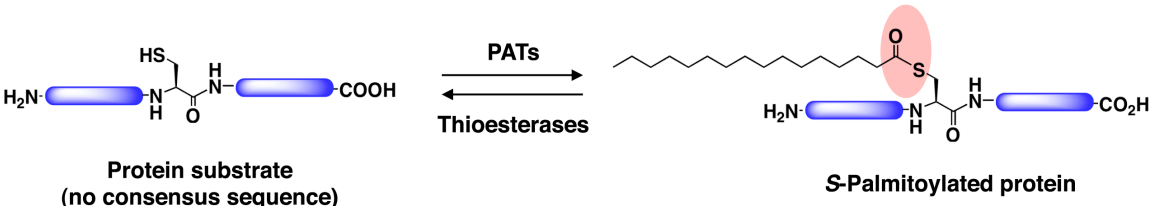

Figure 1.2 | Protein *S*-palmitoylation is a reversible modification. Palmitate is installed on the thiol side chain of a cysteine residue through the formation of a thioester linkage (red). Palmitoylation and depalmitoylation are mediated by a family of palmitoyl acyltransferases (PATs) and thioesterases, respectively. No reliable consensus palmitoylation sequence has been identified.

Nonetheless, recent technical advancements enabled comprehensive global characterization of palmitoyl-proteomes (palmitoylomes) in yeast and mammalian cells, which reveal that ~1-2% of proteomes are modified[10-18]. These studies greatly expanded the known complement of palmitoylated proteins and indicated important roles for this lipid modification as a major cellular regulator in diverse biological processes such as cell death and proliferation, immune signaling and neuronal function (Table 1.1). In this chapter, I will discuss how palmitoylation impacts protein function (Part 1) and how this modification is regulated in cells (Part 2).

Table 1.1 | Representative palmitoylated proteins.

Protein family	Substrate	Reference
Signaling proteins		
Small GTPases	*HRAS, *NRAS	Hancock et al.[20] *Baker et al.[131] *Rocks et al.[22]
	*RHOB	Adamson et al.[167] *Kang et al.[11]
	*Brain-specific CDC42 isoform 2	*Kang et al. [11]
G protein α subunits	*$G\alpha_s$, *$G\alpha_q$, *$G\alpha_{12}$	Linder et al.[219] Wedegaertner et al.[182] *Degtyarev et al.[55] *Wedegaertner et al.[54]
Non-receptor tyrosine kinases	FYN	Koegl et al.[110] Shenoy-Scaria.[115]
	*LCK	Koegl et al.[110] Shenoy-Scaria.[115] *Zhang et al.[52]
Other signaling proteins	GAP43 (neuromodulin)	Skene et al.[183]
	*eNOS	Liu et al.[218] *Ho et al.[40]
	Huntingtin	Yanai et al.[50]
	CaMK1G	Takemoto-Kimura et al.[184]
	GAD65	Christgau et al.
	Stathmin 2 (SCG10)	Grenninglog et al.[217]
Channels, receptors, transporters other transmembrane proteins		
G protein-coupled receptors	Rhodopsin	O'Brien et al.[185]
	*β2-adrenergic receptor	O'Dowd et al.[216] *Mouillac et al.[53]
Ion channels	GluR1, GluR2	Hayashi et al.[215] *Kang et al.[11]
	Large conductance (BK) K^+ channel	Tian et al.[88]
Cell adhesion molecules	Integrin α6	Yang et al.[186]
	CD9 (tetraspannin 29)	Yang et al.[214]
Cell death signaling	FAS	Chakrabandhu et al.[187]

Table 1.1 continued |

Protein family	Substrate	Reference
Adaptors and scaffolds		
	*PSD95 (Post Synaptiic Density protein 95)	Topinka & Bredt[213] *El-Hussini et al.[39]
	GRIP1, GRIP2	DeSouza et al.[212]
	LAT (Linker for Activation of T-cells)	Zhang et al.[31]
Proteins involved in protein sorting and vesicle trafficking		
SNAREs	SNAP25B	Hess et al.[211]
	*Syntaxin1, Syntaxin 6	Martin et al.[13] *Kang et al.[11]
	Synaptobrevin 2	Martin et al.[13] Kang et al.[11]
Synaptotagmins	*Synaptotagmin 1	Heindel et al.[188] *Kang et al.[11]
Others	CSP	Chamberlain & Burgiyne[189]
	*CKAP4 (p63)	Schweizer et al.[210] *Mundy & Warren[56]
	IFITM3	Yount et al.[16]

*Changes in palmitoylation states have been associated with different cellular or physiological states.

Part 1: Palmitoylation-mediated regulation of protein function

Protein targeting and trafficking

Palmitoylation primarily targets proteins to specific membrane compartments in the cell. The small GTPase Ras, an important molecular switch in diverse signaling networks governing cell death, proliferation, differentiation that is well-known for its role in cancer development[19], provides an important paradigm for spatial control mediated by this lipid modification. Nras and Hras are two highly homologous isoforms, differing mainly in their hypervariable C-terminal regions, where Nras and Hras are both prenylated and

either mono- or dual- palmitoylated[2, 20, 21] (Fig. 1.3a). These isoforms have distinct cellular distribution with Hras being more enriched at the plasma membrane relative to the Golgi[22] (Fig. 1.3a). This is dependent on their palmitoylation states since localization of mono-palmitoylated Hras mutants more closely resemble Nras[22] (Fig. 1.3b). Notably, a non-palmitoylated Hras mutant is randomly distributed to all membranes (Fig. 1.3b, C181, 184S), indicating that prenylation alone is insufficient to target proteins to specific membranes[22]. In fact, it is appreciated that other lipid modifications such as myristoylation and prenylation (Fig. 1.1b) act as weak membrane anchors while palmitoylation, although not usually the primary membrane association signal, is a strong membrane anchor that specifies the membrane distribution of a protein[23] (Fig. 1.3d, steps 1-3). The reversibility of palmitoylation is also crucial for its function. Microinjection of a semisynthetic Nras that is irreversibly-linked to palmitate results in non-specific distribution of the protein (Fig. 1.3c), demonstrating that correct localization of Nras requires both palmitoylation and depalmitoylation[22] (Fig. 1.3d). Cycles of palmitoylation and depalmitoylation govern protein-membrane associations, allowing key signaling proteins to shuttle and relocalize between intracellular membrane compartments[22, 24, 25].

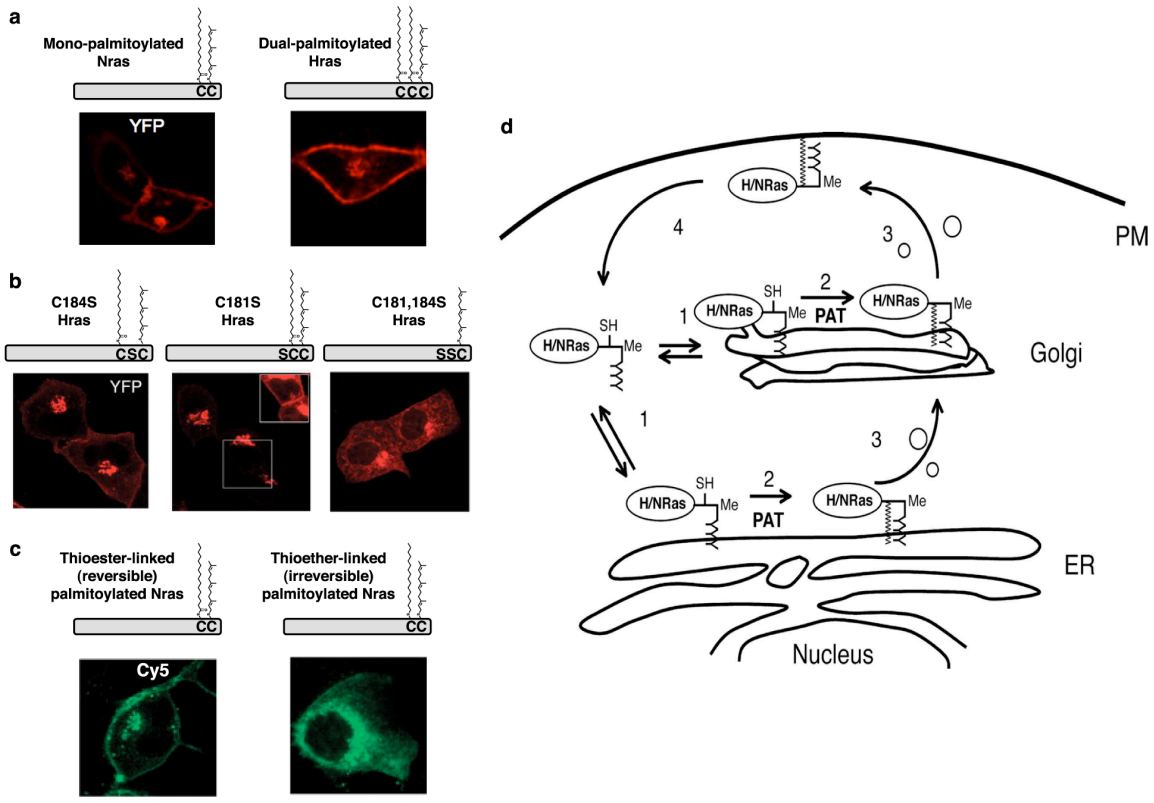

Figure 1.3 | Dynamic palmitoylation regulates localization of Ras isoforms. a, Distinct cellular distribution of two YFP-tagged Ras isoforms, Nras and Hras, which are mono- and dually- palmitoylated, respectively. Both isoforms are also prenylated. **b,** Palmitoylation determines membrane-specific localization of Hras. Cellular distribution of YFP-tagged Hras palmitoylation mutants, C184S, C181S or C181, 184S. Box, overexposed area reveals endoplasmic reticulum (ER) and plasma membrane (PM) localization of the C181S Hras mutant. **c,** Cellular distribution of synthetically-derived Cy5-labeled Nras with either native thioester-linked or a non-cleavable thioether-linked palmitate upon microinjection into cells. **a-c,** Adapted from Rocks et al.[22]. **d,** Model for how palmitoylation regulates Ras trafficking. Newly synthesized Ras is prenylated and reversibly binds ER and Golgi membranes and traffic between them via a soluble cytosolic intermediate (step 1). Palmitoylation by a palmitoyl acyltransferase (PAT) kinetically traps Ras onto membranes in the early secretory pathway (step 2) and enables trafficking to the PM (step 3). Palmitate turnover generates a transiently depalmitoylated pool of protein that is returned to the Golgi and/or ER compartments by non-vesicular transport, where it again can interact with PATs at the Golgi and/or ER and reenter the secretory pathway (step 4). Adapted from Goodwin et al.[24]

Spatial compartmentalization increases the complexity of signal outputs

By influencing their subcellular distribution, dynamic palmitoylation can have critical effects on the function and signaling outputs of proteins as epitomized by compartmentalized Ras signaling. Studies indicate that a Ras protein signals though distinct downstream effectors and pathways from a variety of membrane compartments[22, 26], addressing the conundrum of how a binary molecular switch like Ras, which cycles between GTP-bound active and GDP-bound inactive forms, can selectively control multiple pathways (Fig. 1.4). Unambiguously showed by Onken and colleagues using the single Ras protein in fission yeast[27, 28] (Fig. 1.4b), compartmentalized Ras signaling also explains how the different Ras isoforms in mammals, though highly homologous and indistinguishable in most i*n vitro* assays, perform non-overlapping biological functions[19]. In addition to maintaining the differential subcellular distribution of Hras and Nras isoforms, different de/repalmitoylation kinetics account for isoform-specific activation responses by regulating their partitioning between membrane compartments[22, 24]. It is clear that compartmentalized signaling increases the complexity of signaling outputs but it remains to be determined how palmitoylation, with its potential to impart rapid spatiotemporal control of protein function, affects distribution of signals across multiple platforms and influences the selectivity of signal outputs.

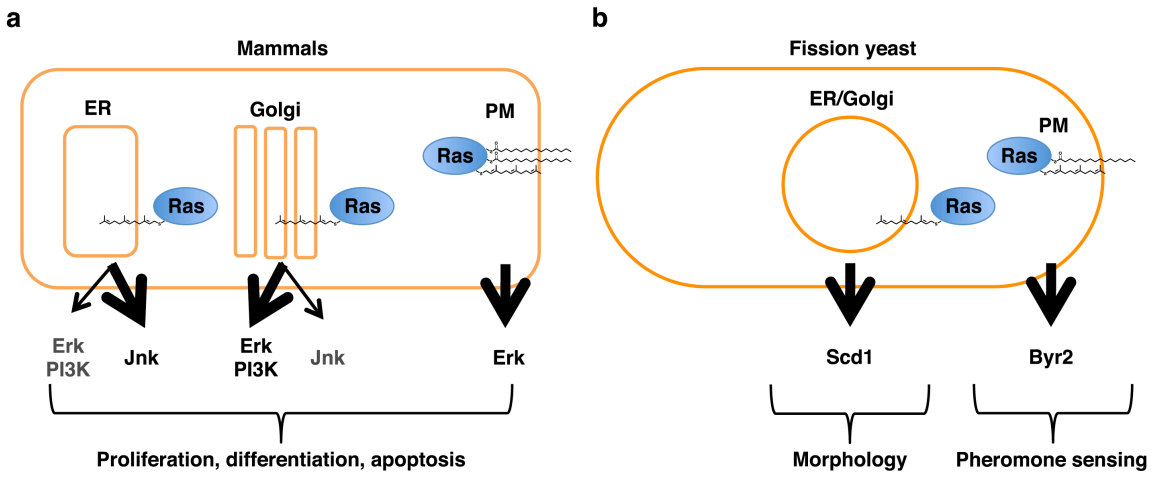

Figure 1.4 | Palmitoylation-modulated compartmentalized Ras signaling increases the complexity of signaling outputs in a, Mammals and **b,** fission yeast. Palmitoylated and non-palmitoylated Ras proteins localize to different membrane platforms, where they signal through different effectors and pathways involved in important cellular processes/events as indicated. PM: plasma membrane.

Membrane microdomains as signaling platforms

Palmitoylation is also important for controlling the lateral segregation of proteins into membrane microdomains such as lipid rafts, which are ordered assemblies of proteins and lipids enriched in sterols and sphingolipids[29]. Several lines of evidence from studies in immune cell signaling suggest that this lipid modification functions modulates raft association of proteins. First, palmitoylation of proteins such as non-receptor tyrosine kinases Lck and Fyn, adaptor LAT, as well as co-receptors CD4 and CD8 are critical for T-cell signaling. Disruption of palmitoylation results in loss of raft association by these proteins, which is concomitant with abrogation of T-cell signaling[3, 30-35]. Second, substitution of palmitate on Lck with a more hydrophilic oxygen-substituted palmitate analog that disrupts lipid packing also reduces raft association and weakens its signaling activity[36]. Third, although artificial targeting of chimeric Lck and LAT constructs to the

plasma membrane without raft association restored their function in T-cell signaling, their signaling properties are altered[37, 38]. Together, these observations strongly indicate palmitoylation-mediated targeting to membrane microdomains can affect the function and signaling outputs of proteins.

How does targeting to membrane microdomains affect protein activity? The concept of compartmentalized signaling described previously can be applied to laterally divided subdomains within the same membrane compartment. Palmitoylation partitions proteins to common membrane microdomains or raft environments that are miscible, facilitating particular protein-protein interactions (Fig. 1.5a). In contrast, interactions between proteins in two non-miscible environments are less favored (Fig. 1.5b). By changing the lateral distribution of proteins within the same membrane compartment, palmitoylation can rapidly and reversibly modulate protein-protein interactions.

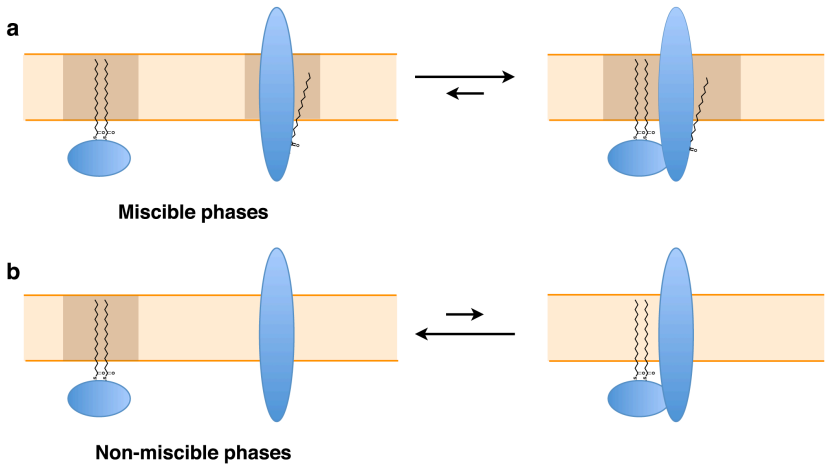

Figure 1.5 | Model for regulation of protein-protein interactions by palmitoylation-mediated microdomain association. a, Palmitoylation targets proteins to common membrane microdomains or raft environments that are miscible, thereby facilitating dynamic protein-protein interactions. **b,** Interactions between proteins in two non-miscible environments are less favored.

Interestingly, many peripheral and transmembrane proteins required for signaling at neuronal and immune synapses are palmitoylated[31, 39-41], suggesting a tantalizing possibility of lipid rafts as signaling platforms where reversible palmitoylation can rapidly regulate signaling strength by coordinating various lipid-protein and protein-protein associations[42].

Beyond membrane targeting

Besides inter- and intra- membrane targeting, palmitoylation controls protein activity in diverse ways such as inducing protein conformational changes[43, 44], modulating protein stability[45-49] and aggregation[50] as well as interacting with a variety of PTMs. Crosstalk between palmitoylation and other PTMs will be elaborated later in this chapter.

Part 2: Regulation of protein palmitoylation

As reviewed in Part 1, palmitoylation controls various aspects of protein distribution and function. Given its versatility and reversibility, palmitoylation is a potential major cellular regulator akin to phosphorylation. If this were true, one expects palmitoylation to be actively regulated and that this will have functional consequences on cellular physiology. This is best exemplified by the neuronal scaffold PSD95. Receptor activity-regulated palmitate turnover of PSD95 modulates synaptic strength and plasticity in post-synaptic neurons by mediating receptor clustering[39, 51]. Importantly, this effect is specific since palmitoylation of other neuronal proteins, GluR2 and GRIP1, is unaffected under the same conditions[51]. Besides neuronal activity, other extracellular signals have been shown to alter the palmitoylation state or rate of palmitate turnover in different cell types (Table 1.1, *proteins). Accelerated depalmitoylation of G-protein subunits, G-protein coupled receptors and a non-tyrosine kinase Lck upon receptor stimulation suggest active regulation of de/re-palmitoylation[52-55]. Additionally, a broader level of control is suggested by global changes in palmitoylomes that are associated with specific physiological states of the cell or organism[11, 56]. While it is clear that this lipid modification is regulated *in vivo*, the field is in its early days and little is known of how these changes in palmitoylation states occur and how they affect cellular function.

Similar to how phosphorylation is regulated by protein kinases and phosphatases, it is conceivable that enzymes catalyzing the palmitoylation and depalmitoylation reactions are regulated. Here, I review the evidence for regulation of these enzymes and

the other mechanisms that modulate protein palmitoylation as well as what these mean in terms of cellular function.

Palmitoyl acyltransferases (PATs)

A family of Asp-His-His-Cys-containing palmitoyl acyltransferases (DHHC-PATs) found in all eukaryotes examined is responsible for most protein palmitoylation events[12]. Discovered in *Saccharomyces cerevisiae*, AKR1[57] and ERF2-ERF4[58] are instrumental towards understanding the enzymology of protein palmitoylation. ERF2 requires an additional cofactor ERF4 for catalyzing palmitate transfer to its substrates[58], as does its mammalian DHHC9 homolog[59], while AKR1 exhibit sufficient activity by itself like most other PATs. ERF2 and AKR1 are integral membrane proteins with 4 and 6 transmembrane domains respectively, with the conserved DHHC domain that is required for catalytic activity facing the cytosol[60] (Fig.1.6a). Demonstrated by two groups using ERF2-ERF4 and mammalian PATs, DHHC2 DHHC3 and DHHC9-GCP16, PATs catalyze palmitoylation via a two-step ping-pong mechanism first involving autopalmitoylation of the enzyme followed by palmitoyl transfer to protein substrates[61, 62]. Although mutation of the conserved cysteine in the DHHC motif abrogates both autopalmitoylation and transfer[57, 58, 61-63], there still lacks definitive evidence that it is the catalytic cysteine due to the current inability to isolate and identify the palmitoyl-enzyme intermediate.

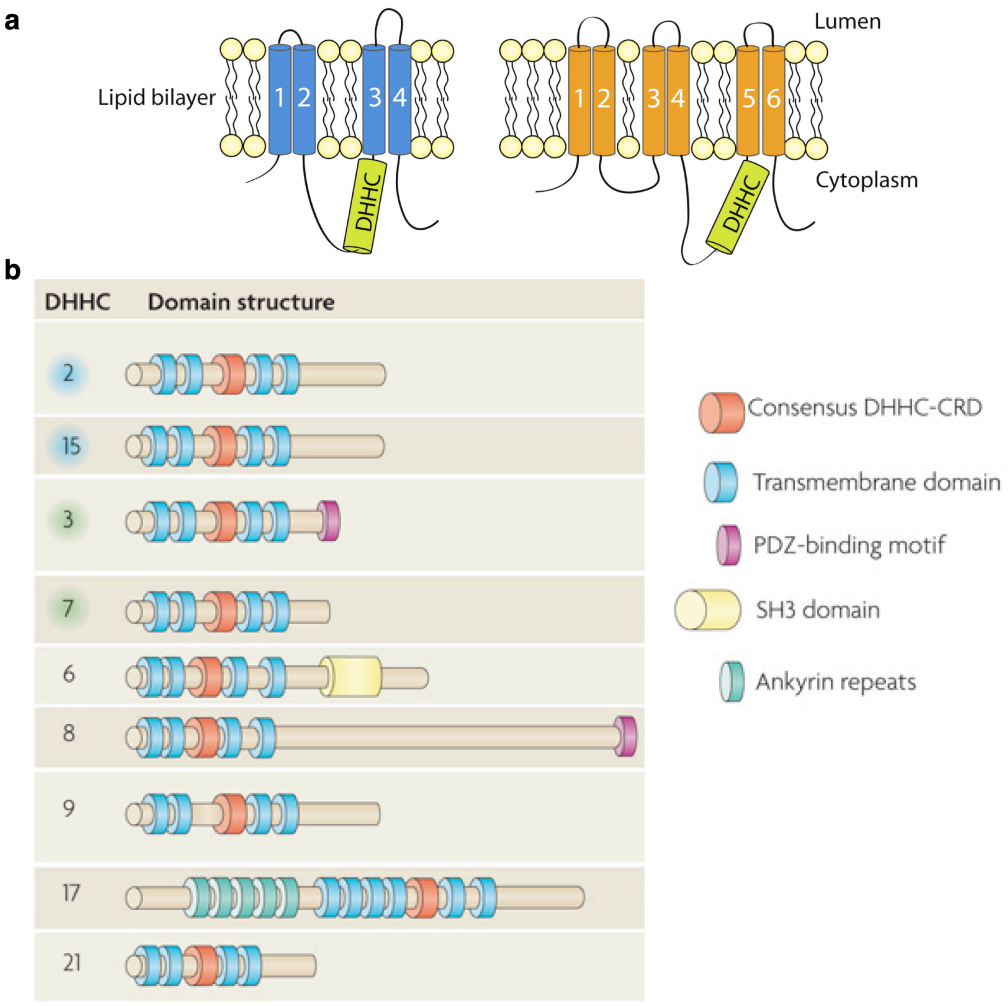

Figure 1.6 | Structure of PATs. a, PATs are integral membrane proteins with typically 4 or 6 predicted transmembrane domains. The conserved DHHC motif required for catalytic activity is located on the cytoplasmic face. Adapted from Young et al.[64] **b,** Domain structures of representative human PATs. Besides a DHHC core domain, each DHHC protein has individual protein–protein-interacting domains such as a PDZ-binding motif, an SH3 domain and ankyrin repeats. Blue and green backgrounds show the DHHC2/15 and DHHC3/7 subfamilies, respectively. Adapted from Fukata et al.[41]

PAT-substrate specificity

The multiple DHHC-containing PATs in an organism, ranging from a handful in unicellular fungi to more than twenty in metazoa, raise intriguing questions about substrate specificity and regulation.

On one hand, most studies support the notion that specific PAT-substrate pairs are needed for palmitate transfer. A systematic screen of all 23 mammalian PATs by gain- and loss- of-function studies revealed that only a subset of PATs (DHHC2, 3 and 7) quantitatively increase palmitoylation of a model substrate PSD95[65]. Palmitoylome analysis of various PAT-deficient mutants in budding yeast provided clear evidence for PAT-substrate specificity with individual PATs showing a preference for substrates with common features[12]. For example, ERF2-ERF4 substrates tend to be heterolipidated (e.g. myristoylated or prenylated), SWF1 substrates tend to be transmembrane proteins and AKR1 preferentially modifies soluble hydrophilic proteins[12]. Evidence of specificity determinants on both substrates[66] and enzymes[67] further supports substrate specificity among members of the PAT family. Huang and co-workers demonstrated that transfer of the HIP14/DHHC17 ankyrin repeat domain to DHHC3 enabled it to modify huntingtin, a HIP14/DHHC17 substrate[67], highlighting the importance and potential of domains outside the DHHC domain in regulating PAT-substrate specificity and function (Fig. 1.6b).

On the other hand, a recent study examining the kinetics of membrane association and partitioning of microinjected semisynthetic fluorescent lipopeptides suggested that protein palmitoylation was neither stereoselective nor sequence-specific and that substrate specificity was not required for dynamic palmitoylation in cells[68]. This is

supported by Hou and colleagues, who showed strong biochemical and functional overlap between the different PATs in budding yeast[69]. A potential concern for these studies is the use of non-physiological concentrations of substrates and/or enzymes, which may be accompanied by loss of PAT specificity.

Nonetheless, it is evident and consistent among the different studies that there is to a certain extent, biochemical and functional overlap between multiple PATs in organisms[12, 65, 68, 69], which makes understanding their roles in regulating global protein palmitoylation and cellular physiology challenging.

Differential regulation of PATs

Physiological state-dependent changes in the palmitoylation of individual proteins and in palmitoylomes suggest mechanisms by which PATs "sense" regulatory inputs and coordinate differential modification of its substrates. To date, there is little evidence for regulation of PATs and how it impacts protein palmitoylation as well as cellular function.

Specific PATs were found to have different subcellular locations and tissue-specific distribution[70, 71], suggesting the possibility that PAT localization and expression levels may be important for cellular function. As the first documentation of differential PAT regulation, Noritake and colleagues showed in neurons that activity-sensitive DHHC2 translocation enhances PSD95 palmitoylation and synaptic receptor clustering[51]. Although how PAT localization is determined and altered in response to synaptic activity is unclear, such stimulus-specific compartmentalization of PAT function may be a general mechanism to regulate protein palmitoylation. Recent studies by the Chamberlain lab

identified sorting signals on several PATs that target these enzymes to defined membrane compartments as well as regulate PAT cycling between compartments[72, 73].

PATs may also be regulated by PTMs such as palmitoylation and ubiquitination[18, 74, 75]. Interestingly, ubiquitination and subsequent proteasome-mediated degradation of DHHC5 were observed when cultured neural stem cells were induced to differentiate[74]. Nonetheless, it remains to be determined how induced PAT degradation affects substrate palmitoylation and impacts neuronal differentiation. From a bigger picture, are PATs modified by other PTMs and how do they regulate PAT function?

Further supporting that PATs have distinct substrates and modulate specific physiological functions, misregulation and mutation of specific PATs in mammals are involved in different neurological and developmental defects as well as various cancers (Table 1.2). Given the importance of PAT-mediated palmitoylation in many biological systems, it is important to elucidate mechanisms that control PAT activity in physiologically relevant contexts.

Table 1.2 | PATs involved in human diseases

Disease	Model	PAT	Observations	Reference
Neurological diseases				
Huntington disease (HD)	*In vitro*	ZDHHC17 /HIP14	Weaker huntingtin (HTT)–HIP14 interaction and reduced palmitoylation in presence of disease-causing mutation in HTT.	Singaraja et al[190] Huang et al.[209]
	Mouse	ZDHHC17 /HIP14	Reduced HTT palmitoylation in mouse model of HD.	Yanai et al.[50]
	Mouse	ZDHHC17 /HIP14	Phenotype in mice lacking HIP14 resembles mouse model of HD.	Singaraja et al.[208]
	In vitro	ZDHHC13 /HIP14L	Reduced HTT palmitoylation *in vitro.*	Saleem et al.[191]
	Mouse	HIP14, HIP14L	HTT modulates HIP14 and HIP14L activity.	Huang et al.[75]
Alzheimer's	*In vitro*	ZDHHC12	DHHC12 is involved in amyloid protein precusor metabolism (including Aβ production).	Mizumaru et al.[192]
Schizophrenia	Human	DHHC8	Associated with patients with schizophrenia.	Liu et al.[207]
	Mouse	ZDHHC8	Pre-pulse inhibition deficit in female knockout mice.	Mukai et al.[193]
	Mouse	ZDHHC8	Defective neuron morphology and reduced dendrite spine density. ZDHHC8 palmitoylates PSD95.	Mukai et al.[206]
X-linked mental retardation (XMLR)	Human	DHHC9	Severe nonsyndromic XLMR, epileptic seizures, dysmorphic facial appearance.	Raymond et al.[194]
	Human	DHHC15	Moderate XLMR in males. Developmental delay.	Mansouri et al.[205]
Non-neurological developmental defects				
Multiple defects	Mouse	ZDHHC13 /HIP14L	Knockout mice have shortened life spans, global amyloidosis, and hair, skin, and bone abnormalities.	Saleem et al.[191]
Hair and skin defects	Mouse	ZDHHC21	Loss of ZDHHC21 function results in skin homeostasis and hair follicle differentiation.	Mayer et al.[204] Mill et al.[195]
Cancers				
Various cancers and metastasis	Human	DHHC2	Potential tumor suppressor genes for various cancers are mapped to chromosomal region 8p22 that contains the *DHHC2* gene	Oyama et al.[203] Qin et al.[196]
Bladder cancer	Human	DHHC11	Increased copy number of chromosome region containing *DHHC11* gene in bladder cancers with high malignant potential.	Yamamoto et al.[202]

Table 1.2 continued |

Disease	Model	PAT	Observations	Reference
Non-small lung cancer	Human	DHHC11	Increased copy number of chromosome region containing *DHHC11* gene in non-small cell lung cancers.	Kang et al.[198]
Colorectal cancer	Human	DHHC9	*DHHC9* transcript is upregulated in the majority of microsatellite stable colorectal tumors but not in other common cancers.	Mansilla et al.[201]
Cellular transformation	Murine cell line Human	DHHC20	DHHC20 overexpression induces cellular transformation. Overexpressed in several human tumors (ovarian, breast and prostate)	Draper et al.[199]
Cellular transformation	Murine cell line	ZDHHC17 /HIP14	HIP14 overexpression induces cellular transformation.	Ducker et al.[200]

Depalmitoylating enzymes/ protein thioesterases

In contrast to the large PAT family, few protein thioesterases with depalmitoylating activity have been identified and they are relatively uncharacterized. Biochemical efforts to purify depalmitoylating enzymes have yielded lysosomal palmitoyl protein thioesterase 1 (PPT1) and cytosolic acyl protein thioesterase 1 (APT1), both of which can depalmitoylated proteins *in vitro*[76-78].

PPT1, a lysosomal protein is responsible for degrading palmitoylated proteins, is thought to be topologically incompatible with depalmitoylating cytoplasmic proteins[79]. Nonetheless, recent studies show that PPT1 is also found in presynaptic compartments in neurons and that it may play a role in synaptic vesicle cycling[80, 81].

Consistent with its ability to depalmitoylate Hras and $G\alpha_i$ *in vitro*[77], APT1 overexpression promoted depalmitoylation of $G\alpha_s$ and eNOS in mammalian cultured cells[82] and disruption of APT1 function in budding yeast resulted in decreased palmitate turnover on GPA1, the yeast Gα homolog[78]. Treatment of cells with an inhibitor

(Palmostatin B) designed to target APT1, an α/β serine hydrolase with a canonical serine/ histidine/aspartate catalytic triad[83, 84], increased steady state Ras palmitoylation and cellular redistribution of Ras proteins[84]. While this study provides the first evidence that Ras is a substrate of APT1 in cells, it is possible that this is due to off-target effects of Palmostatin B on other similar serine hydolases and protein thioesterases including PPT1 and APT2[83], which has been shown to deacylate GAP43 in cells[85]. Recently, APT1 was implicated in neuronal morphogenesis when it was found to be a target of a neuronal enriched microRNA, miR138[86]. Down-regulation of APT1 function was associated with increased association of $G\alpha_{13}$ with the membrane and higher dendritic spine volume[86]. It would be interesting to see if other palmitoylated proteins in neurons[41] are actually APT1 substrates and if they contribute to neuron morphogenesis and activity.

Given the limited number of APT1 substrates that are validated *in vivo* compared to diverse proteins that undergo regulated palmitate turnover[14], it remains to be determined if PPT1, APT1 and their related isoforms are the main deacylating enzymes or if there are potentially more enzymes to be uncovered. As with discovery of the PATs, identification of the thioesterases would allow perturbation of the palmitoylation/ depalmitoylation cycle and yield insights into the regulation and physiological function of dynamic palmitoylation.

Accessibility of modification sites

Protein palmitoylation can be modulated by mechanisms that influence the accessibility of substrates or modification sites to the palmitoylation or depalmitoylation enzymatic machinery. An example is the promotion of Ras depalmitoylation by prolyl isomerase FKBP12[87] (Fig. 1.7). Ahearn and co-workers showed that FKBP12 binds to Hras in a palmitoylation-dependent manner and regulates its trafficking by promoting depalmitoylation through cis-trans isomerization of a peptidyl-prolyl bond close to palmitoylated cysteines. Inhibition of FKBP12 prolyl isomerase activity by a variety of chemical inhibitors such as FK506, rapamycin and cycloheximide increases Hras steady state palmitoylation[87]. While only proteins with proline residues close to palmitoylation sites can potentially be regulated by this mechanism, it is conceivable that any changes in protein conformation that influence the accessibility of the modification sites, can affect the palmitoylation/depalmitoylation cycle.

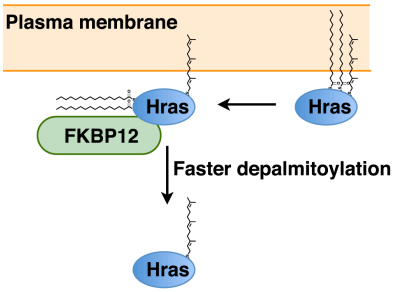

Figure 1.7 | Controlling depalmitoylation by altering the accessibility of modification sites. FKBP12 binds Hras and promotes its depalmitoylation by *cis-trans* isomerization of a peptidyl-prolyl bond in proximity to the palmitoylated cysteines.

Substrate accessibility can also be modulated by crosstalk between different PTMs. Negatively-charged phosphate groups may prevent palmitoylation of an adjacent cysteine by preventing association with membranes, where PATs are localized (Fig 1.8a, 1). In a reciprocal manner, one would also expect palmitoylation to prevent phosphorylation by blocking access of kinases to nearby serine, threonine or tyrosine residues[88-91] (Fig. 1.8a, 2). Nitrosylation competes with the PATs for modification sites (Fig. 1.8b). PSD95 is physiologically nitrosylated at the same cysteines that are palmitoylated and physiologically produced nitric oxide (NO) inhibits PSD95 palmitoylation and synaptic clustering *in vivo*, demonstrating direct competition between these cysteine modifications[40]. Since NO is an established modulator of many biological processes including synaptic transmission[92], dynamic reciprocity between nitrosylation and palmitoylation may explain how synaptic activity regulates PSD95 palmitoylation as well as synaptic clustering and activity. Further examination of palmitoylated substrates for competing cysteine modifications (e.g. nitrosylation and sulfhydration) would help determine if this is a general mechanism for regulating protein palmitoylation.

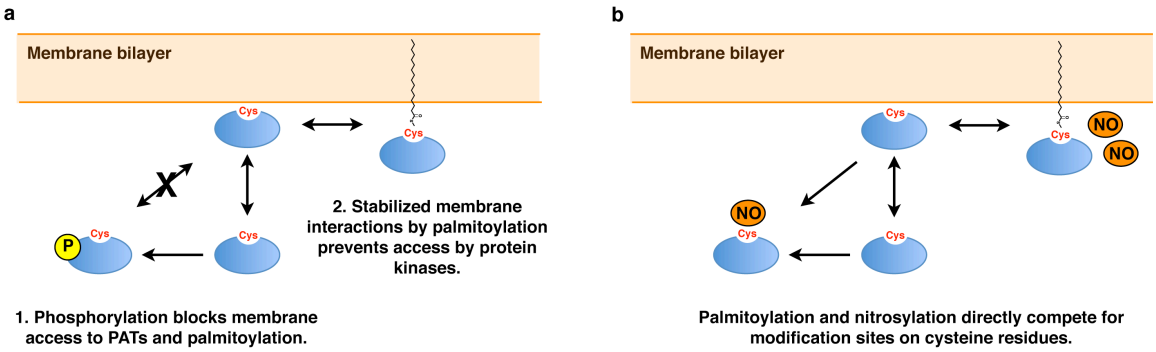

Figure 1.8 | Interplay between palmitoylation and other PTMs. a, Proximity-dependent reciprocal regulation between phosphorylation and palmitoylation. (1) Negatively-charged phosphate group (P, yellow circle) prevents palmitoylation of an adjacent cysteine (Cys, red) by blocking membrane interaction. (2) Palmitoylation-mediated membrane association prevents access of protein kinases to an adjacent phosphorylation site. **b,** Direct competition for modification sites. (1) Nitrosylation (NO (nitric oxide, orange circle) may prevent palmitoylation by direct competition for cysteine residues (Cys, red) and vice versa. Nitrosylation may deplete the pool of depalmitoylated substrates available for repalmitoylation. Other cysteine modifications may have similar regulatory effects. Note that these examples are not mutually exclusive, nor do they illustrate the full range of effects that these PTMs have on each other.

While it is clear that protein palmitoylation is important for protein function and is regulated *in vivo*, the identity and physiological roles of mechanisms that regulate palmitoylation is limited. In this thesis, I describe the development of chemical tools that improves the detection and identification of dynamically palmitoylated proteins, present the fission yeast S*chizosaccharomyces pombe* as a new model organism useful for PAT studies and demonstrate a physiologically important mechanism for regulating protein palmitoylation.

CHAPTER 2

BIOORTHOGONAL DETECTION OF PROTEIN FATTY-ACYLATION IN MAMMALIAN CELLS

Introduction

Many cellular proteins are covalently modified by lipids, the addition and removal of which regulates diverse biological processes ranging from cellular growth and differentiation to lymphocyte activation and synaptic transmission. In eukaryotes, fatty acids, isoprenoids and glycosylphosphatidylinositols constitute the three prevalent forms of lipid modifications. In this chapter, I will be focusing on the two major forms of protein fatty-acylation, *S*-palmitoylation and *N*-myristoylation, which are characterized by the chain length of the acyl group attached to proteins (Table 2.1).

S-Palmitoylation, also known as *S*-acylation, is the only characterized reversible lipid modification that takes place on the thiol side chains of cysteine residues post-translationally via a thioester linkage[1]. Although it typically involves attachment of a saturated 16-carbon palmitate to proteins, incorporation of longer fatty acids with different degrees of unsaturation have been reported[3-5]. Unlike *N*-myristoylation, there is no unique consensus palmitoylation motif, making it difficult to accurately predict palmitoylated proteins and modification sites. The functional role of palmitoylation in physiology and disease is covered in Chapter 1.

Table 2.1 | *N*-Myristyolation and *S*-palmitoylation are two major forms of protein fatty-acylation in eukaryotes.

***N*-Myristoylation**	***S*-Acylation (*S*-Palmitoylation)**
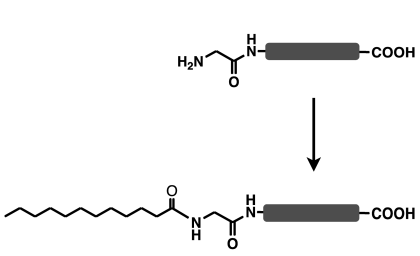	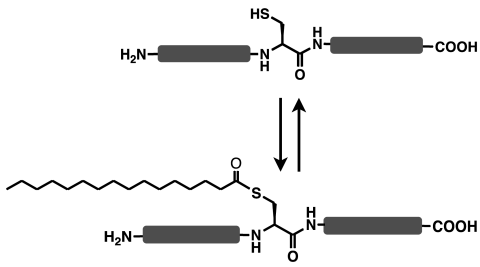
Co-translational modification	Post-translational modification
Covalent attachment of a myristoyl (C14:0) group	Covalent attachment of a long chain acyl group such as palmitoyl (C16:10), stearoyl (C18:0), palmitoleoyl (16:1) etc.
Modification of N-terminal glycine residues via amide linkages MGXXXS/T signature sequence (X=any residue)	Modification of cysteine residues via thioester linkages No unique canonical *S*-acylation motif
Irreversible	Reversible
Mediated by N-myristoyltransferases (NMT)	Acylation mediated by palmitoyl acyltransferases (PATs) Deacylation mediated by protein thioesterases
Autoradiographic detection: Radiolabeled fatty acids (^{3}H, ^{14}C and ^{125}I) Western blot detection: Azido-fatty acids and Staudinger ligation	Autoradiographic detection: Radiolabeled fatty acids (^{3}H, ^{14}C and ^{125}I) Western blot detection: Azido-fatty acids and Staudinger ligation Acyl-biotin exchange (ABE)

Myristoylation is the irreversible attachment of a saturated 14-carbon myristate to N-terminal glycine resides of proteins that is mediated by *N*-myristoyltransferases (NMTs)[93]. Although myristoylation predominantly occurs during protein translation, it can occur post-translationally on N-terminal glycine residues revealed by proteolytic cleavage of protein substrates[94]. Studies indicate that myristoylation promotes weak transient protein-membrane associations that would be further stabilized by a second signal such as palmitoylation[23]. In addition to being an essential modification[95, 96], protein myristoylation has been implicated in infectious and neurological diseases as well as various cancers[97]. This is exemplified by different classes of myristoyl switch proteins, of which conformation changes modulates accessibility of the myristate group and thus their interactions with the membranes and other proteins[98-102].

Given the critical role of fatty-acylation in modulating protein behavior, the ability to detect, characterize and probe their involvement in cellular function is important. Traditional autoradiographic detection of radioactive (^{3}H or ^{14}C) fatty acids that are metabolically incorporated into proteins, while effective, requires exposure times spanning days or weeks. Radioactive iodinated (I^{125})-fatty acids improves detection time but are hazardous and not readily available[103]. These limitations are circumvented by two different approaches of visualizing fatty-acylated proteins using streptavidin immunoblotting (Fig. 2.1). First, the acyl-biotin exchange protocol (ABE) involves the covalent attachment of biotin-HPDP (*N*-[6-(biotinamido)hexyl]-3′-(2′-pyridyldithio)propionamide) to free thiols on proteins that are liberated by hydroxylamine cleavage of thioester-linked palmitate groups[104] (Fig. 2.1a). The combination of ABE

with mass spectrometry-based proteomics using multidimensional protein identification technology to yeast and neurons has revealed many new *S*-palmitoylated proteins in eukaryotes[11, 12]. However, this approach is limited to *S*-acylated proteins since the amide linkages of myristoylated proteins are resistant to hydroxylamine[1]. Furthermore, it is limited to the analysis of steady state palmitoylation. Developed by my research advisor, Dr. Howard Hang, the second approach allows visualization of both myristoylated and palmitoylated proteins. This bipartite labeling approach involving metabolic incorporation of azide-functionalized fatty acids followed by selective addition of phosphine-biotin probes via Staudinger ligation[105] (Fig. 2.1b). While these complementary approaches offer rapid and convenient detection of fatty-acylation, immunoblotting methods are not ideal for analyzing quantitative changes in protein fatty-acylation necessary for investigating dynamics or regulatory mechanisms.

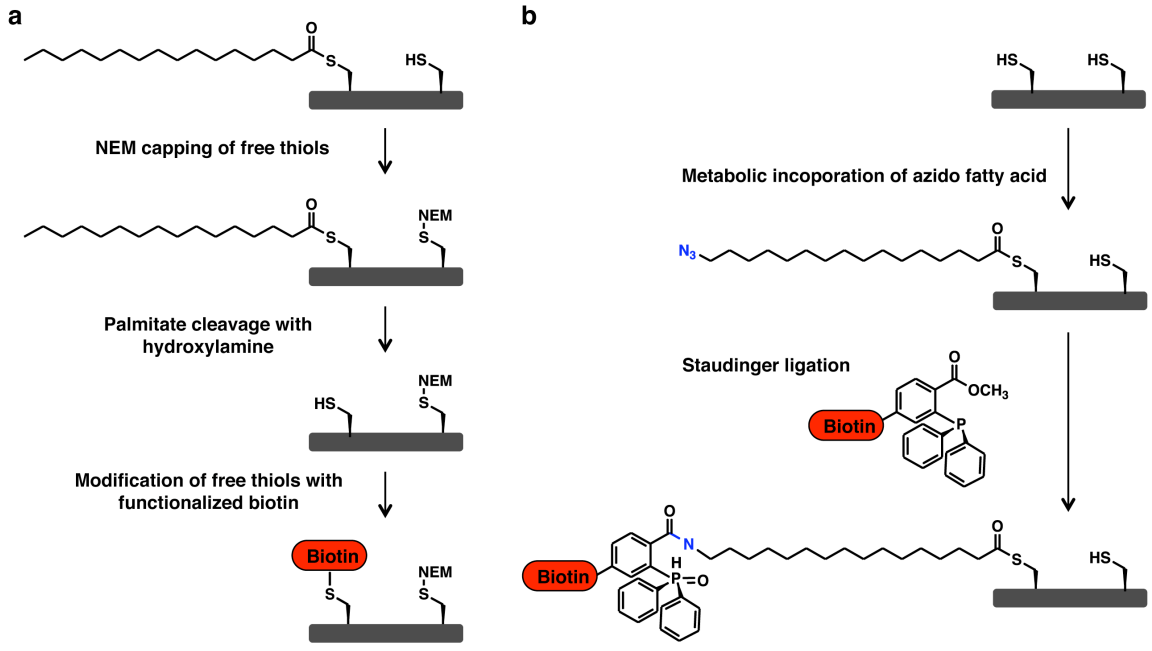

Figure 2.1 | Non-radioactive immunoblot detection of fatty-acylated proteins in eukaryotes. **a,** Acyl-biotin exchange. **b,** Metabolic labeling and Staudinger ligation.

I initiated this thesis by developing bioorthogonal methods for improved fluorescent detection of endogenously expressed fatty-acylated proteins in mammalian cells. Through comparative analysis of substrates representing different classes of fatty-acylated proteins, I demonstrated the fatty acid chemical reporters are indeed taken up by cells and specifically incorporated into proteins at canonical modification sites via native linkages. Furthermore, I showed that alkynyl-fatty acid chemical reporters, in combination with in-gel fluorescence scanning, provide superior and quantitative detection of fatty-acylated proteins. Finally, Dr. Lun Tsou and I developed a tandem labeling and detection method to simultaneously monitor dynamic palmitoylation and protein turnover. The sensitivity and efficiency of this approach should facilitate the functional characterization of cellular factors and drugs that modulate palmitoylation dynamics.

Results

Bioorthogonal detection of protein fatty-acylation in mammalian cells

Advances in bioorthogonal labeling methods employing copper(I)-catalyzed Huisgen [3 + 2] cycloaddition (CuAAC) or "click chemistry" reaction between alkyl azides and alkynes (Fig. 2.2b) offered an opportunity to improve the analysis of fatty-acylated proteins using chemical reporters. To that end, a fellow graduate student in the lab, Guillaume Charron, synthesized a series of azido- and alkynyl-fatty acids of different lengths (Fig. 2.2c) as potential chemical reporters as well as a panel of biotinylated (alk-biotin, az-biotin) and fluorescent (alk-rho, az-rho) detection tags (Fig. 2.2d). Together with another graduate student in the lab, John Wilson, we optimized bioorthogonal reaction conditions and showed that fluorescence detection of fatty-acylated proteins in whole cell lysates using alkynyl chemical reporters is more sensitive compared to radioactive and immunoblot detection methods described previously.

Analysis of protein fatty-acylation at the proteome level, while important, is biased towards highly abundant proteins in cells where the dynamic range of protein concentrations can span more than seven orders of magnitude[106-108]. By immunopurifying proteins of interest prior to CuAAC (Fig. 2.2a), I was able to detect chemical reporter incorporation into substrates representing different classes of fatty-acylated proteins: *S*-palmitoylated Linker for Activation of T-cells (LAT)[31], *N*-myristoylated and *S*-palmitoylated Lck[109, 110], as well as *S*-palmitoylated and *S*-prenylated Ras[2, 20, 21] (Fig. 2.3). Fluorescence at the expected molecular weight of each substrate was only observed in samples that were metabolically labeled with the fatty acid chemical reporters (Fig 2.3b).

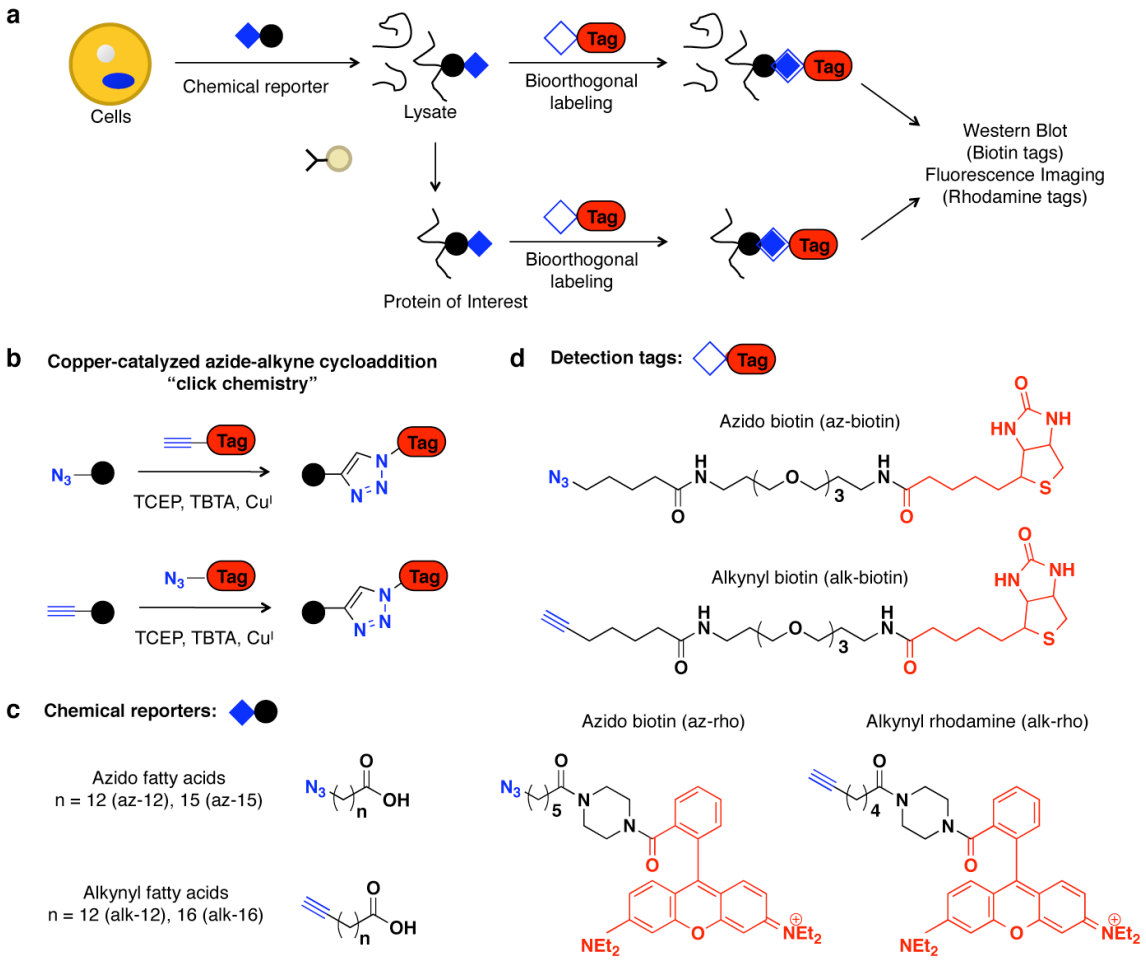

Figure 2.2 | Analysis of protein fatty-acylation with chemical reporters. a, Metabolic labeling of mammalian cells with chemical reporters and bioorthogonal labeling of proteins. **b,** Copper(I)-catalyzed Huisgen [3 + 2] cycloaddition or "click chemistry" enables selective covalent attachment of detection tags to azido or alkynyl substrates. **c,** Fatty acid chemical reporters. **d,** Clickable detection tags.

As a first indication of the specificity of these fatty-acylation chemical reporters, no fluorescent signal was observed for p53, a non-acylated protein (Fig. 2.3b). This approach allows analysis of less abundant proteins and focused studies of individual proteins of interest, detection of which may not be readily apparent at the lysate level.

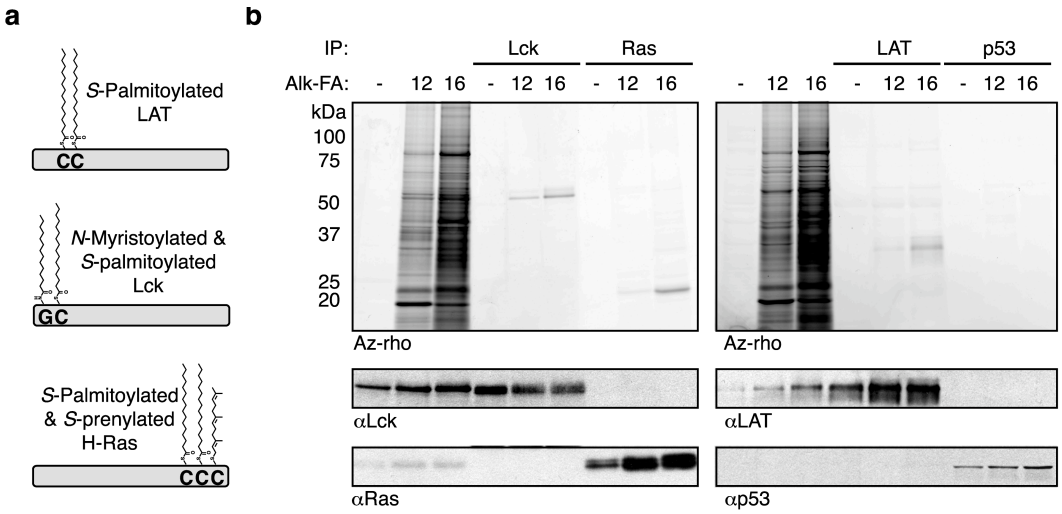

Figure 2.3 | Robust fluorescent detection of fatty-acylated proteins. a, Schematic representation of lipidation sites for LAT (*S*-palmitoyl-Cys26, *S*-palmitoyl-Cys29), Lck (*N*-myristoyl-Gly2, *S*-palmitoyl-Cys3, *S*-palmitoyl-Cys5) and H-Ras (*S*-palmitoyl-Cys181, *S*-palmitoyl-Cys184, *S*-prenyl-Cys186), which represent different classes of fatty-acylated proteins. **b,** In-gel fluorescent detection of fatty-acylated proteins in lysates and of immunopurified proteins. p53, non-fatty-acylated protein.

Fatty acid chemical reporters exhibit chain-length dependent labeling of N-myristoylated and S-palmitoylated proteins

The ability to assess chemical reporter incorporation into individual proteins allows evaluation of different detection methods and specificity of the chemical reporters. For these studies, Jurkat cells were metabolically labeled with azido- or alkynyl- fatty acids and their incorporation into LAT, Lck and Ras was detected using biotinylated or fluorescent detection tags. Fluorescent detection of immunopurified fatty-acylated proteins was markedly improved compared to detection by streptavidin blotting (Fig. 2.4). Longer palmititc acid analogues (az-15, alk-16), which should be incorporated into all three *S*-acylated proteins, was nearly undetectable by streptavidin blotting (Fig. 2.4a) but robustly visualized by in gel fluorescence scanning (Fig. 2.4b). Shorter myristic acid

analogues (az-12, alk-12), which should label *N*-myristoylated proteins, are preferentially incorporated into Lck and to a lesser extent into LAT and Ras by fluorescence (Fig. 2.4b). This is not unexpected since *S*-acylation involves a heterogenous composition of fatty acids[3-5].

It is unclear why detection of *S*-acylated proteins is more efficient with myristic acid compared to palmitic acid analogues by streptavidin blotting. It is possible that az-12 or alk-12 labeled proteins transfer more efficiently from the gel to the membrane and are thus better detected by streptavidin blot than the more hydrophobic az-15 or alk-16 proteins. Variability in protein transfer efficiency would be circumvented by direct in-gel fluorescent detection, which is the more consistent and reproducible detection method over the multiple repeats of this experiment (data not shown). Notably, the orientation of alkyne and azide functional groups also influence overall detection sensitivity, with the alkynyl-chemical probes giving higher signal-to-noise compared to their azide counterparts (Fig. 2.4b). This is consistent with studies using alkyne- or azide-functionalized chemical probes[111, 112]. Overall, these experiments demonstrate that alkynyl-fatty acid chemical reporters, in combination with in-gel fluorescence detection, afford optimal detection of fatty-acylated proteins.

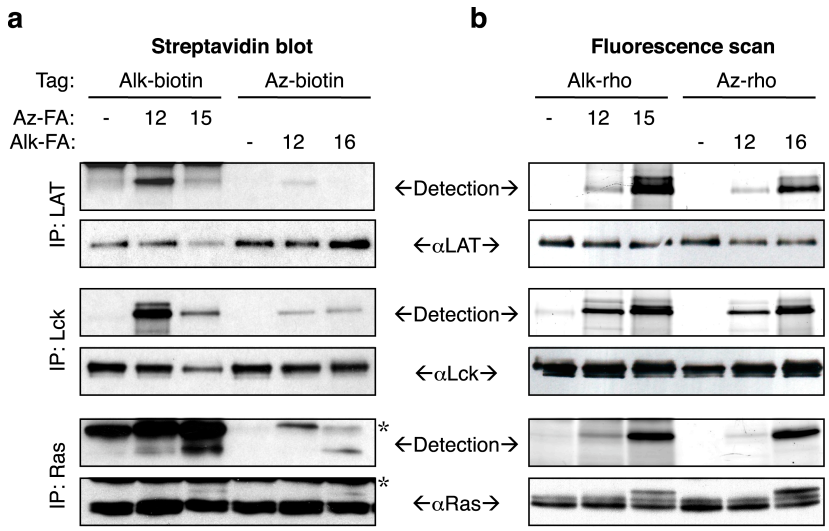

Figure 2.4 | Alkynyl chemical reporters, in conjunction with in-gel fluorescence scanning, affords optimal detection of fatty-acylated proteins. a, Comparative analysis of click chemistry orientation with LAT, Lck and Ras by streptavidin blotting and **b,** in gel-fluorescence scanning. *non-specific bands.

Fatty acid chemical reporters are incorporated into proteins at canonical modification sites via native linkages

In-gel hydroxylamine treatment of alkynyl-fatty acid-labeled Lck and LAT reduced the fluorescent signal derived from alk-16 on both proteins, but did not alter the alk-12 labeling of Lck (Fig. 2.5a). We also analyzed the specificity of our fatty acid chemical reporters with wild-type and mutant constructs of p59 Fyn[113], a well-characterized *N*-myristoylated and *S*-palmitoylated Src-family kinase, by overexpression in HeLa cells, metabolic labeling and immunoprecipitation (Fig. 2.5b, c). Fatty-acylation of wild-type Fyn is readily detected with alk-12 and alk-16 labeling, whereas the *N*-myristoylation G2A mutant exhibited significantly reduced alk-12 labeling and was undetectable with alk-16. The dual *S*-palmitoylation-deficient C3,6S mutant was efficiently labeled with alk-12 and not with alk-16. These results are quantitatively identical to previously

described experiments using radiolabeled fatty acids, which also demonstrated residual labeling of G2A mutant Fyn with a ^{125}I-myristic acid analogue and no labeling with ^{125}I-palmitic acid analogue[3, 113]. These experiments also support the model that *N*-myristoylation precedes *S*-palmitoylation and highlight the possibility of fatty-acylation at N-terminal alanine residues. Collectively, our experiments with cell lysates and specific proteins demonstrate that alk-12 labels *N*-myristoylated and *S*-acylated proteins, whereas longer-chain fatty acid chemical reporters such as alk-16 preferentially target *S*-acylated proteins.

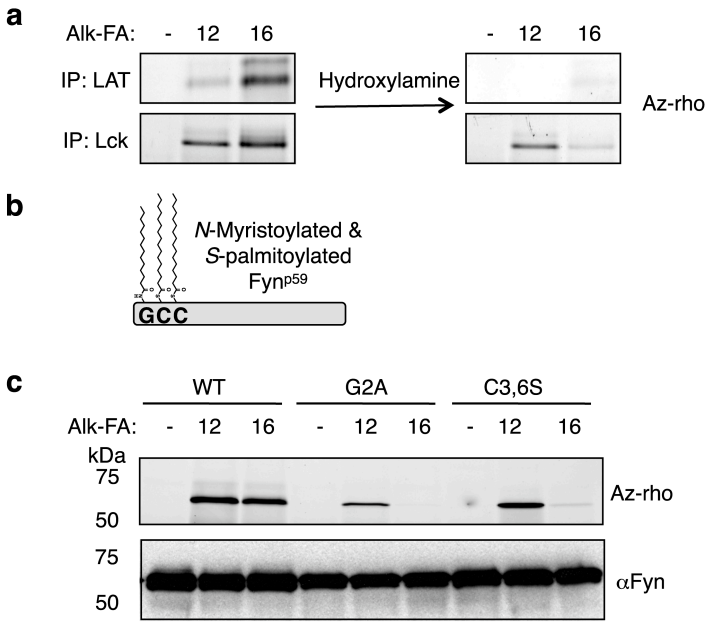

Figure 2.5 | Fatty acid chemical reporters exhibit linkage and residue specific labeling of proteins. a, Hydroxylamine sensitivity of alkynyl-fatty acid Lck and LAT labeling in Jurkat cells. Shown are fluorescence scans of the same gel before and after hydroxylamine treatment. **b,** Schematic representation of lipidation sites of Fyn (*N*-myristoyl-Gly2, *S*-palmitoyl-Cys3, *S*-palmitoyl-Cys6). **c,** Comparative analysis of the acylation states of wild type (WT), G2A mutant and C3,6S mutant Fyn in HeLa cells.

Tandem fluorescence imaging of two different protein modifications

An opportunity to visualize two distinct chemical reporters in the same sample arose when Dr. Tsou developed a set of clickable fluorescent detection tags (az/alk-Cyfur) with near-IR photophysical properties that are orthogonal to the rhodamine detection tags[114]. The following studies were done in close collaboration with Dr. Tsou.

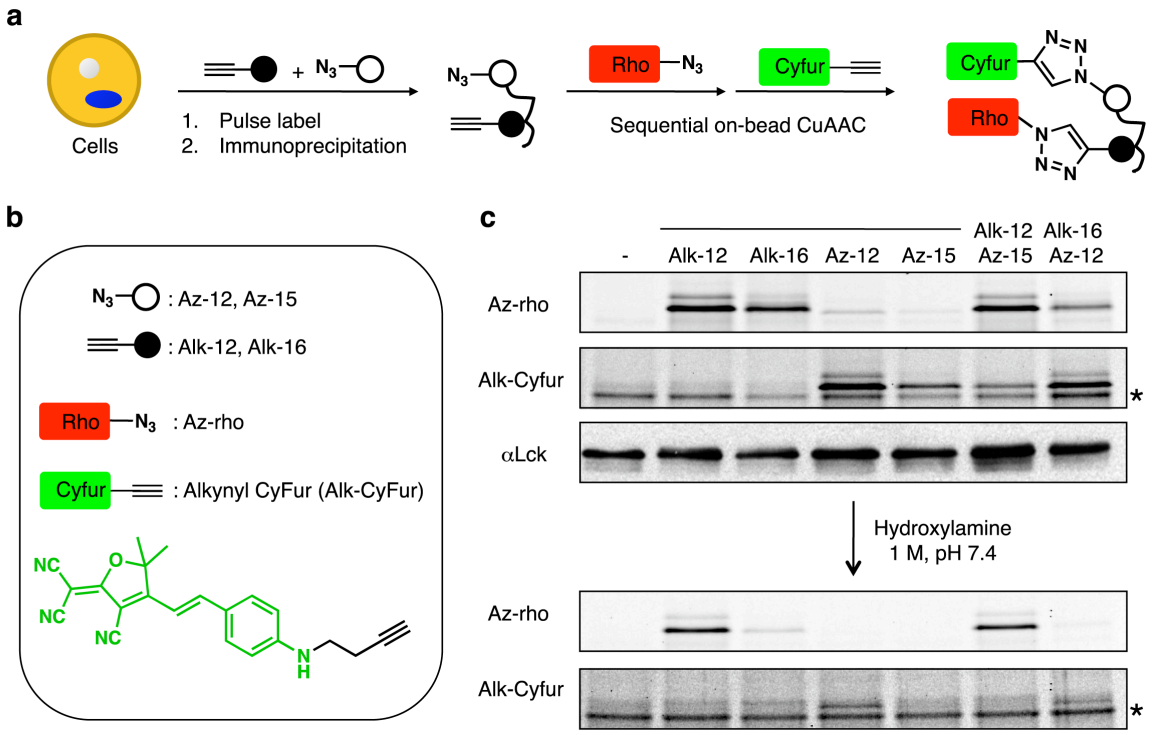

Figure 2.6 | Tandem orthogonal imaging of two different protein modifications. a, Following metabolic labeling with two chemical reporters, immunopurification and sequential click chemistry reactions with orthogonal detection tags allow simultaneous visualization of two protein modifications. **b,** Fatty acid chemical reporters and clickable fluorescent detection tags. **c,** Tandem detection of az-12 and alk-16 on Lck using alk-Cyfur and az-rho respectively. Western blot is probed for Lck. Lower panels are fluorescence scans of the same gel after hydroxylamine treatment. *, non-specific bands.

To explore the simultaneous metabolic labeling and detection of two distinct chemical reporters, we focused on Lck, an *N*-myristoylated and *S*-palmitoylated non-receptor tyrosine kinase required for T-cell activation[110, 115, 116] and exploited the chain-length specificity between different fatty acid chemical reporters (Fig. 2.5a). Lck was immunopurified from Jurkat T-cells that were metabolically labeled with either one or both of the myristate (az-12/alk-12) and palmitate (az-15/alk-16) analogs and subjected to sequential on-bead CuAAC reactions with az-rho and alk-Cyfur (Fig. 2.6a, b). Washes after the first reaction removes excess reagents that could quench the second CuAAC reaction. Orthogonal visualization of the two chemical reporters was achieved with in-gel fluorescence scanning. At 532 nm excitation/580 nm emission, az-rho signal was observed for samples labeled with alkynyl-fatty acid reporters (alk-12 and alk-16), while alk-Cyfur fluorescence at 633 nm excitation/670 nm emission was only detected in with samples exposed to azido-fatty acid reporters (az-12 and az-15) (Fig. 2.6c, upper panel). Consistent with the differential biochemical reactivity of thioester and amide linkages[1], in-gel hydroxylamine treatment selectively diminished fluorescence associated with thioester-linked palmitate analogs (az-15/alk-16) compared to amide-linked myristate analogs (az-12/alk-12) (Fig. 2.6c, lower panel). These results demonstrate that both sets of fatty acid chemical reporters are specifically incorporated by *N*-myristoylation and *S*-palmitoylation cellular machinery through native chemical linkages. For the first time, we show sensitive fluorescent detection of dually-modified proteins using two distinct chemical reporters in parallel. Our tandem imaging method is complementary to copper-

mediated and copper-free click chemistry strategies that have been used for time-resolved imaging of single biosynthetic pathways[117-120].

Measuring palmitate turnover on proteins using tandem fluorescence imaging

Next, we determined if we can measure palmitate cycling on proteins by using the tandem imaging method to orthogonally monitor palmitoylation and protein synthesis[52]. Traditionally, palmitoylation turnover rates are obtained from pulse chase studies using ^{3}H-palmitate and ^{35}S-methionine, with limitations associated with autoradiographic detection. To monitor palmitate cycling with fluorescence, we envisioned a pulse-chase experiment employing distinct chemical reporters with orthogonal readouts (Fig. 2.7a) – one to monitor dynamic palmitoylation and the other to function as an internal control for protein turnover. Since myristoylation is primarily a co-translational and constitutive modification[1], a myristate analog should function as an efficient chemical reporter for the amount and loading of myristoylated proteins.

We first evaluated whether incorporation of alk-16 into *S*-acylated proteins is reversible in cells. Lck was immunopurified from Jurkat cells that were pulse-labeled with az-12 and alk-16 followed by a 10-fold excess palmitate chase for different lengths of time (Fig. 2.7a). Compared to the relatively constant signal of az-12 labeling of Lck, the fluorescent signal from alk-16 labeling decayed over time (Fig. 2.7b-d). No decrease of az-12 signal was observed with excess myristate as the chase additive over 6 hours (Fig. 2.8a), demonstrating that az-12 is an effective chemical reporter of constitutive *N*-myristoylation and protein loading. If alk-16 is efficiently recognized by cellular

thioesterases, we expect the calculated palmitate half-life on Lck using our method to agree with that of a previously reported pulse-chase study using ^{3}H-palmitate and ^{35}S-methionine[109].

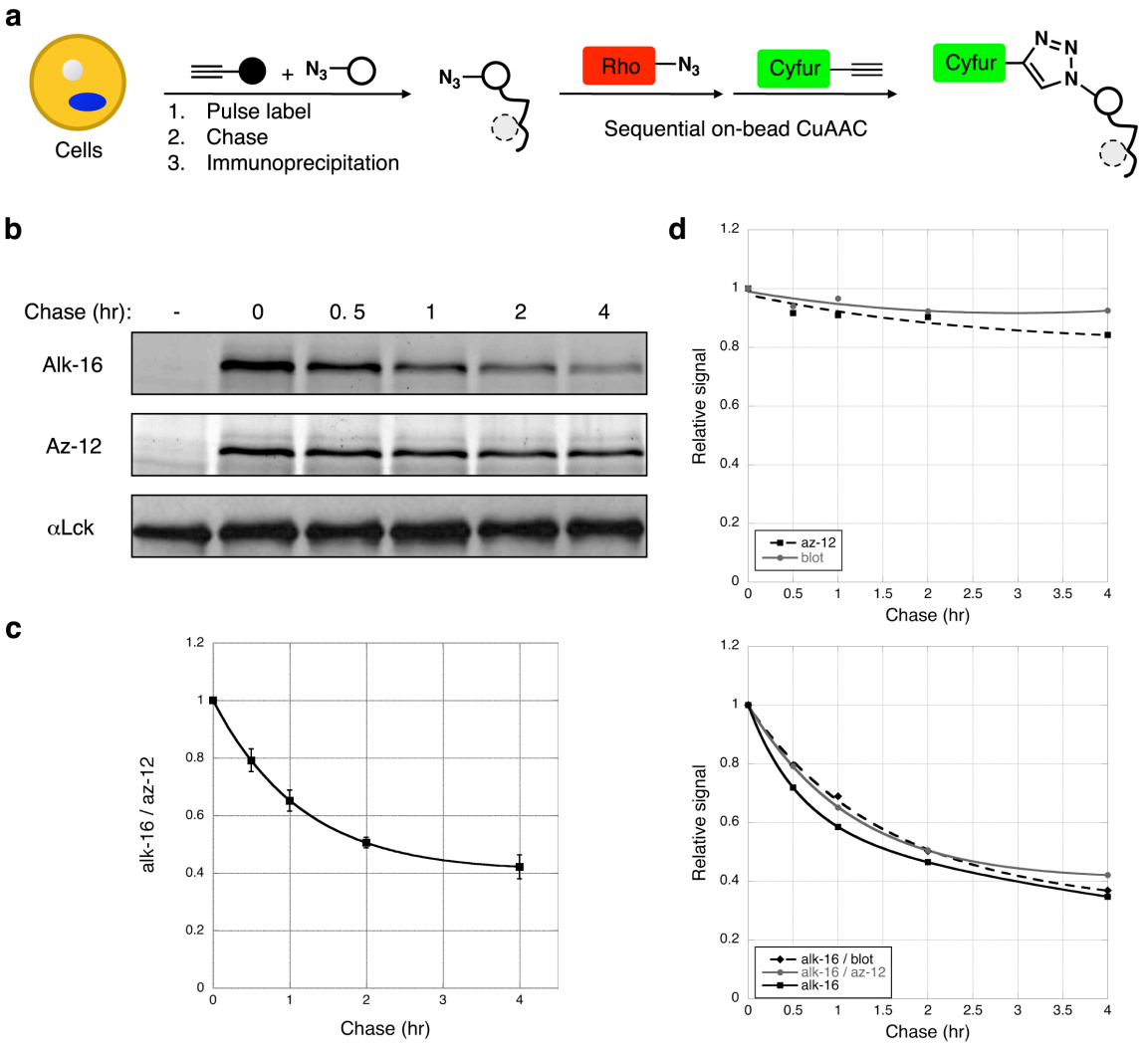

Figure 2.7 | Measuring palmitate turnover on Lck using the tandem imaging method. a, Scheme of pulse-chase experiment. **b,** Pulse-Chase analysis of Lck. **c,** Data from multiple chase experiments (n=10). Data points from the same chase times, after normalizing alk-16/az-12 signals, were compiled and displayed as average values ± s.e.m. **d,** Plots of relative signals for alk-16, az-12 fluorescence and anti-Lck blot intensities in the pulse-chase experiments.

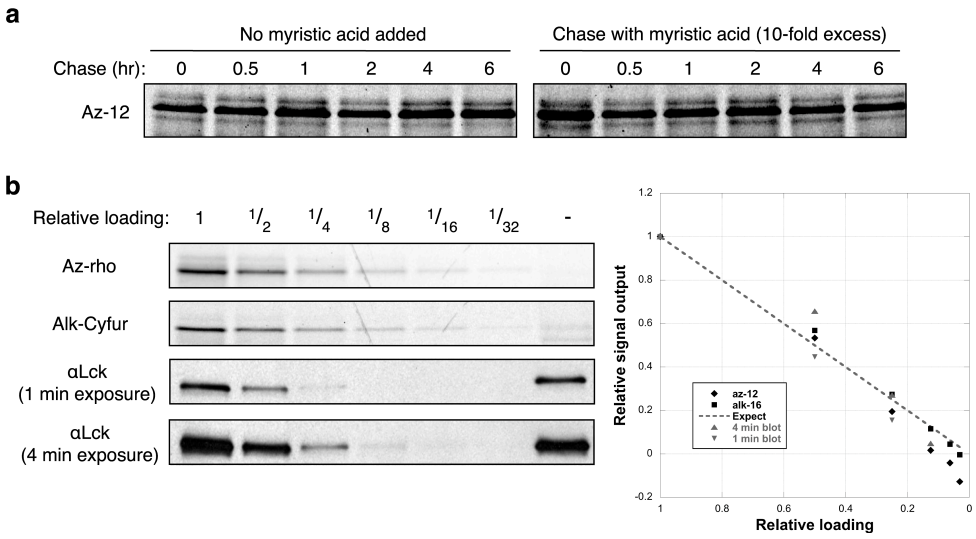

Figure 2.8 | Pulse-Chase controls. a, In-gel fluorescence scanning in the alk-Cyfur channel shows no significant turnover of az-12 on Lck upon chasing in the presence of excess myristate. **b,** The range of in-gel fluorescence intensities is linear compared to the amount of labeled substrate.

After confirming our fluorescence measurements are in the linear range (Fig. 2.8b) and normalizing alk-16 to az-12 fluorescent signals, our calculated palmitate half-life on Lck is ~50 minutes (Fig. 2.7c), which is comparable to that reported by Paige et. al. under similar experimental conditions[109]. Parallel analysis of another fatty-acylated kinase, Fyn[110, 113], from the same lysates confirmed dual and specific labeling with the fatty acid reporters. The calculated palmitate turnover rate of Fyn is longer than Lck (Fig. 2.9) and is consistent with the reported estimate of 1.5-2 hours[121]. These results demonstrate that the fatty acid reporters and our tandem imaging method can be used to efficiently and accurately evaluate *S*-palmitoylation turnover on endogenously expressed proteins.

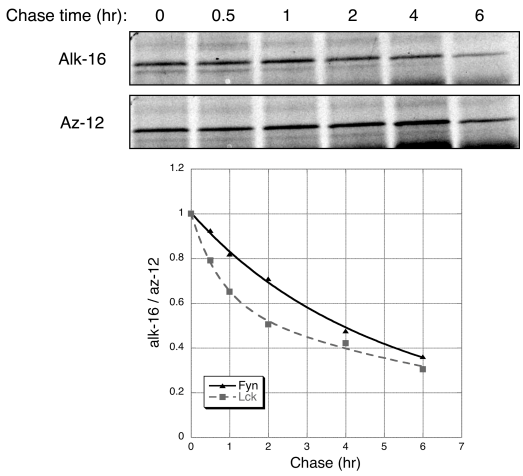

Figure 2.9 | Pulse-Chase analysis of Fyn. Data from a single pulse-chase experiment after normalizing alk-16/az-12 signals relative to that of Lck.

Pevandate stimulation accelerates palmitate cycling on Lck

Since receptor stimulation has been shown to increase palmitate turnover on various proteins including G-protein subunits and G-protein coupled receptors[53-55] and palmitoylation of Lck is crucial for T-cell activation[38, 122, 123], we asked whether T-cell activation affects palmitate cycling on Lck. We utilized pervandate (PV), a phosphatase inhibitor, since it has been shown to trigger an activation response similar to that of TCR cross-linking[124]. Anti-phosphotyrosine immunoblots revealed substantial increase in protein phosphorylation upon PV-treatment (Fig. 2.10) and mobility shift of Lck due to phosphorylation was also evident from anti-Lck blots and in-gel fluorescence scans (Fig. 2.10).

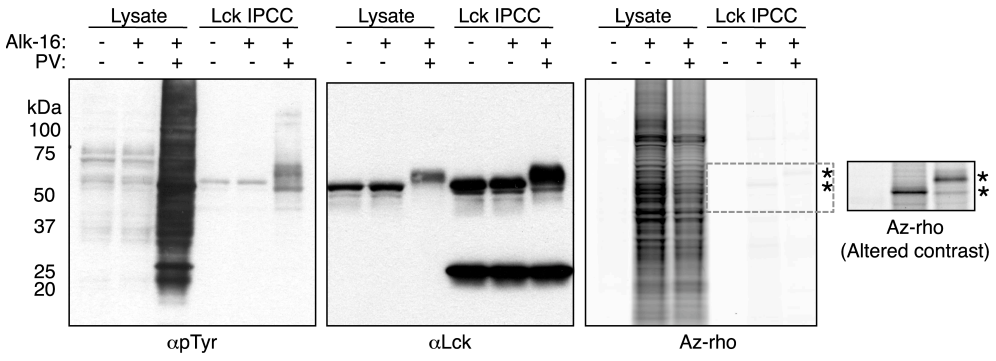

Figure 2.10 | Pervanadate stimulation of Jurkat T-cells increases protein phosphorylation and alters Lck electrophoretic mobility. Analysis of phosphoproteins and Lck electrophoretic mobility in cells with or without pervanadate (PV) treatment. IPCC, immunoprecipitation-click chemistry.

PV treatment resulted in 2-3 fold increase in palmitate cycling on Lck ($t_{1/2}$ ~15 min) that was reproduced over several experiments (n = 7) (Fig. 2.11a), suggesting T-cell activation increases dynamic palmitoylation of Lck. The increase in alk-16 signal at later time points suggest recycling of alk-16 from cellular palmitoyl-CoA pools, which has been attributed to the discrepancy of palmitate half-life measurements obtained in pulse chase experiments and imaging studies. Palmitate half-life measurements based on pulse-chase experiments are in the order of minutes or hours and are often inconsistent with rapid physiological responses that can occur on the seconds time scale. Photo-activation/ bleaching of palmitoylated proteins fused to fluorescent proteins estimate protein-bound palmitate to turnover in milliseconds or seconds[22, 24], but these experiments only measure the protein trafficking and do not the directly evaluate the lipidation state of the protein.

We initially performed 2 hr pulses of the az-12 and alk-16 chemical reporters to compare our results with reported ^{3}H-palmitate pulse-chase studies[109]. To address the effects presented by recycling analog pools, we repeated the experiments with a shorter pulse time (30 min) prior to chasing with excess palmitate, which has been demonstrated to minimize recycling of substrates in pulse-chase studies[125]. The absolute fluorescence intensities observed for both az-12 and alk-16 were lower overall but they remained in the linear range. Consistent with less recycling of alk-16, shorter pulses yielded a faster palmitate half-life of ~30 min on Lck compared to the ~50 min obtained with longer 2 hr pulses and the normalized alk-16 signal plateaus at a lower level with shorter pulses (Fig. 2.11b). The increase in palmitate turnover on Lck upon PV stimulation, however, persists with shorter pulse times with an estimated half-life of <5 min (Fig. 2.11c). Notably for

PV-treated cells, recovery of alk-16 signal was observed even with a shorter pulse time, which can be attributed to the rapid recycling of alk-16. These results demonstrate our tandem imaging method can reveal rapid rates of palmitate cycling on proteins that are closer to values obtained using fluorescence microscopy and that T-cell stimulation with PV accelerates palmitate cycling on Lck.

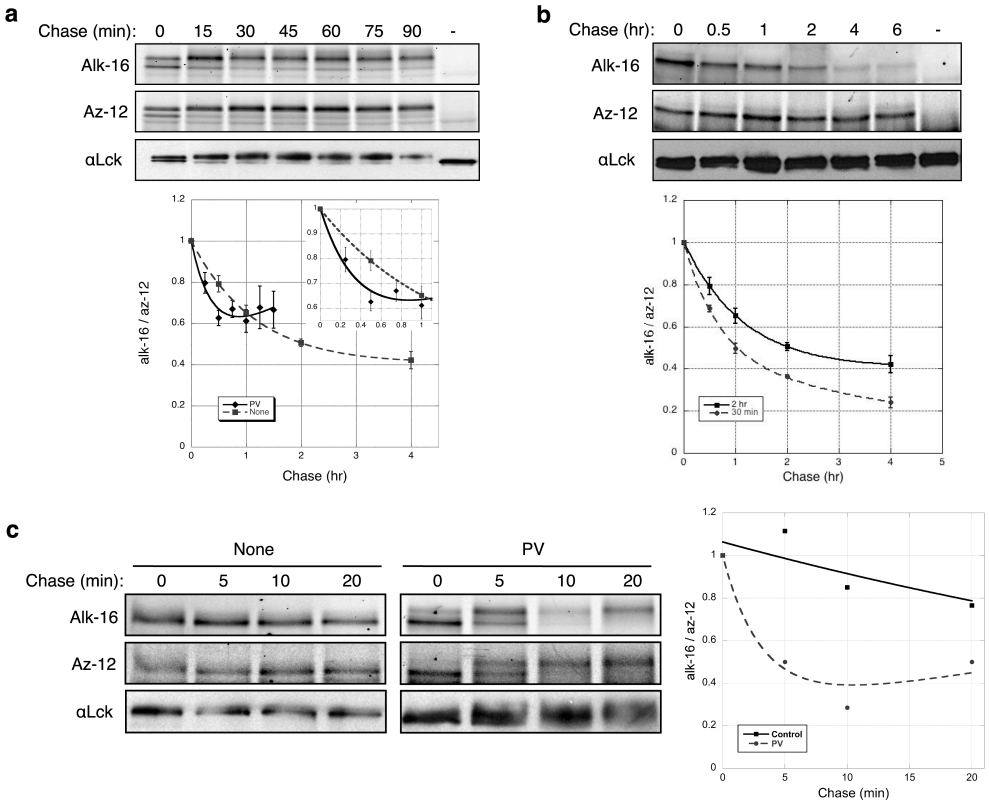

Figure 2.11 | Pervanadate stimulation of Jurkat cells accelerates palmitate cycling on Lck. a, Pulse-chase analysis of Lck in the presence of 0.1 mM pervanadate (PV). PV activation data from multiple pulse-chase experiments (n = 7). Data points from the same chase times, after normalizing alk-16/az-12 signals, were compiled and displayed as average values ± s.e.m. (Inset). **b,** Pulse-chase analysis of Lck upon PV treatment with a shorter pulse time. **c,** PV activation data averaged from two pulse-chase experiments with a shorter pulse time.

Pharmacological perturbation of Lck palmitate cycling

Efforts to identify enzymes that can depalmitoylate proteins have revealed APT1 and PPT1 as candidates[76-78]. Since both enzymes are predicted to be serine hydrolases based on sequence homology and structure studies, we investigated the effect of a broad-spectrum serine hydrolase inhibitor on Lck depalmitoylation. Addition of methyl arachidonyl fluorophosphonate (MAFP) during the chase significantly retarded palmitate turnover on Lck (Fig. 2.12a), suggesting that serine hydrolases that are sensitive towards the reactive fluorophosphonate group of MAFP may contribute to Lck depalmitoylation in T-cells. In contrast, incubation with another broad-spectrum serine hydrolase inhibitor, phenylmethylsulfonyl fluoride (PMSF) had no apparent effect on the initial rate of palmitate removal (Fig. 2.12b). Structural studies suggest that the bulky aromatic group of PMSF sterically hinders its binding to the active site of lipid serine hydrolases such as PPT1[126]. Since PPT1 resides in lysosomal compartments that are not topologically compatible with cytosolic depalmitoylation reactions[79], and APT1 depalmitoylation activity has only been demonstrated for limited substrates, enzyme(s) that deacylate Lck in cells remain unclear. Nonetheless, our results with mechanism-based inhibitors suggest that serine hydrolases with active sites similar to that of PPT1 may contribute to the observed thioesterase activity on Lck.

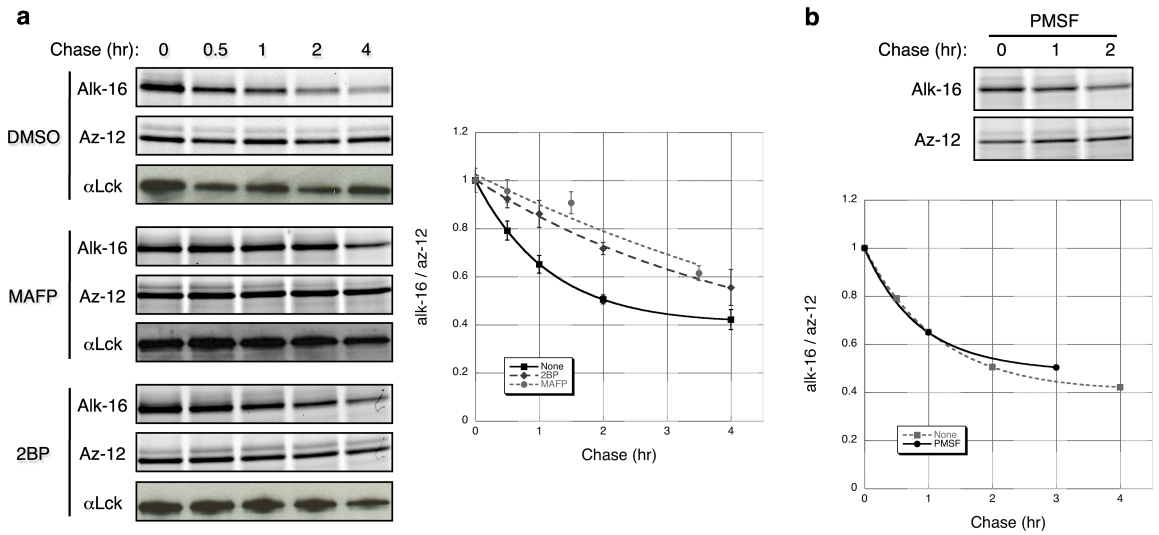

Figure 2.12 | Pharmacological perturbation of palmitate turnover on Lck. a, Pulse-chase analysis of Lck in the presence of chemical inhibitors. Data from multiple pulse-chase experiments (n = 2). Data points from the same chase times, after normalizing alk-16/az-12 signals, were compiled and displayed as average values ± s.e.m. **b,** Pulse-chase analysis of Lck in the presence of PMSF. Data from pulse-chase experiment after normalizing alk-16/az-12 signals compared to chase conditions without chemical inhibitors.

We also assessed the effect of 2-bromopalmitate (2BP), a PAT inhibitor commonly used to block protein palmitoylation[30, 127]. Interestingly, 2BP also decreased Lck depalmitoylation rate (Fig. 2.12a). The actual targets of 2BP in cells are unknown and several enzymes have been suggested to interact with 2BP[128]. It is possible that 2BP, which harbors a reactive α -bromo-carboxyl functional group poised for nucleophilic attack, might also inhibit putative thioesterases. This raises concerns over the use of 2BP as a specific PAT inhibitor in cells and subsequent interpretation of the data. Collectively, these experiments demonstrate that such a dual detection method can be used to evaluate effects of chemical inhibitors on palmitate turnover. Development of more specific

inhibitors using this assay should facilitate discovery and characterization of cellular factors that perturb palmitate turnover in cells.

Tandem imaging method can be generalized to include alternative chemical reporters

To evaluate the utility of our tandem imaging method beyond *N*-myristoylated proteins, we employed a general chemical reporter of protein synthesis. Azidohomoalanine (AHA, Fig. 2.13a), a well-described azide-bearing methionine surrogate shown to label newly synthesized proteins with no observed toxicity, is an attractive alternative[129, 130]. We used an HA-tagged H-Ras^{G12V} construct to analyze another class of *S*-palmitoylated proteins. In-gel fluorescence analysis of purified HA-tagged H-Ras^{G12V} expressed in HeLa cells that were metabolically labeled with alk-16 and AHA showed incorporation and orthogonal detection of both chemical reporters (Fig. 2.13b).

We then compared our tandem imaging pulse-chase data with reported radioactive studies of H-Ras variants[131]. Palmitate removal rates on oncogenic H-Ras isoforms have been experimentally shown to be ~1 hr[131]. Pulse-chase analysis revealed significantly faster chase kinetics for alk-16 than AHA, demonstrating dynamic *S*-palmitoylation and minimal turnover of H-Ras^{G12V} in the time points analyzed (Fig. 13b, c). The HA-tagged H-Ras^{G12V} construct appeared as doublets by Cyfur fluorescence and anti-HA western blot, but only the upper band is modified by alk-16 as observed with az-rho fluorescence, suggesting the slower migrating polypeptide is the lipid-modified isoform of H-Ras^{G12V} under these conditions. Average Cyfur fluorescence across both H-Ras^{G12V} isoforms was used for data normalization since both exhibited similar turnover rates. The palmitate

half-life on H-Ras^{G12V} was calculated to be ~50 min using our tandem imaging method over several experiments (n = 5) (Fig. 2.13b). This is consistent with the reported experimental palmitate turnover rates of other oncogenic H-Ras variants[131]. Based upon these experimental rates of palmitate cycling and GTP-binding measurements, the calculated palmitate half-life of fully GTP-bound H-Ras is less than 10 min. The combined use of alk-16 with AHA should enable tandem fluorescence imaging of palmitate turnover on any *S*-acylated protein. Given its modularity and the wide spectrum of chemical reporters currently available[132], this tandem imaging approach can be readily adapted to study other dynamic protein modifications.

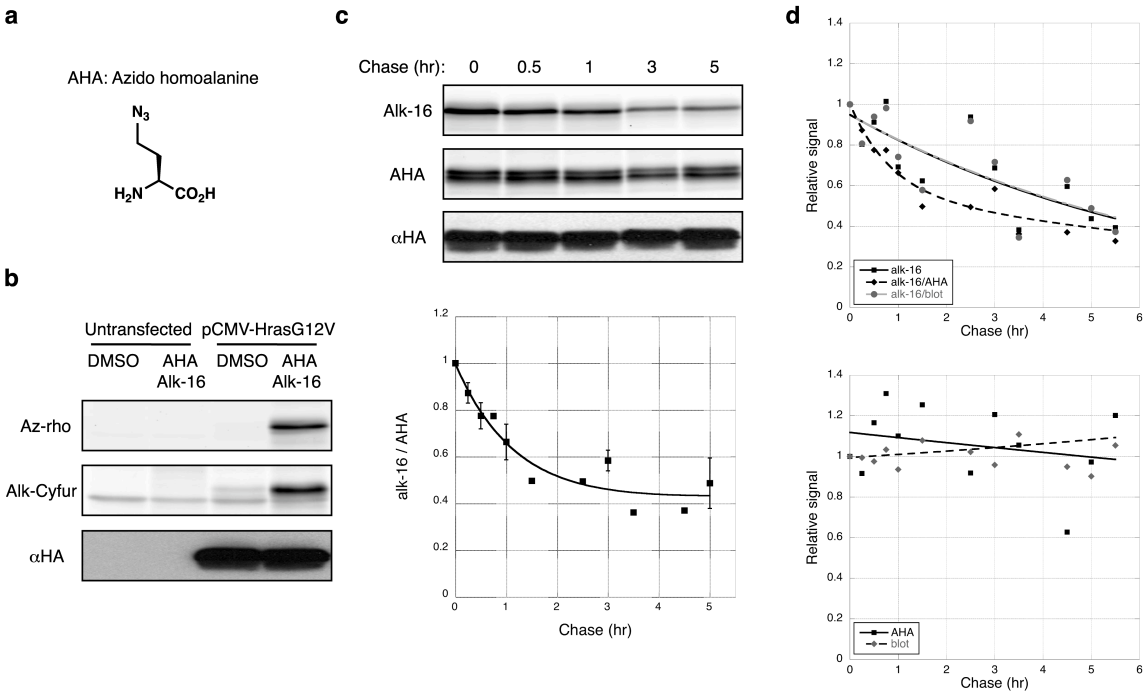

Figure 2.13 | Use of a general protein synthesis chemical reporter extends the tandem imaging method beyond *N*-myristoylated proteins. a, Amino acid chemical reporter for protein synthesis. **b,** Tandem detection of AHA and alk-16 on H-Ras^{G12V} in transfected HeLa cells. Western blot is probed for the N-terminal HA epitope on H-Ras^{G12V}. **c,** Pulse-Chase analysis of H-Ras^{G12V} with AHA and alk-16. Data from multiple pulse-chase experiments (n = 5). Data points from the same chase times, after normalizing alk-16/AHA signals, were compiled and displayed as average values ± s.e.m. **d,** Plots of relative signals for alk-16, AHA fluorescence and anti-HA blot intensities in the pulse-pulse-chase experiments.

Summary and Discussion

In this chapter, we have expanded the chemical toolbox for monitoring two major forms of protein fatty-acylation, *N*-myristoylation and *S*-palmitoylation, in mammalian cells. First, we established that fatty acid chemical reporters, combined with improved bioorthogonal labeling conditions using CuAAC, enables specific and sensitive fluorescent detection of protein myristoylation and palmitoylation. We further extended this approach to enable tandem fluorescent detection of two protein modifications on proteins of interest and showed that this tandem imaging method can be used to efficiently monitor dynamic protein palmitoylation in cells.

I have shown that sensitivity of the bioorthogonal labeling approach enables robust detection of endogenously expressed fatty-acylated proteins within minutes after gel electrophoresis compared to days or weeks with radioactive analogues. Furthermore, in-gel fluorescence detection of fatty-acylated proteins circumvents the need to transfer proteins onto membranes for immunoblotting, which can be problematic for hydrophobic polypeptides, and thus provides a more direct and quantitative means to detect protein fatty-acylation as well as measure palmitoylation dynamics in cells. These significant improvements in the detection of protein fatty-acylation offer new opportunities to interrogate the functions and regulatory mechanisms of protein fatty-acylation, in physiology and disease.

There are caveats to the bioorthogonal labeling approach described in this chapter. First, it is likely that the fatty acid chemical reporters might be metabolized into longer or shorter fatty acids such as acetate and be non-specifically installed onto proteins. While

this is not evident from the fact that the myristate and palmitate analogs preferentially label myristoylated and palmitoylated proteins respectively and do not label p53, an acetylated protein (see Fig. 2.4), crosstalk between different fatty acid pools in the cell can be reduced by minimizing metabolic labeling times. Second, most likely due to low incorporation efficiency of the AHA methionine surrogate into proteins cells, we were unable to detect AHA labeling of endogenous proteins and detection was possible only upon overexpression. As a result, non-myristoylated proteins like H-Ras will have to be overexpressed for us to measure palmitate turnover rates using the tandem detection method (see Fig. 2.13). This problem may be circumvented by the use of other chemical reporters for protein synthesis that are more efficiently incorporated into proteins.

Application of our new tools revealed accelerated palmitate cycling of Lck upon T-cell stimulation, which raises several interesting questions. Studies demonstrate that Lck palmitoylation is required for proper T-cell activation by targeting Lck to the plasma membrane and maintaining its lipid raft association[122, 123]. Nonetheless, the physiological consequences of increased palmitate cycling rate during cellular stimulation is unclear. Live cell imaging studies suggest that Lck is dynamically recruited and distributed to the periphery of immunological synapses during cellular activation[33]. It is therefore possible that increased palmitate turnover upon T-cell activation serves to limit the proportion of raft-associated Lck and its access to downstream substrates or activators. Notably, accelerated palmitate turnover upon cellular stimulation have also been observed for other proteins including G-protein coupled receptors and neuronal scaffold PSD95[39, 53-55], although how palmitate cycling on these proteins is modulated to be determined. For Lck,

it is possible that protein thioesterase activity is stimulated by downstream effects of TCR signaling such as release of calcium from intracellular stores in the ER. Alternatively, activated and phosphorylated Lck may assume a conformational change favorable towards spontaneous or enzymatic deacylation. Since protein thioesterases with depalmitoylating activity towards Lck are yet to be identified, mechanistic insights into the regulation of activity-induced palmitate turnover remain elusive.

To understand basic control mechanisms of protein palmitoylation, I was motivated to use the genetically amendable fission yeast as a model because of its relatively simple palmitoylation machinery compared to metazoans. This transition to fission yeast will be further developed in the next chapter.

Materials and Methods

Cell culture growth. Jurkat (human T-cell lymphoma) cells were propagated in RMPI 1640 supplemented with 10% fetal bovine serum, 100 U/mL penicillin and 100 μg/mL streptomycin in a humidified CO_2 incubator at 37 °C. Cell densities were maintained between 1 x 10^5 and 2 x 10^6 cells per mL. HeLa cells were cultured in DMEM, supplemented with 10% fetal bovine serum (FBS), 100 U/mL penicillin with 100 μg/mL streptomycin and maintained in a humidified 37 °C incubator with 5% CO_2.

Transfection of wild type, G2A, C3,6S Fyn constructs and HA-tagged H-Ras^{G12V}. For transfection studies, HeLa cells were grown in a 10 cm culture plate supplemented with DMEM containing 10% fetal bovine serum in a humidified CO_2 incubator to approximately 90% confluence before transfection with 12-15 μ g of DNA using Lipofectamine 2000 (Invitrogen). The human Fyn constructs, wild-type and mutant Fyn cDNAs cloned into eukaryotic expression vector pCMV5 as well as N-terminal HA-tagged H-Ras^{G12V} (PCNC10) construct were kindly provided by Dr. Marilyn Resh (Memorial Sloan-Kettering Cancer Center). Cells were transfected about 16 hours prior to metabolic or pulse-chase labeling.

Metabolic labeling with fatty acid chemical reporters. Jurkat and HeLa cells were treated for 2 hours with 20 μM az-12, az-15, alk-12, alk-14 or alk-16 (50 mM DMSO stock solutions) using the corresponding media for the respective cell types in the humidified CO_2 incubator at 37 °C. The same volume of DMSO was used in the negative

control. Following metabolic labeling, cells were harvested, washed once with ice-cold PBS and pelleted at 1000 *g* for 5 min. Cells were directly lysed or flash frozen in liquid nitrogen and stored at -80 °C prior to lysis. No significant loss of signal was observed for frozen cell pellets.

Pulse-Chase labeling. Jurkat T-cells were labeled with 20 μM az-12 and 20 μM alk-16 in RMPI 1640 supplemented with 2% charcoal-filtered fetal bovine serum, 100 U/mL penicillin and 100 μg/mL streptomycin. For H-Ras studies, transfected HeLa cells were incubated with 1 mM azidohomoalanine (AHA) and 20 μM alk-16 in methonine-free DMEM (Invitrogen) supplemented with 2% charcoal-filtered fetal bovine serum. The same volume of DMSO was used in the negative controls. After 2 hours or 30 minutes incubation, the labeled cells were chased with pre-warmed RMPI 1640 or DMEM containing 200 μM palmitate, 10% fetal bovine serum and/or 100 U/mL penicillin and 100 μg/mL. 100 μM 2-bromopalmitate (2BP) (Fluka), 20 μM (MAFP) (Sigma) or 200 μM phenylmethylsulfonyl fluoride (PMSF) were added to the chase medium to investigate the effects of small molecule inhibitors on palmitate turnover. To determine palmitate turnover upon T-cell activation, 100 mM pervanadate, freshly prepared by dissolving sodium orthovanadate in 300 mM H_2O_2, was added to the chase medium for a final pervanadate concentration of 0.1 mM. Samples were taken at various time points during the chase, washed once with PBS and flash frozen in liquid nitrogen and stored at -80 °C prior to lysis.

Preparation of cell lysates. Frozen Jurkat or HeLa cell pellets were lysed in chilled Brij lysis buffer (1% Brij-97, 150 mM NaCl, 50 mM triethanolamine pH 7.4, 10× Roche EDTA-free protease inhibitor cocktail, 10 mM PMSF) with vigorous vortexing (3 x 20 s), placing tubes on ice during intervals to avoid heating of samples. For analysis of protein phosphorylation after T-cell stimulation, 1:50 dilution of phosphatase inhibitor cocktail 2 (Sigma) was included in the lysis buffer. Lysates were spun at 1,000 g for 5 minutes at room temperature to remove cellular debris. Typical lysate concentrations of 4-8 mg/ml were obtained, as quantified using the BCA assay (Pierce).

Lysate CuAAC / click chemistry. Cell lysates (50 μg) in 44.5 μL RIPA lysis buffer were reacted with 5.5 μL freshly premixed click chemistry reaction cocktail [azido- or alkynyl-detection tag (100 μM, 5 mM stock solution in DMSO), tris(2-carboxyethyl)phosphine hydrochloride (TCEP) (1 mM, 50 mM freshly prepared stock solution in deionized water), tris[(1-benzyl-1*H*-1,2,3-triazol-4-yl)methyl]amine (TBTA) (100 μM, 2 mM stock solution in 1:4 DMSO:t-butanol) and $CuSO_4 \cdot 5H_2O$ (1 mM, 50 mM freshly prepared stock solution in deionized water)] for a total reaction volume of 50 μL for 1 h at room temperature. The reactions were terminated by the addition of ice-cold methanol (1 mL), placed at −80 °C overnight and centrifuged at 18000*g* for 10 min at 4 °C to precipitate proteins. The supernatant from the samples was discarded. The protein pellets were allowed to air-dry for 10 min, resuspended in 25 μL of SDS buffer (4% SDS, 50 mM triethanolamine pH 7.4, 150 mM NaCl). 8.7 μL 4×LDS sample buffer (Invitrogen) and 1.3 μL 2-mercaptoethanol were then added and the samples were heated for 5 min at 95

°C; 20 μL of the sample was loaded per gel lane for separation by SDS-PAGE (4−20% Bio-Rad Criterion Tris-HCl gel).

Immunoprecipitation-CuAAC. LAT, Lck and Ras proteins were immunoprecipitated from 200 μg Jurkat cell lysate using the following antibodies at recommended concentrations: mouse anti-Lck ($p56^{lck}$) monoclonal (Clone 3A5, Thermo Scientific), rat anti-v-H-ras (Ab-1) monoclonal (Y13-259 agarose conjugate, Calbiochem), and rabbit anti-LAT polyclonal (Upstate). A rabbit anti-Fyn polyclonal (Upstate) was used to immunoprecipitate wild-type and mutant Fyn proteins HeLa cell lysates. Upon incubation at 4 °C for an hour with 25 μL of packed protein A-agarose beads (Roche) with an end-over-end rotator (Barnstead/Thermolyne), the beads were washed three times with ice-cold RIPA lysis buffer (1% Triton X-100, 1% sodium deoxycholate, 0.1% SDS, 10 mM Tris pH 7.4, 150 mM NaCl). The beads were resuspended in 20 μL of resuspension buffer (4% SDS, 50 mM triethanolamine pH 7.4, 150 mM NaCl) and 2.25 μL freshly premixed click chemistry reagents (same as above) were added. After 1 hour at room temperature, the reaction mixture was diluted with 8.7 μL 4× LDS sample buffer and 1.3 μL 2-mercaptoethanol and separated by SDS-PAGE. A separate gel was loaded for Western blot analysis.

Sequential on-bead CuAAC. Lck and Fyn proteins were immunoprecipitated from 0.6-1 mg of Jurkat cell lysate using antibodies described above. For HA-tagged H-Ras^{G12V} immunoprecipitation, 15 μL of anti-HA beads (Monoclonal anti-HA agarose conjugate,

clone HA-7) was added to 200-300 μg of HeLa cell lysates. After 2 hours incubation on a platform rocker at 4 °C, the beads were washed three times with 1 mL of ice-cold RIPA buffer. The beads were resuspended in 20 μL of PBS and 2.25 μL freshly premixed az-rho click chemistry reaction cocktail described above for a total approximate reaction volume of 25 μL for 1 hour at room temperature. The beads were washed three times with 1mL of ice-cold RIPA buffer and resuspended in 20 μL of SDS buffer. For the second CuAAC reaction, 2.25 μL of freshly premixed click chemistry reagents (alk-Cyfur in place of az-rho) were added. After 1 hour at room temperature, the reaction mixture was diluted with 8.7 μL 4× LDS sample buffer and 1.3 μL 2-mercaptoethanol, heated for 5 min at 95 °C, and 20 μL was loaded per gel lane for separation by SDS-PAGE. A separate gel was loaded for Western blot analysis.

In-gel fluorescence scanning. Proteins separated by SDS-PAGE were visualized by incubating the gel in 40% methanol, 10% acetic acid for at least 1 hour and directly scanning it on a GE healthcare Typhoon 9400 variable mode imager. Rhodamine-associated signal was detected at excitation 532 nm/emission 580 nm while orthogonal detection of Cyfur-associated signal was achieved at excitation 633 nm/emission 670 nm.

In-gel hydroxylamine treatment. After an initial fluorescence scan to determine pretreatment fluorescence, the gel was rinsed with deionized water and soaked in freshly prepared 1 M hydroxylamine (pH 7.4) for 2 hours at room temperature on a shaker. The gel was subsequently rinsed with deionized water and incubated with shaking for 2 hours

in 40% methanol, 10% acetic acid at room temperature prior to scanning for post-treatment fluorescence.

Western blots. Proteins separated by SDS-PAGE were transferred to nitrocellulose membranes (50 mM Tris, 40 mM glycine, 0.0375% SDS, 20% MeOH in deionized water, Bio-Rad Trans-Blot Semi-Dry Cell, 20 V, 40 min), which were blocked with 10% non-fat milk, 5% BSA, 0.1% Tween-20 in PBS (0.1% PBST) and washed with 0.1% PBST before incubation with appropriate antibodies. Membranes were incubated with a mouse anti-Lck ($p56^{Lck}$) monoclonal (Clone 3A5, Invitrogen) followed by light chain-specific HRP-conjugated affiniPure goat anti-mouse secondary (Jackson Immunoresearch Laboratories) for anti-Lck blots. Likewise, anti-Fyn and anti-LAT blots were treated with mouse anti-Fyn monoclonal (S1, Chemicon) and mouse anti-LAT monclonal (2E9, Upstate) respectively and followed by goat anti-mouse HRP-conjugated secondary antibody (Upstate). Anti-HA blots were treated with rabbit anti-HA polyclonal (CloneTech) followed by goat anti-rabbit HRP-conjugated secondary antibody (Upstate). Anti-phosphotyrosine blots were blocked with 5% BSA, 0.1% PBST prior to incubation with HRP-conjugated anti-phosphotyrosine mouse monoclonal (PY99, Santa Cruz). Blots were developed using the enhanced chemiluminescent kit (GE Healthcare).

Image processing and calculations. All images were processed and analyzed using the ImageJ software. A rectangular box was tightly selected around the band(s) of interest and average fluorescence intensity at mid-length of the box was measured. Dimensions of the box were maintained within the same experiment. No event of signal saturation was observed in this study. Background signal from non-specific labeling was removed by subtracting measurements of the DMSO sample from each of the data points. The ratio of background-corrected alk-16 to az-12 associated fluorescent signals accounted for protein load and turnover at each time point of a pulse-chase analysis. To allow comparison between pulse-chase experiments, alk-16/az-12 values within each dataset were normalized such that alk-16/az-12=1 at T=0 hours, which was defined as the earliest of three consecutive time points during which a decrease of alk-16/az-12 was initially observed. Since values obtained under some conditions tested did not form a straight line when plotted on a logarithmic scale, which was observed by others (50), data for each protein or chase condition was fitted to a two-phase exponential decay model using the KaleidaGraph graphing and data analysis software. The equation used was a biphasic exponential decay line m1*exp(-m2*m0)+m3*exp(-m4*m0), which starts at m1+m3 and decays with rate constants m2 and m4. The half-life of protein-bound palmitate ($t_{1/2}$) was defined as the length time required for the normalized alk-16/az-12 signal to decrease halve if decay was to occur solely at the initial rate, which is ln(2)/m2 with m1=0.5.

CHAPTER 3

RHEOSTATIC CONTROL OF PROTEIN PALMITOYLATION REGULATES MEIOTIC COMMITMENT IN FISSION YEAST

Introduction

With advancements in biochemical methods for the detection and identification of palmitoylated proteins, including those described in Chapter 2, it is evident that reversible protein palmitoylation is subjected to regulation *in vivo* at the level of individual proteins as well as the level of the palmitoylomes. Changes in the protein palmitoylation states and in the repertoire of modified proteins associated with different physiological states[11, 39, 54, 56] hint at the potential of this lipid modification to be a major cellular regulator akin to phosphorylation. Nonetheless, little is known of about how these changes are coordinated with physiological states and how they affect cellular function.

The family of DHHC-containing PATs is known to be responsible for most protein palmitoylation events and genes encoding PATs are found in all eukaryotes, ranging from a handful in unicellular fungi to more than twenty in metazoa (Fig. 3.1a, b). The multiple PATs in an organism raises intriguing questions about substrate specificity and regulation. Specific PATs were found to have different subcellular locations and tissue-specific distribution[70, 71], suggesting the possibility that PATs play diverse roles in cells. Nonetheless, understanding their roles in regulating global palmitoylation and cellular physiology has been difficult due to extensive biochemical and functional overlap among multiple PATs[12, 67-69].

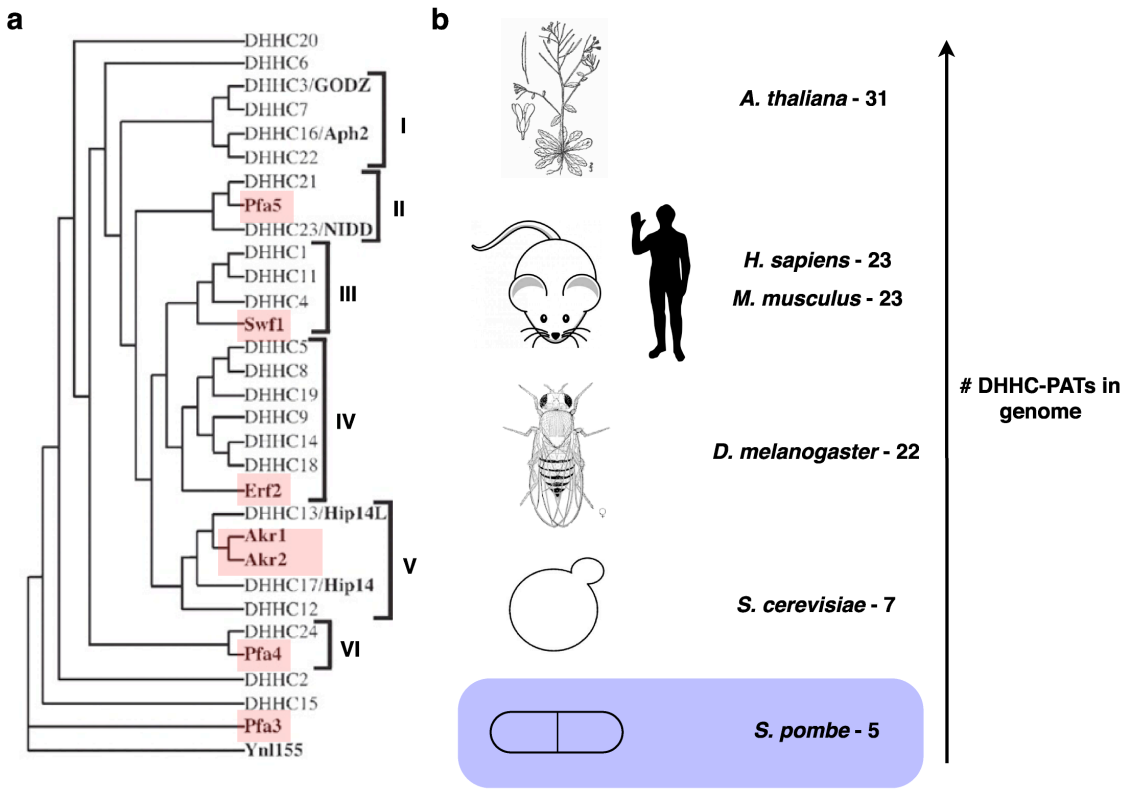

Figure 3.1 | Model organisms used for PAT studies. a, Phylogenetic clustering of human and *S. cerevisiae* (Red) DHHC-containing PATs based on ClustalX alignment of the 51 amino acid DHHC core sequence. Six potential subfamilies (I-VI) are indicated by brackets. Adapted from Mitchell et al.[133] **b,** Model organisms used in PAT studies and the number of DHHC-containing PATs encoded in each genome. Blue: *S. pombe* PATs have not been studied.

I chose to work in the fission yeast *Schizosaccharomyces pombe* because of its simple palmitoylation machinery compared to other model organisms that are traditionally used in PAT studies (Fig. 3.1b). Like the budding yeast *Saccharomyces cerevisiae, S. pombe* is genetically amendable and has proven to be a useful model for fundamental principles and mechanisms such as cell cycle control, genome organization and signal transduction. Although studies of *S. pombe* PATs have not been reported, its simple PAT network should facilitate the functional dissection of individual PATs. A study

on compartmentalized Ras signaling provided further motivation to move into fission yeast. Onken et al. showed that the only Ras protein in *S. pombe*, Ras1, controls cell morphology and mating depending on its subcellular location, which in turn depends on its palmitoylation state[28]. The combination of a simple PAT network and a highly conserved protein substrate with distinct palmitoylation-dependent outputs that are easily scored make *S. pombe* an attractive model to study basic control mechanisms of protein palmitoylation.

In this chapter, I showed that the chemical tools that we have previously developed in mammalian cells also works in fission yeast. Combining chemical and genetic approaches, I showed that physiological control of PAT levels underlies differential modification of its cognate substrates in distinct cellular states, shaping the palmitoylome, which in turn plays a critical role in meiotic commitment. Based on these results, I propose that rheostatic control of single or multiple PAT activities quantitatively regulates global protein palmitoylation, which can have important consequences on cellular events.

Results

S. pombe has a simplified PAT network

In contrast to metazoa and budding yeast, where high functional redundancy among multiple PATs has been reported[68, 69], the fission yeast genome contains only five open reading frames that encode proteins containing the conserved DHHC motif preceded by a cysteine-rich domain, which is a characteristic feature of PATs (Fig. 3.2a). This less complex PAT network allows me to more easily dissect the functional contribution and regulation of individual PATs.

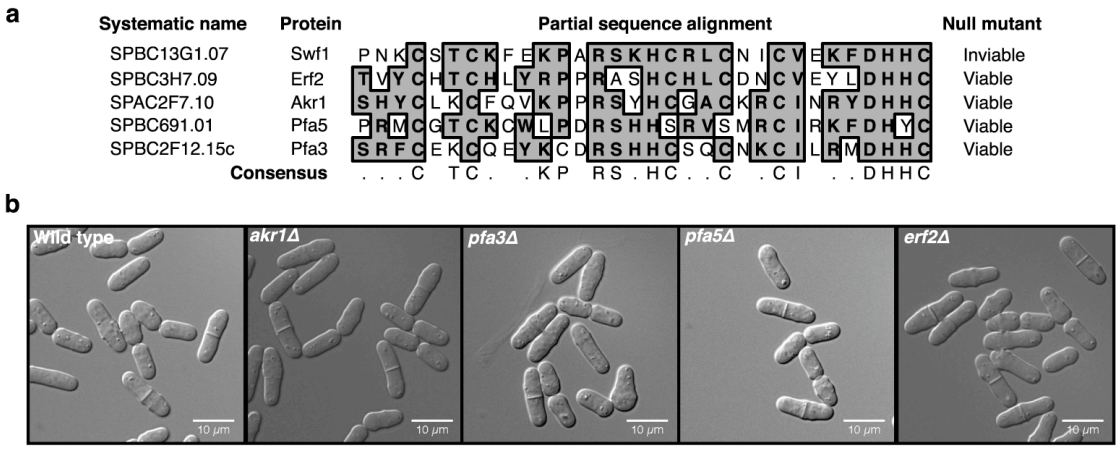

Strain	Length at division (μm)	Generation time (min)
Wild type	14.4 ± 1.0	125
akr1Δ	14.9 ± 0.7	130
pfa3Δ	15.1 ± 0.8	130
pfa5Δ	14.7 ± 0.9	127
erf2Δ	15.8 ± 0.9	131

Figure 3.2 | DHHC-PATs in *S. pombe.* a, Partial sequence alignments and consensus sequence of the five DHHC-containing PATs encoded in the *S. pombe* genome. Viability of null mutants are also indicated. **b,** Growth and morphological phenotypes of cells with individual PAT deletions. Notably, *erf2*Δ and *erf4*Δ cells are viable at 32 °C and 34 °C but inviable at 36 °C. DIC images (Top panel) as well as measurements of cell lengths (n=20) at division and generation times (Bottom panel) of indicated strains.

Of the five PATs, only Swf1 was essential for viability[134] while deletions of the remaining PATs had no effect on cell growth or morphology under exponential vegetative growth conditions at 32 °C. (Fig. 3.2). Notably, *erf2*Δ and *erf4*Δ cells are inviable at 36 °C. I focused on the Erf2 PAT and its accessory protein Erf4, whose roles in meiosis are suggested by their strongly regulated expression during this major transitional event in fission yeast[135, 136]. This system, where PAT regulation is linked to a highly coordinated biological process, provides a good model to study how regulation of PATs affects global protein palmitoylation and its functional consequences.

Erf2 PAT function regulates meiosis in S. pombe

Fission yeast cells proliferate in the haploid state but when nutrients become limiting, cells of opposite mating types conjugate to form a diploid zygote. These diploid cells replicate their genome and then undergo two successive nuclear divisions to yield four haploid nuclei that mature into spores, completing meiosis (Fig. 3.3a). To specifically investigate a potential role for Erf2 in meiosis as well as circumvent the mating defect of haploid *erf2Δ* cells (Fig. 3.6c), I constructed stable diploids containing a temperature-sensitive allele of the Pat1 meiotic repressor, *pat1-114*, which can be used to synchronously induce meiosis[137-139] (Fig 3.4a). Consistent with genome-wide expression studies[135, 136], transcript levels of *erf2* and *erf4* were significantly upregulated in synchronized meiotic cells compared to vegetative cells (Fig. 3.3b). Expression of *erf2* and *erf4* was also induced by overproduction of the meiosis-specific Mei4 transcription factor (Fig. 3.3c). Compared to *erf2*$^{+}$ cells, *erf2Δ* mutants were delayed in meiotic entry,

as determined by the onset of S phase (Fig. 3.4b), and in meiotic progression (Fig. 3.4c, d). The striking increase in the length of *erf2Δ* cells suggests that they continued vegetative growth during this delay (Fig. 3.4d). Taken together, these observations indicate a role for Erf2 in regulating meiotic entry, suggesting that changes in global protein palmitoylation are critical determinants in meiotic commitment.

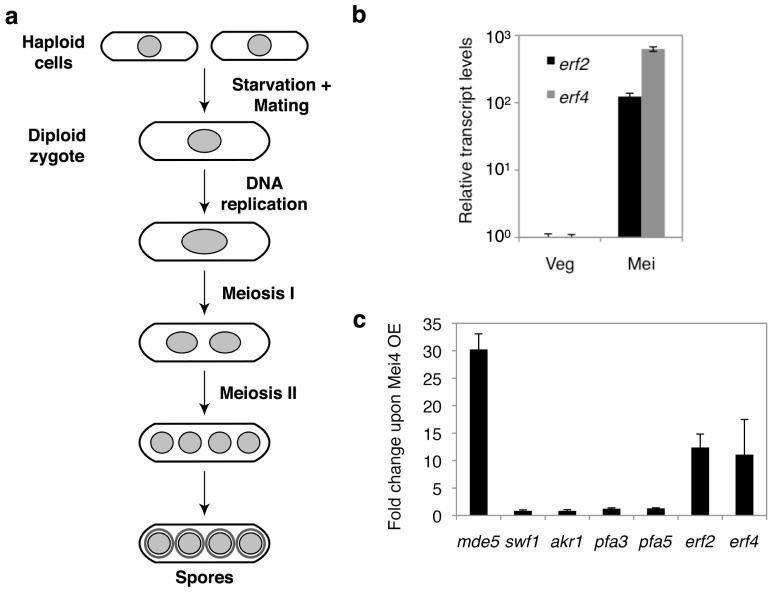

Figure 3.3 | *erf2* and *erf4* expression are strongly regulated during meiosis in fission yeast. a, Schematic representation of the fission yeast sexual differentiation process. Haploid cells conjugate to form a diploid zygote, which undergoes meiosis to yield four haploid nuclei that matures into spores. **b,** qPCR analysis of *erf2* and *erf4* transcripts in vegetative (Veg) and meiotic (Mei, 8 h after meiotic induction) *pat1-114/pat1-11*4 cells. **c,** qPCR analysis of indicated transcripts in vegetative haploid cells overexpressing (OE) Mei4 from a thiamine-repressible promoter. Fold change, transcript levels after 24 hours in thiamine-free medium compared to that in thiamine-containing medium. *mde5* is a known Mei4 target gene. **b, c,** All transcript levels were normalized to *act1* mRNA. Error bars, s.d.

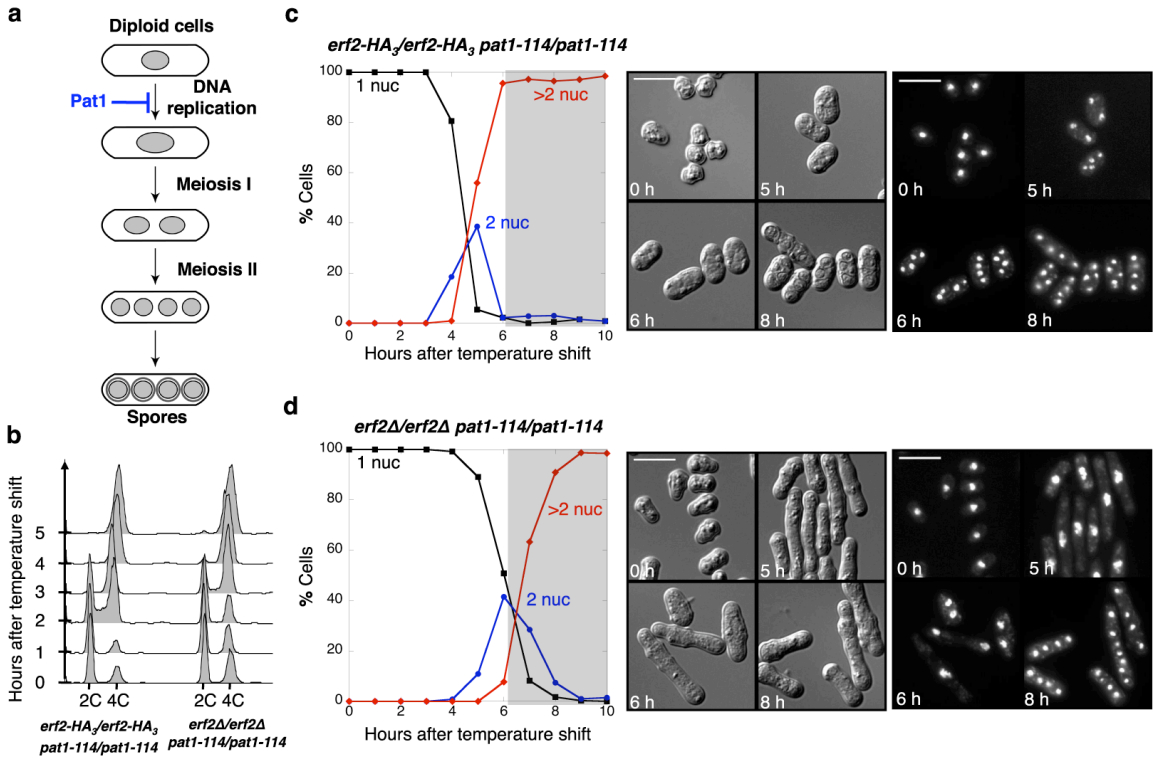

Figure 3.4 | *erf2Δ* cells are delayed in meiotic entry. a, Pat1 is repressor of meiosis. Synchronous meiosis in diploid *pat1-114/pat1-114* cells was induced by shifting nitrogen-starved cultures to restrictive temperature (see Methods). **b,** DNA content analysis of indicated strains after meiotic induction. **c, d,** Percentage of cells with 1, 2 or >2 nuclei were determined by counting ≥ 200 DAPI-stained cells of the indicated strains at hourly intervals after meiotic induction (left panel). Shaded area facilitates comparison between the two strains. Representative DIC (middle panel) and DAPI (right panel) images of cells at indicated times after temperature shift. Scale bars, 10 μm.

Chemical tools also work in fission yeast

To assess Erf2-dependent modulation of the palmitoylome during meiosis, we employed the alkyne-functionalized palmitate chemical reporter described in Chapter 2, alk-16[140], together with bioorthogonal labeling (Fig. 3.5a), which allows superior fluorescent detection of the modification compared to conventional radiolabeled lipids in mammalian and yeast cells (Fig. 3.5b-d). This bipartite bioorthogonal labeling approach enabled robust visualization of global and individual palmitoylated proteins such as Ras1 without overexpression (Fig. 3.5b). Alk-16 labeling of Ras1 was competed away by palmitic acid in a dose-dependent manner (Fig. 3.5c). Additionally, preincubating cells with broad-spectrum palmitoylation inhibitor 2-bromopalmitate or post-CuAAC cleavage of thioesters with hydroxylamine greatly diminished the fluorescence signal observed for Ras1 (Fig. 3.5d). In contrast, pretreating cells with protein synthesis inhibitor cycloheximide had minimal effect on Ras1 labeling (Fig. 3.5d). Collectively, these experiments established alk-16 as a specific and robust reporter for post-translational protein *S*-palmitoylation in fission yeast at endogenous substrate and enzyme concentrations.

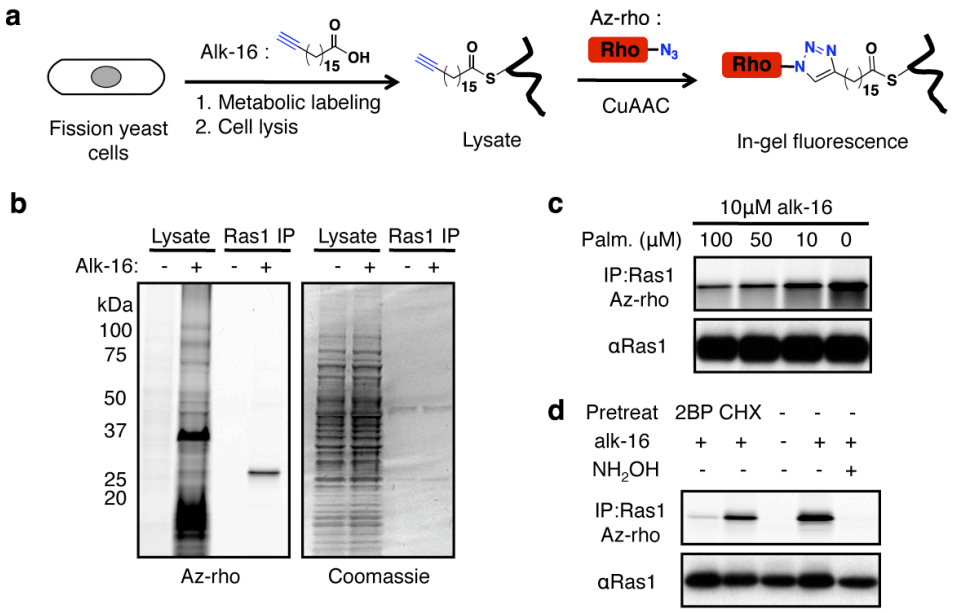

Figure 3.5 | Chemical tools work in fission yeast. a, Schematic representation of the bioorthogonal detection protocol. Alk-16: alkyne-functionalized palmitate reporter. Az-rho: azide-functionalized rhodamine fluorophore. CuAAC: copper-catalyzed azide-alkyne cycloaddition. **b,** In-gel fluorescent detection of alk-16 labeled proteins in lysates and immunopurified Ras1. **c, d,** Fluorescent detection of immunopurified Ras1, a known palmitoylated protein, from alk-16 labeled cells (top panels). Western blots are probed for Ras1 (bottom panels). Palmitate (Palm) competes with alk-16 labeling in a dose-dependent manner. Ras1 fluorescence signal was greatly diminished by preincubating cells with a general palmitoylation inhibitor 2-bromopalmitate (2BP) or by post-CuAAC cleavage of palmitoylation thioester linkages with hydroxylamine (NH_2OH). Pretreatment of cells with the protein synthesis inhibitor cycloheximide (CHX) had little effect on post-translational Ras1 labeling by alk-16.

Ras1 is a substrate of the Erf2-Erf4 PAT complex

Using this system, I showed that the Erf2-Erf4 PAT complex and not two of the other putative PATs is required for the incorporation of alk-16 onto Ras1 (Fig. 3.6a), a known palmitoylated protein whose modification has been implicated in pheromone signaling[28]. Incorporation of alk-16 directly requires Erf2 PAT activity as re-introduction of Erf2, but not a catalytically inactive DHHC→DHHA mutant[58, 62], rescued the Ras1 palmitoylation defect in *erf2*Δ cells (Fig. 3.6b). Since palmitoylation of Ras1 has been implicated in pheromone signaling[28], these observations are consistent with the mating defect of *erf2*Δ cells (Fig. 3.6c). Akr1 may substitute for Erf2 function since deletion of *akr1* in an *erf2Δ* background further decreased mating efficiency although no mating defect was observed for *akr1Δ* cells. This is not surprising given the redundancy between the multiple budding yeast and mammalian PATs[68, 69]. Collectively, these experiments demonstrate that Erf2-Erf4 is able to specifically incorporate alk-16 into its substrates and that this method can be used to profile Erf2 substrates.

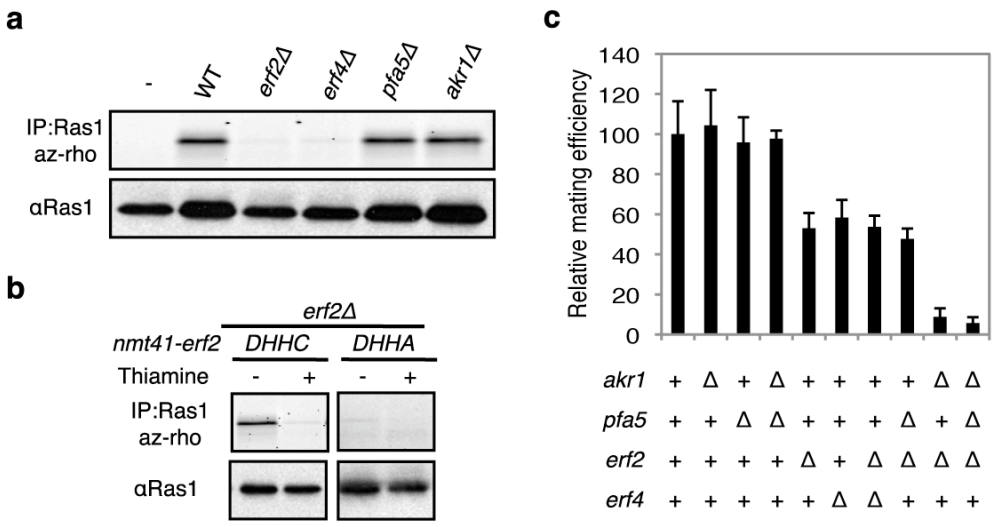

Figure 3.6 | Ras1 is a substrate of the Erf2-Erf4 PAT complex. a, b, Alk-16-associated fluorescence of immunopurified Ras1 from cells with the indicated PAT deletions (top panels). Western blots are probed for Ras1 (bottom panels). Wild type (*DHHC*) or catalytic inactive (*DHHA*) Erf2 was expressed from a thiamine-repressible promoter in *erf2*Δ cells. **c,** *erf2*Δ and *erf4*Δ cells are defective in mating. Mating efficiency is quantified as the percentage of diploid zygotes/spore-containing asci after 2 days in nitrogen-free medium normalized to wild type (n≥200). Error bars, s.d.

Erf2 drives changes in the palmitoylome during meiosis

The significantly elevated *erf2* transcript levels in meiotic cells and the phenotypes of *erf2*Δ cells support its role in orchestrating meiosis-specific protein palmitoylation (Fig. 3.3). To determine whether increased *erf2* expression alone has an impact on the meiotic palmitoylome, I profiled palmitoylated proteins by in-gel fluorescence in diploid cells undergoing synchronous meiosis. A distinct meiotic palmitoylome with a prominent band at approximately 23 kDa is established following the striking increase in Erf2 protein levels (Fig. 3.7a), which reflects the reported *erf2* transcription profile during meiosis[135, 136]. This specific palmitoylome requires Erf2 activity, as modification of those prominent substrates was not observed in either *erf2*Δ or *erf4*Δ cells undergoing meiosis (Fig. 3.7b, c). Ras1 was also palmitoylated in an Erf2-Erf4 dependent manner in meiotic cells (Fig. 3.7c, lower panel), suggesting a role for Ras1 in meiosis[141]. Since the salient features of the meiotic palmitoylome were still observed when two of the other putative PATs are deleted (Fig. 3.7c), I concluded that Erf2 is the primary PAT driving changes in the protein palmitoylation during meiosis.

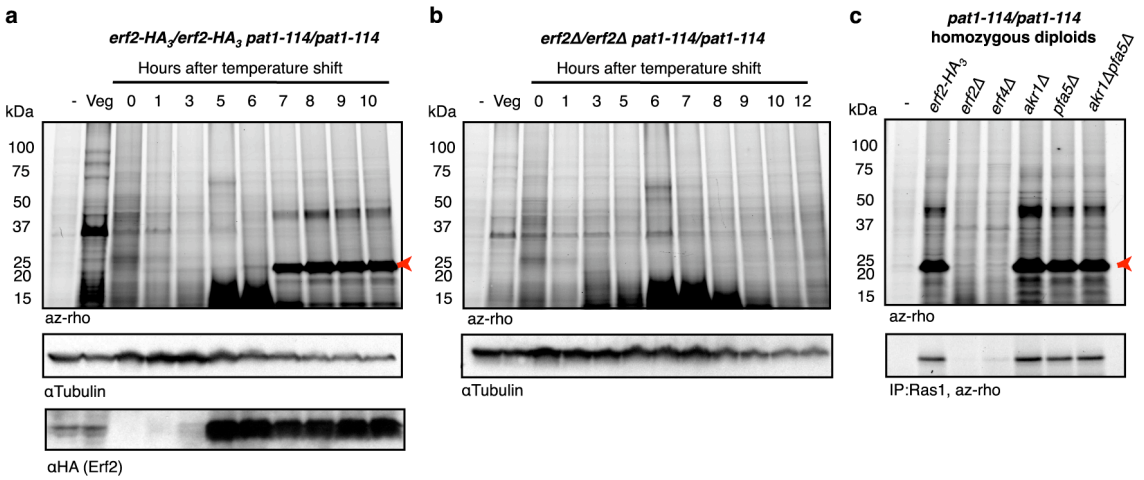

Figure 3.7 | The Erf2-Erf4 PAT is required for meiotic-specific protein palmitoylation. a, b, Fluorescence profiles of palmitoylated substrates in *erf2-HA₃/erf2-HA₃ pat1-114/pat1-114* and *erf2*Δ*/erf2*Δ *pat1-114/pat1-114* cells undergoing synchronized meiosis (top panels). At the indicated times after meiotic induction, aliquots of the culture were pulse-labeled with alk-16. Western blots were probed for tubulin and HA (middle and bottom panels). **c,** Fluorescence detection of palmitoylated substrates (top panel) and Ras1 palmitoylation (bottom panel) in homozygous diploid *pat1-114/pat1-114* cells with the indicated PAT deletions 8 h after meiotic induction. (-): DMSO control. Veg: vegetative cells. Red arrowhead points to the major substrate ~25 kDa that is specifically modified by Erf2 in meiotic cells.

Isp3 and Rho3 are selectively palmitoylated by Erf2 in meiotic cells

To identify the major Erf2 substrates that are preferentially palmitoylated during meiosis, I affinity purified alk-16 labeled proteins in meiotic *erf2*$^{+}$, vegetative *erf2*$^{+}$, and meiotic *erf2*Δ cells using a cleavable azido-biotin tag (Supplementary Fig. 3.8a, b). Recovered proteins were subsequently identified by gel-based proteomics, and those with ≥ 2-fold spectral counts in alk-16 samples compared to the corresponding DMSO controls were further studied. Proteins enriched in meiotic *erf2*$^{+}$ cells were subjected to two filter criteria, excluding those also enriched in (1) meiotic *erf2*Δ cells and (2) vegetative *erf2*$^{+}$ cells (Fig. 3.8c). Notably, Ras1 was excluded by the second filter because it was equally recovered in both meiotic and vegetative *erf2*$^{+}$ cells, consistent with the biochemical analyses (Fig. 3.9d). Of the 238 remaining candidates (Appendix 1), we focused on Isp3 and Rho3 (Fig. 3.8e) as they were the most highly enriched proteins with molecular weights matching the prominent ~23 kDa band we previously observed (Fig. 3.8d).

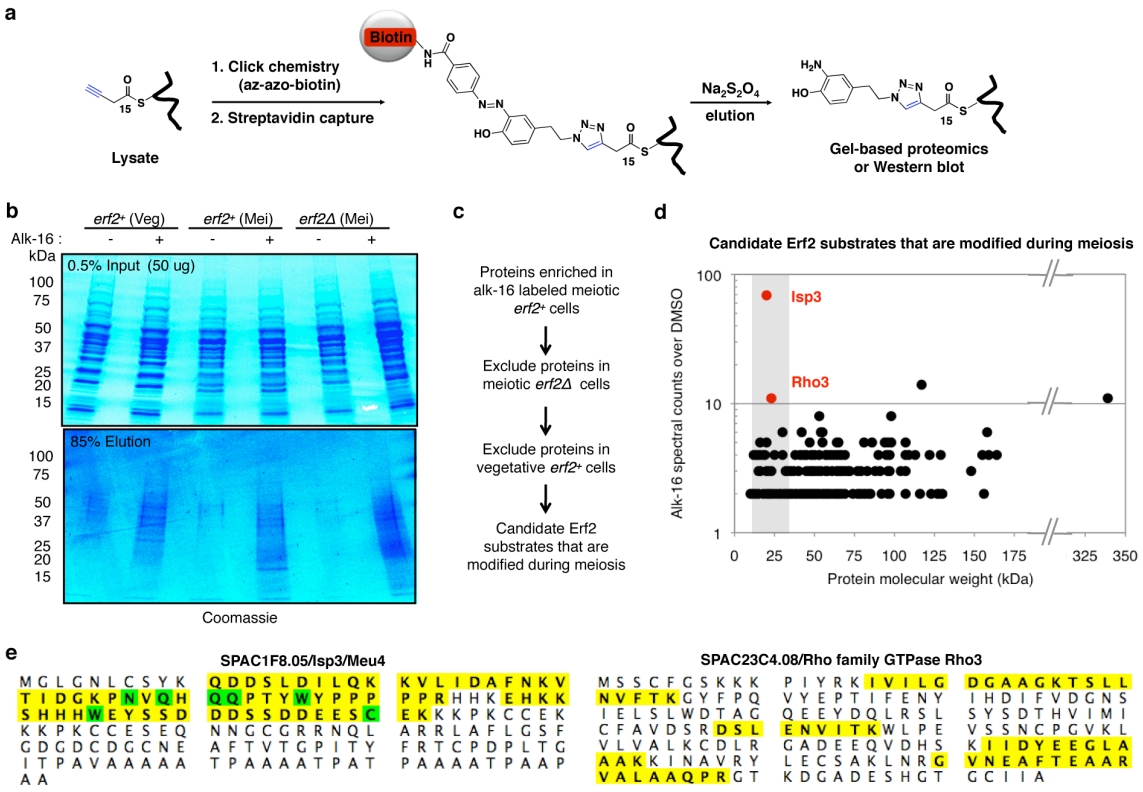

Figure 3.8 | Identification of Erf2 substrates that are selectively palmitoylated during meiosis. a, Schematic representation of the selective enrichment protocol of alk-16 modified proteins from cell lysates using streptavidin beads. Az-azo-biotin: Azide-functionalized biotin probe with an azobenzene cleavable linker. CuAAC: copper-catalyzed azide-alkyne cycloaddition. **b, c,** Filter criteria for candidate substrates that are palmitoylated by Erf2 during meiosis. **d,** Each of the 238 candidates from (**c**) is represented as a data point reflecting its molecular weight and enrichment (net spectral counts) in alk-16 over DMSO labeled *erf2*$^{+}$ meiotic cells. Isp3 and Rho3 are the top two candidates with molecular weights ~23 kDa (shaded). **e,** Amino acid sequences of Rho3 and Isp3, both of which were validated to be Erf2 substrates that are selectively palmitoylated in meiotic cells. Yellow: identified peptides. Green: modified amino acids in identified peptides (e.g. oxidation, carbamidomethylation).

Cognate Erf2 substrates are differentially modified in distinct cellular states

Isp3, an abundant spore protein specifically expressed in meiotic cells[142] (Fig. 3.9c), was the most heavily modified species since the ~23 kDa band was lost in *isp3*Δ cells and HA_3-tagging of Isp3 reduced the electrophoretic mobility of the major fluorescent band (Fig. 3.9a). I also confirmed that Rho3, a Rho GTPase involved in polarized growth[143], is an Erf2 substrate (Fig. 3.9b) that is differentially modified with between meiotic and vegetative cells (Fig. 3.9d). This suggests a mechanism by which changes in the palmitoylome can be mediated by the regulation of a single PAT (Fig. 3.9e). Given that Erf2 expression is low in vegetative cells and high in meiotic cells, I reasoned that the differential modification of Erf2 substrates could be a consequence of PAT levels.

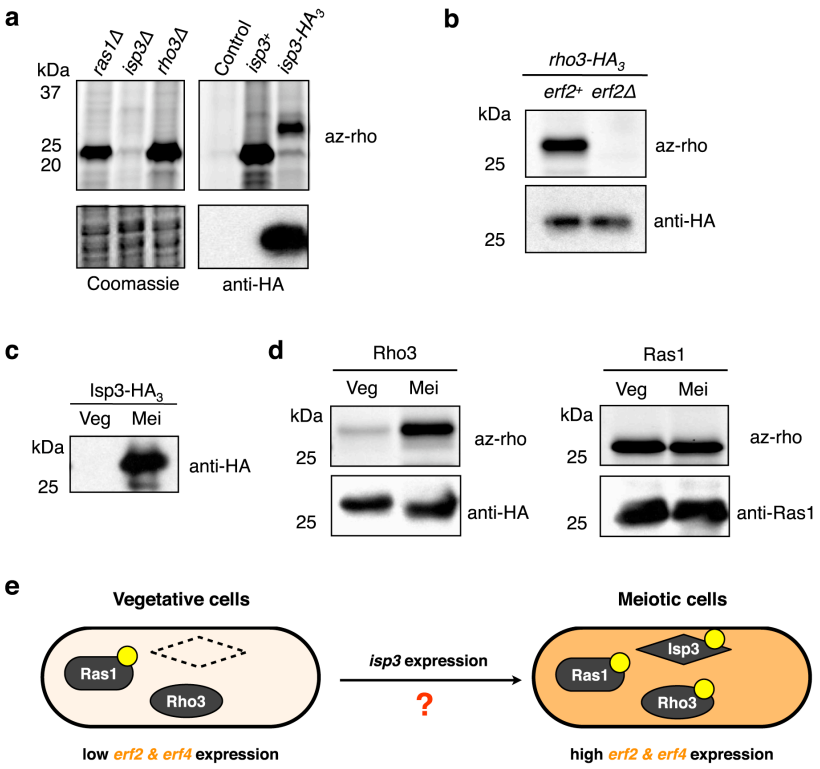

Figure 3.9 | Erf2 substrates are differentially modified in vegetative and meiotic cells. a, Fluorescence profiles of meiotic cells with indicated gene deletions or those expressing endogenous or tagged Isp3 (top panels). Control: *isp3*$^{+}$ cells labeled with DMSO instead of alk-16. Bottom panels: Coomassie or western blot probed for HA. **b,** Palmitoylation of Rho3-HA$_3$ in meiotic *erf2*$^{+}$ and *erf2*Δ cells (top panel). Western blot is probed for HA (bottom panel). **c,** Isp3-HA$_3$ expression as determined by anti-HA blot of lysates from cells in indicated cellular states. Veg: vegetative cells. Mei: meiotic cells. **d,** Rho3 and Ras1 palmitoylation states in vegetative and meiotic cells (top panels). Western blots were probed for Ras1 or HA (bottom panels). **a-d,** Synchronous meiosis in indicated diploid *pat1-114/pat1-114* cells was induced by shifting nitrogen-starved cultures to restrictive temperature (see Methods). Meiotic cells refer to cells 8 h after the temperature shift. **e,** While differential palmitoylation of Isp3 in meiotic and vegetative cells can be explained by meiosis-specific *isp3* expression, the differential modification of Ras1 and Rho3 is mediated by an alternative mechanism. Yellow circles represent palmitoylation of the indicated Erf2 substrates.

Erf2-Erf4 PAT levels shape the meiotic palmitoylome

To test this hypothesis, I reduced *erf2* expression in diploid cells undergoing synchronized meiosis, achieving intermediate and low expression relative to wild type (Fig. 3.10a, top). Although all three substrates require Erf2 for palmitoylation, Ras1, Rho3 and Isp3 were differentially modified as a consequence of altering *erf2* levels (Fig. 3.10a). Ras1 was efficiently palmitoylated at low *erf2* expression levels, and its palmitoylation was unaltered at higher levels. In contrast, reducing *erf2* expression decreased Rho3 and Isp3 palmitoylation with different sensitivities. This demonstrates that modulation of PAT levels can differentially alter the palmitoylation of individual substrates and suggests that the strong upregulation of *erf2* expression during meiosis is needed to establish the distinctive features of the meiotic palmitoylome.

If physiological control of Erf2-Erf4 abundance solely accounts for the palmitoylome changes observed upon meiosis, it is predicted that increasing Erf2-Erf4 levels in haploid vegetative cells would yield a palmitoylome similar to that of meiotic cells. To test this, I focused on Ras1 and Rho3 as model substrates since *isp3* expression is restricted to meiotic cells (Fig. 3.9c). Ras1 palmitoylation was insensitive to increases in Erf2-Erf4 levels (Fig. 3.10b), consistent with our results in meiotic cells. In contrast, while individual overexpression of *erf2* and *erf4* had no impact on Rho3 modification, a striking increase in Rho3 palmitoylation was observed when the effective Erf2-Erf4 PAT concentration was increased by co-overexpression of *erf2* and *erf4* (Fig. 3.10b, strains 4-7). Intermediate overproduction of Erf2-Erf4 resulted in a modest increase in Rho3 palmitoylation, indicating a dose-dependent function of PAT activity (Fig. 3.10b, strain

8). Importantly, although *erf2* and *erf4* were expressed from heterologous promoters, their levels were in fact within physiological range, with the highest and lowest levels being comparable to those attained by meiotic and vegetative cells respectively (Fig. 3.3b and 3.10a, b). These results demonstrate that rheostatic control of protein palmitoylation by varying PAT levels is a mechanism by which cells finely shape the palmitoylome and that this may play a key role in cellular transitions such as meiosis.

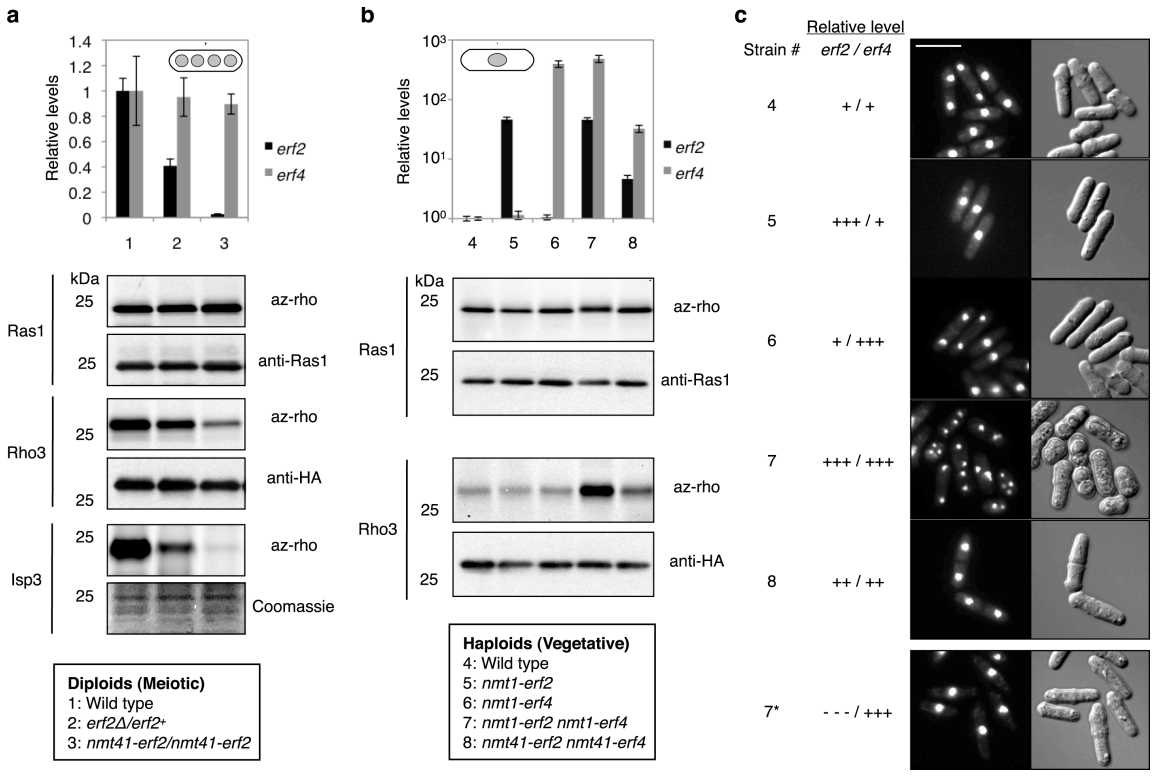

Figure 3.10 | Physiological changes in Erf2-Erf4 levels underlie the differential modification of cognate substrates in meiotic and vegetative cells. a, Labels are indicated in box. qPCR analysis of *erf2* and *erf4* transcripts normalized to *act1* mRNA levels in indicated *pat1-114/pat1-114* strains 8 h into synchronous meiosis (top panel). Error bars, s.d. Palmitoylation of cognate Erf2 substrates were analyzed from the same lysate of each strain (bottom panels). Ras1 and Rho3-HA_3 were immunopurified and their levels were determined by Ras1 and HA immunoblots respectively. Isp3 palmitoylation was monitored at the lysate level since it accounts for most of the fluorescence at ~23 kDa (Isp3 is unstable upon immunoprecipitation, data not shown). **b,** Labels are indicated in box. Overexpression of *erf2* and/or *erf4* from thiamine-repressible *nmt* promoters in the indicated vegetative *pat1-114* cells was achieved by switching them into thiamine-free medium for 24 h. qPCR analysis (top panel) as well as palmitoylation of Ras1 and Rho3 (bottom panels) were performed as described in (**a**). Isp3 is not expressed in vegetative cells.Cells were maintained at permissive temperature throughout this experiment (See Methods). **c,** DAPI (left) and DIC (right) images of indicated cells 96 h after *erf2* and/or *erf4* overexpression. Strain 7*: *nmt1-erf2 (DHHA) nmt1-erf4*. Scale bars, 10 µm.

Erf2-Erf4 overproduction is sufficient to induce a meiotic phenotype in vegetative cells

If PAT-mediated changes in global protein palmitoylation are critical in meiotic entry, then increasing Erf2-Erf4 levels in vegetative cells may be sufficient to trigger meiosis in the absence of nutritional cues. Strikingly, overexpression of *erf2* and *erf4* in proliferating haploid cells induced a meiotic phenotype (Fig. 3.10c, strain 7). A significant reduction in growth rate with time, accompanied by a reduction in cell length at division and a transient G1 delay (Fig. 3.11a-c) was observed. At 96 hours after induction, a significant proportion of cells had >2 nuclei (Fig. 3.11d). These cells were appeared to be undergoing a meiotic program since deletion of *mei4*, which is required for meiotic but not mitotic divisions, resulted in the disappearance of cells with >2 nuclei and accumulation of misshapen cells with a single nucleus (Fig. 3.11f). The appearance of spores that are resistant to β-glucuronidase digestion, which specifically kills vegetative cells further suggested that these cells were indeed undergoing sexual differentiation program (Fig. 3.11e). While Erf2-induced haploid meiosis produced mainly inviable spores, overexpression *erf2* and *erf4* in diploid cells also induced a meiotic phenotype and yielded viable spores (Fig. 3.13). Under these same conditions, non-overexpressing cells continued normal vegetative growth over the course of the experiment (Fig. 3.12). Overall, these results demonstrate that increasing the levels of a single PAT activity is sufficient to induce sexual differentiation in otherwise proliferating cells and implicate the control Erf2-Erf4 activity levels as a major determinant in *S. pombe* meiotic commitment.

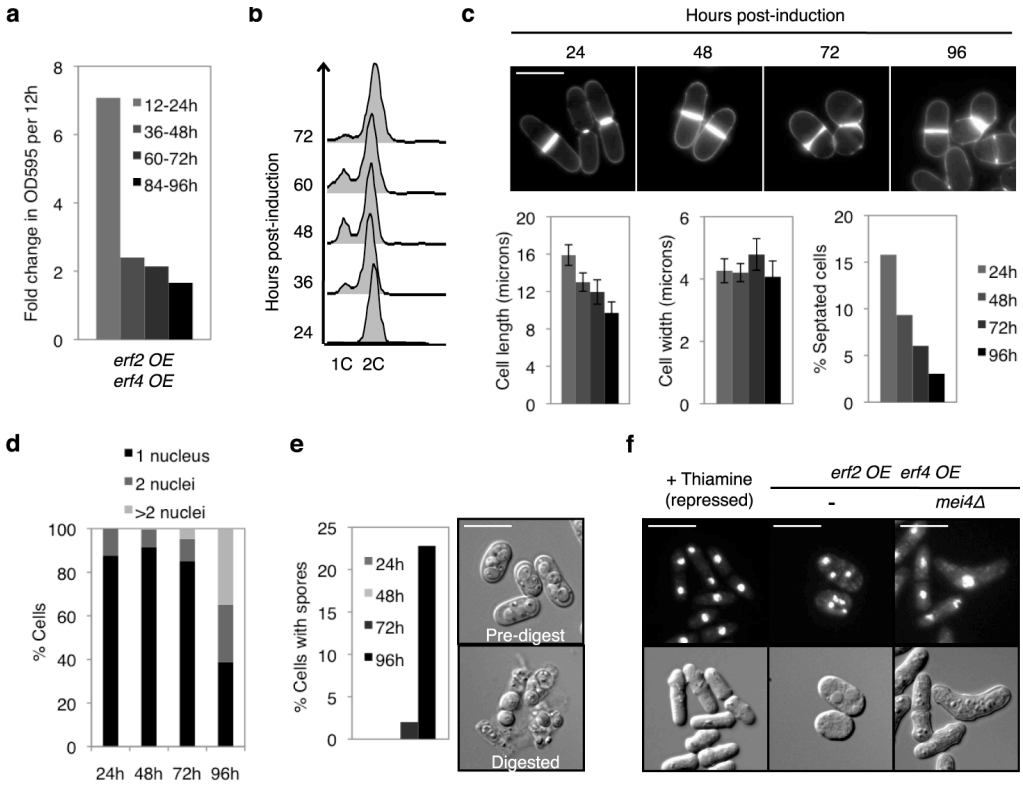

Figure 3.11 | Overproduction of Erf2 and Erf4 in proliferating cells induce a meiotic phenotype. a-e, *erf2 OE erf4 OE:* strain 7 from Fig. 3.10 that co-overexpresses *erf2* and *erf4* at high levels. These cells were grown in the presence of nutrients at permissive temperature, and co-overexpression of *erf2* and *erf4* was induced by switching cells to thiamine-free medium (See Methods). Indicated times or time intervals refers to time after induction of *erf2* and *erf4* co-overexpression. **a,** Fold change in OD_{595} of cultures during indicated 12 h intervals. OD_{595} was maintained < 0.6 (See Methods). **b,** DNA content analysis. **c,** Blankophor staining of cells (top panels). Dimensions of septated cells (cell length and width, n=20) and percentage of septated cells (septation index, n≥200) were determined by measuring and counting blankophor-stained cells (bottom panels, left to right). Error bars, s.d. **d**, Percentage of cells with 1, 2 or >2 nuclei (n≥200) was determined by DAPI staining. **e,** Left panel, percentage of cells with spores (n≥200) at indicated times post-induction. Right panel, DIC images of cells 96 h post-induction before and after β-glucuronidase digestion, which specifically kills vegetative cells but not spores. **f,** DAPI (top) and DIC (bottom) images of indicated *erf2* and *erf4* co-overexpressing cells 96 h post-induction. Scale bars, 10 μm.

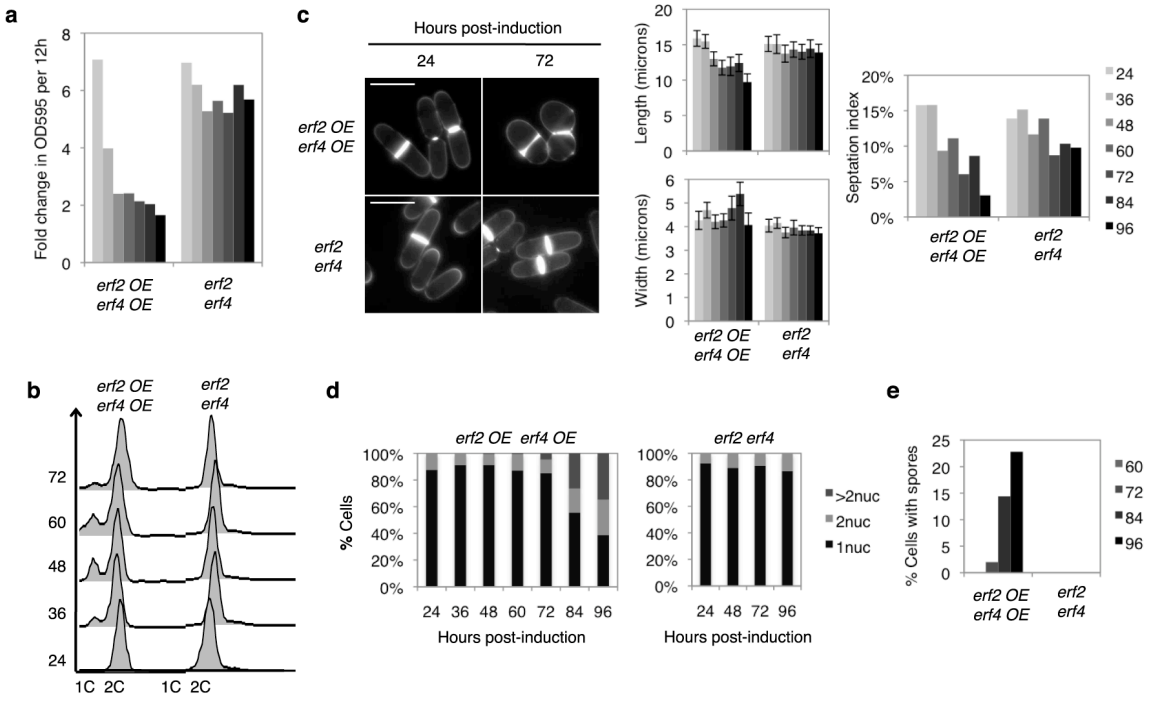

Figure 3.12 | Non-overexpressing *pat1-114* cells continue vegetative growth under the same conditions. *erf2 OE erf4 OE:* strain 7 from Fig. 3.10 that co-overexpresses *erf2* and *erf4* at high levels. *erf2 erf4*: strain 4 from Fig. 3.10 that expresses erf2 and erf4 at endogenous levels. These cells were grown in the presence of nutrients at permissive temperature, and co-overexpression of *erf2* and *erf4* was induced by switching cells to thiamine-free medium (See Methods). Indicated times or time intervals refers to time after the switch to thiamine-free medium. **a,** Fold change in OD_{595} of cultures during indicated 12 h intervals. OD_{595} was maintained < 0.6 (See Methods). **b,** DNA content analysis. **c,** Blankophor staining of cells (left panels).Scale bars, 10 μm. Dimensions of septated cells (cell length and width, n=20, middle panels) and percentage of septated cells (septation index, n≥200, right panel) were determined by measuring and counting blankophor-stained cells. Error bars, s.d. **d,** Percentage of cells with 1, 2 or >2 nuclei (n≥200) was determined by DAPI staining of the indicated strains. **e,** Percentage of cells with spores at indicated times post-induction (n≥200).

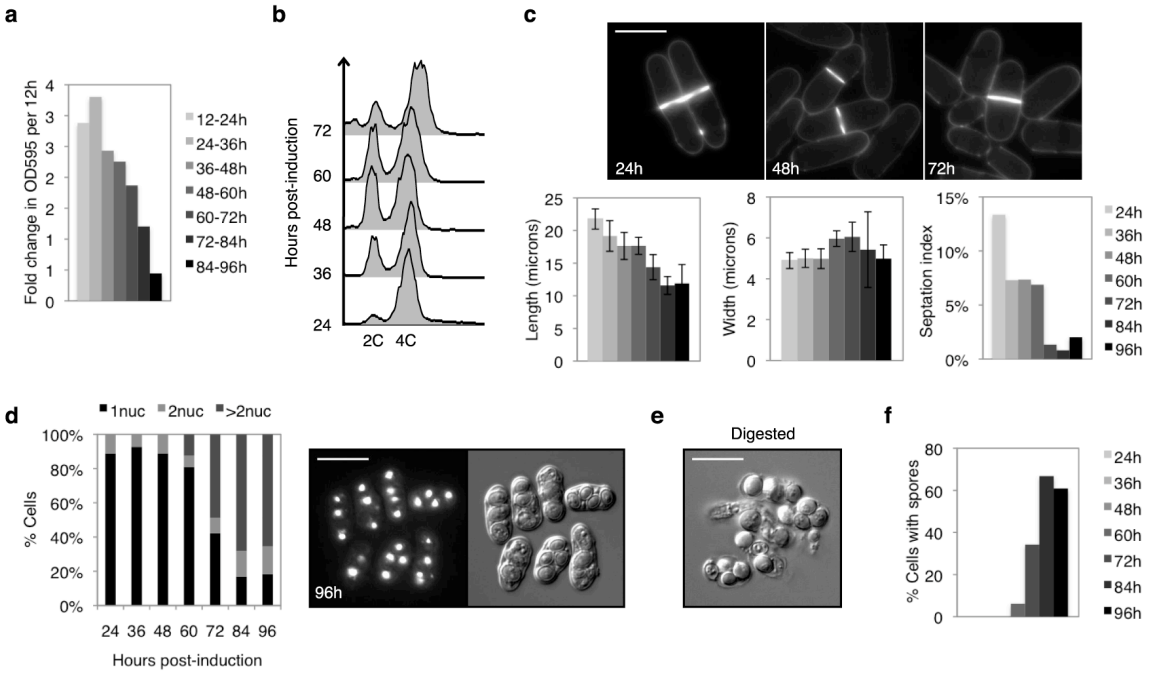

Figure 3.13 | Ectopic meiosis in diploid cells co-overexpressing *erf2* and *erf4* yields viable spores. Strain 7 from Fig. 3.10 was diploidized and grown in the presence of nutrients at permissive temperature, and co-overexpression of *erf2* and *erf4* was induced by switching cells to thiamine-free medium (See Methods). Indicated times or time intervals refers to time after the switch to thiamine-free medium. **a,** Fold change in OD_{595} of cultures during indicated 12 h intervals. OD_{595} was maintained < 0.6 (See Methods). **b,** DNA content analysis. **c,** Blankophor staining of cells (top panels). Dimensions of septated cells (cell length and width, n=20) and percentage of septated cells (septation index, n≥200) were determined by measuring and counting blankophor-stained cells (bottom panels, left to right). Error bars, s.d. **d,** Percentage of cells with 1, 2 or >2 nuclei (n≥200) was determined by DAPI staining (left panel). DAPI and DIC images of cells 96 h post-induction (right panels). **e,** DIC image of cells 96 h post-induction after β-glucuronidase digestion, which specifically kills vegetative cells but not spores. **f,** Percentage of cells with spores (n≥200). Viable colonies were obtained after plating β-glucuronidase digested cells at 84 h and 96 h. Scale bars, 10 μm.

Erf2-induced meiotic phenotype is dependent on PAT activity levels

Consistent with the rheostat model (Fig. 3.10), this meiotic phenotype was dependent on high PAT levels, as cells continued vegetative growth when *erf2* and *erf4* are expressed at low (Fig. 3.11f, +Thiamine) or intermediate levels (Fig. 3.10c, strain 8). Critically, meiotic induction was not observed in cells co-overexpressing a catalytically inactive Erf2 mutant and Erf4 (Fig. 3.10c, strain 7*) or in cells overproducing either Erf2 or Erf4 alone (Fig. 3.10c, strains 5 and 6), highlighting the requirement for a functional and active PAT complex. Together with the meiotic delay observed in *erf2*Δ cells, these results demonstrate that modulation of Erf2-Erf4 activity levels through changes in the expression of each subunit is a key step for meiotic commitment.

Rho3 function is required for Erf2-induced meiosis

As *erf2* and *erf4* expression are upregulated in cells undergoing normal meiosis when encountering low nitrogen conditions[136], these results suggest that PAT level-mediated modulation of the palmitoylome is a major determinant of meiotic entry. What are the cellular factor(s) involved in this process? As meiosis can be induced by Erf2-Erf4 overproduction, I reasoned that Erf2-Erf4 substrates involved in triggering meiosis would have to be present in vegetative cells and sensitive to Erf2-Erf4 levels for their palmitoylation state (Fig. 3.14a). One such substrate is Rho3 (Fig. 3.9b, d, and 3.10b). I found that Rho3, but not Ras1, is required for the meiotic phenotype triggered by Erf2-Erf4 overexpression in haploid cells (Fig. 3.14b). This is clearly dependent on the Exo70 subunit of the exocyst complex and the Formin For3 (Fig. 3.14b), both effectors of Rho3,

suggesting a novel role for Rho3 in meiotic control in fission yeast, potentially through its function in polarized exocytosis that is likely to be regulated by its palmitoylation state[143, 144].

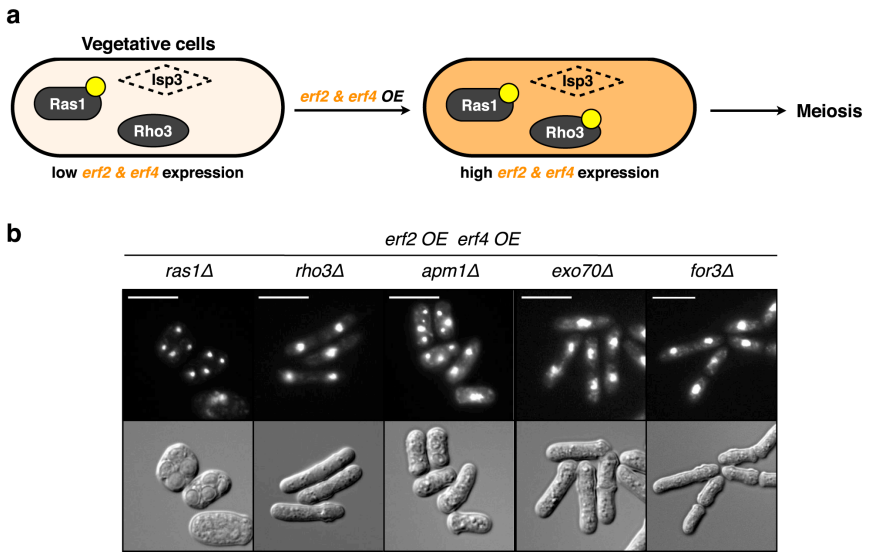

Figure 3.14 | A novel function of Rho3 in *S. pombe* meiotic control. a, As meiosis can be induced by Erf2-Erf4 overproduction, the cellular factor(s) involved in Erf2-mediated meiotic control should be present in vegetative cells. Yellow circles represent palmitoylation of the indicated Erf2 substrates. **b,** DAPI (top) and DIC (bottom) images of *erf2* and *erf4* co-overexpressing cells with indicated deletions 96 h post-induction. Scale bars, 10 μm. Rho3 in *S. pombe* regulates polarized cell growth through For3 and Exo70, both of which are required for the observed meiotic phenotype. Rho3 has also been implicated in Golgi/endosome trafficking through Apm1 but Apm1 function is not required for Erf2-Erf4 induced meiosis.

Erf2 function is required for proper Rho3 localization in vegetative and meiotic cells

Since palmitoylation has been shown to control protein function by changing protein distribution between the plasma and intracellular membranes, in collaboration with Dr. Pei-Yun Jenny Wu, we asked if Erf2-mediated palmitoylation of Rho3 affects its subcellular localization during ectopic meiosis. While Rho3 normally localizes to cell tips and septa in vegetative cells[144], enhanced enrichment at cell tips was observed with Erf2-Erf4 overexpression (Fig. 3.15a), which coincided with increased Rho3 palmitoylation (Fig. 3.10b). Interestingly, Rho3 relocalized to what appeared to be prespore surfaces encapsulating individual nuclei as cells completed meiosis (Fig. 3.15a). This redistribution of Rho3 from cell tips to prespore surfaces was also observed under more physiological conditions, during meiosis in diploid cells induced by Pat1 inactivation after nitrogen starvation (Fig. 3.15b). Rho3 localization in both vegetative and meiotic cells requires palmitoylation by Erf2 (Fig. 3.15c), which was also visualized at forespore surfaces during meiosis (data not shown). Taken together, these data suggest that Erf2-Erf4 regulates Rho3 function, and potentially its role in polarized exocytosis, by altering its subcellular distribution.

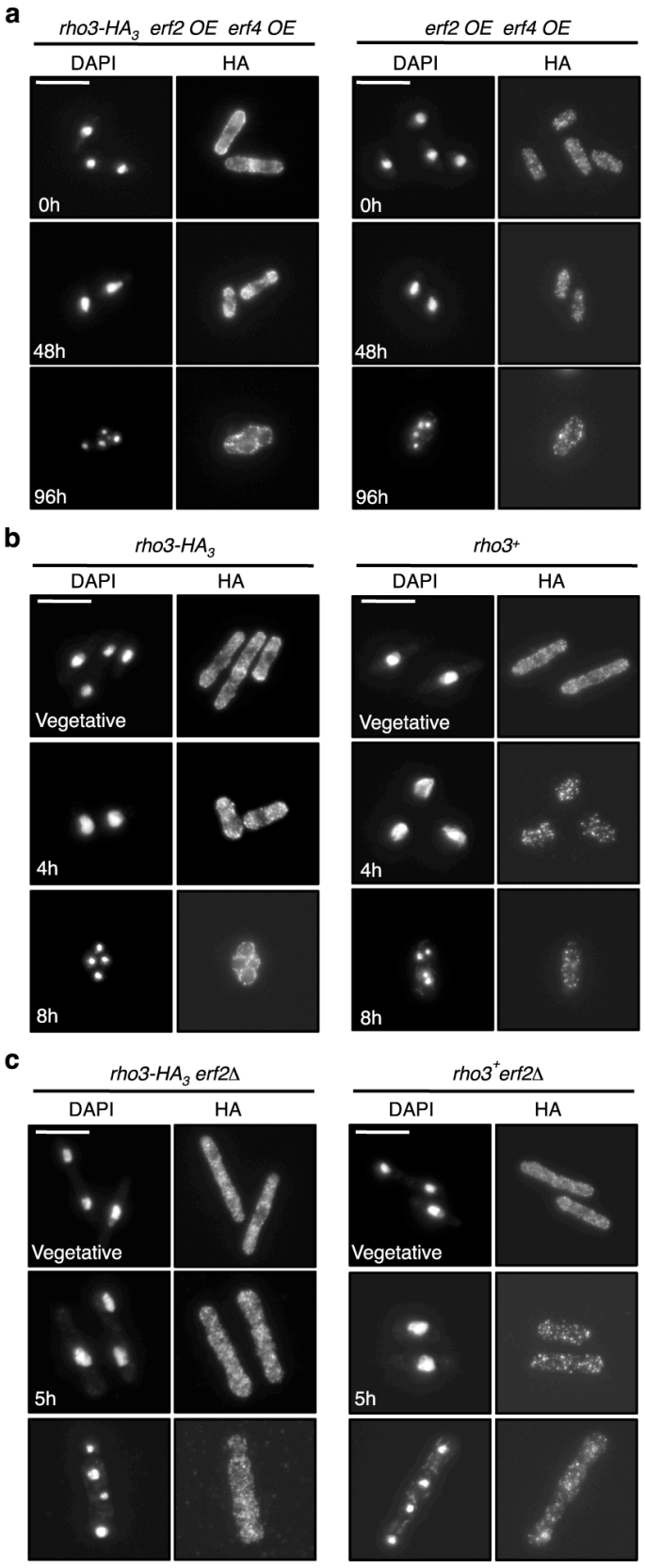

Figure 3.15 | Erf2-dependent Rho3 localization in vegetative and meiotic cells. Immunofluorescence localization of Rho3-HA$_3$ and DAPI images (left panels). Background anti-HA immunofluorescence and respective DAPI images (right panels). Images are maximum intensity projections. Scale bars, 10 μm. **a,** Haploid cells were grown in the presence of nutrients at permissive temperature. Co-overexpression of *erf2* and *erf4 (erf2 OE erf4 OE*) was induced by switching cells to thiamine-free medium (See Methods). Indicated times refers to time after the switch to thiamine-free medium. **b, c**, Meiosis in homozygous diploid *pat1-114/pat1-114* cells with the indicated genotypes was induced by shifting the culture to restrictive temperature for the indicated times. Later time points were taken for *erf2*Δ cells to compensate for the meiotic delay in these cells (Fig. 3.4).

Summary and Discussion

In this chapter, we demonstrated that PAT levels matter. Physiological control of PAT levels underlie the differential modification of distinct substrates in vegetative and meiotic cells and palmitoylome changes mediated by control of the level of Erf2-Erf4 activity are sufficient to induce meiosis in fission yeast. We propose that rheostatic control of single or multiple PAT activities quantitatively regulates palmitoylomes, which we showed have important consequences on cellular events.

This study showcases fission yeast as a relevant and complementary model organism for PAT studies. Consistent with studies in budding yeast and mammals[12, 65, 67], I showed that fission yeast PATs can have different substrate preferences and that specific PAT-substrate pairs are needed for efficient palmitate transfer. Notably, the Erf2-Erf4:Ras1 PAT:substrate pairing in fission yeast is reminiscent of the ERF2-ERF4:RAS1/RAS2 and DHHC9-GCP16:H-/N-Ras pairs in budding yeast and human, respectively [58, 59]. This suggests an evolutionary selection for specific cognate PAT:substrate pairs, which would be unlikely if PATs have extensive overlapping substrate preferences and were able to freely substitute for each other. Furthermore, from the relatively few PAT paralogs in fission yeast, I surmised that there would be less functional redundancy between the enzymes, enabling us to distinguish the functional contributions of individual PATs. This is evident from the requirement of Swf1 for cell viability, which is the first report of an essential DHHC-PAT and supports the view that PATs occupy functional niches. Furthermore, I showed biochemically a clear requirement for Erf2 in Ras1 and Rho3 palmitoylation in fission yeast, in contrast to reports in budding yeast[12, 63]. The

unambiguous PAT-substrate pairs in fission yeast facilitated this study and given the apparent parallels of PAT-mediated protein palmitoylation between yeasts and metazoa, studying this simple machinery will provide insights into equivalent controls in mammals.

It remains to be determined how levels of a PAT affect its substrate specificity. One possibility is a difference in catalytic efficiency (k_{cat}/K_M) and this is supported by the discovery of specificity determinants on both the PATs and their substrates that dictate enzyme-substrate interactions[66, 67]. In addition, level-dependent changes in PAT localization might alter substrate availability. For example, DHHC2 translocates to post-synaptic membranes upon neuronal stimulation, where it increases palmitoylation and synaptic targeting of PSD95[51]. In this study, however, changes in PAT localization are unlikely to account for the difference in Ras1 and Rho3 palmitoylation since both substrates are localized to the same compartments in vegetative cells[28, 144]. Alternatively, there may be depalmitoylating thioesterases or competing cellular factors that target substrates differentially[40, 84, 86, 87].

As global proteomic studies rapidly expand the known list of proteins that are reversibly modified with this lipid moiety[10-18], palmitoylation is proposed to be a major cellular regulator. This is supported by expression profiling experiments in flies and humans in which transcript levels of specific PATs vary widely across tissues[70, 71]. Neuronal differentiation signals were found to induce the PAT degradation via the ubiquitin-proteosome pathway[74]. In addition, PAT overexpression is associated with a variety of human cancers and induces cellular transformation (summarized in Table 1.2).

Along with these results, this study suggests critical roles for the control of PAT levels and regulation of palmitoylomes in cellular development and disease. Although the palmitoylation machinery is more elaborate in multicellular eukaryotes, the conservation of PAT function and of specific PAT:substrate pairs between yeast and humans[12, 58, 59] indicates that the conclusions of this study are relevant in predicting regulatory roles of palmitoylation in major developmental transitions in metazoa.

Materials and Methods

Genotype of haploid S. pombe strains used.

Strain	Genotype	Source
PN1	*h-*	Nurse lab
PN4	*h+*	Nurse lab
Mz53	*h- erf2Δ::NatMX6*	This study
Mz56	*h+ erf2Δ::NatMX6*	This study
Mz166	*h- erf4Δ::KanMX6*	This study
Mz170	*h+ erf4Δ::KanMX6*	This study
Mz126	*h- akr1Δ::KanMX6*	This study
Mz132	*h+ akr1Δ::KanMX6*	This study
Mz120	*h- pfa5Δ::KanMX6*	This study
Mz124	*h+ pfa5Δ::KanMX6*	This study
Mz184	*h- erf2Δ::NatMX6 erf4Δ::KanMX6*	This study
Mz188	*h+ erf2Δ::NatMX6 erf4Δ::KanMX6*	This study
Mz254	*h- akr1Δ::KanMX6 pfa5Δ::KanMX6*	This study
Mz257	*h+ akr1Δ::KanMX6 pfa5Δ::KanMX6*	This study
Mz108	*h+ erf2Δ::NatMX6 leu1-32::pDUAL(leu1 nmt41:HFY-erf2) ade-M216 ura4-D18*	This study
Mz199	*h+ erf2Δ::NatMX6 leu1-32::pDUAL(leu1 nmt41:HFY-erf2(DHHA)) ade-M216 ura4-D18*	This study
YN464 (FY12642)*	*h- leu1 pREP1(nmt1:mei4)*	Nakase et al.[197]
Mz471	*h- pat1-114 nmt1:erf2::KanMX6 rho3-HA$_3$::KanMX6*	This study
Mz492	*h- pat1-114 nmt1:erf4::KanMX6 rho3-HA$_3$::KanMX6*	This study
Mz476	*h- pat1-114 nmt1:erf2::KanMX6 nmt1:erf4::KanMX6 rho3-HA$_3$::KanMX6*	This study
Mz504	*h- pat1-114 nmt41:erf2::KanMX6 nmt41:erf4::KanMX6 rho3-HA$_3$::KanMX6*	This study
Mz556	*h- pat1-114 leu1-32::pDUAL(leu1 nmt1:erf2(DHHC))*	This study
Mz560	*h- pat1-114 leu1-32::pDUAL(leu1 nmt1:erf2(DHHA))*	This study
Mz518	*h- nmt1:erf2::KanMX6 nmt1:erf4::KanMX6 rho3-HA$_3$::KanMX6*	This study
Mz534	*h- pat1-114 nmt1:erf2::KanMX6 nmt1:erf4::KanMX6 mei4Δ::natMX6 ura4-D18*	This study
Mz488	*h- pat1-114 nmt1:erf2::KanMX6 nmt1:erf4::KanMX6 rho3Δ::kanMX6 ura4-D18*	This study
Mz587	*h- pat1-114 nmt1:erf2::KanMX6 nmt1:erf4::KanMX6 ras1Δ::ura4$^+$ ura4-D18*	This study
Mz629	*h- pat1-114 nmt1:erf2::KanMX6 nmt1:erf4::KanMX6 apm1Δ::ura4$^+$ ura4-D18*	This study
Mz634	*h- pat1-114 nmt1:erf2::KanMX6 nmt1:erf4::KanMX6 exo70Δ::ura4$^+$ ura4-D18*	This study
Mz567	*h- pat1-114 nmt1:erf2::KanMX6 nmt1:erf4::KanMX6 for3Δ::ura4$^+$ ura4-D18*	This study

Genotype of diploid S. pombe strains used.

Strain	Genotype	Source
Mz5d	*h-/h- pat-114/pat1-114 erf2-HA$_3$::KanMX6/erf2-HA$_3$::KanMX6*	This study
Mz9d	*h-/h- pat-114/pat1-114 erf2Δ::NatMX6/erf2Δ::NatMX6*	This study
Mz21d	*h-/h- pat-114/pat1-114 erf4Δ::KanMX6/erf4Δ::KanMX6*	This study
Mz25d	*h-/h- pat-114/pat1-114 akr1Δ::KanMX6/akr1Δ::KanMX6*	This study
Mz29d	*h-/h- pat-114/pat1-114 pfa5Δ::KanMX6/pfa5Δ::KanMX6*	This study
Mz17d	*h-/h- pat-114/pat1-114 akr1Δ::KanMX6/akr1Δ::KanMX6 pfa5Δ::KanMX6/pfa5Δ::KanMX6*	This study
Mz60d	*h-/h- pat-114/pat1-114 ras1Δ::KanMX6/ras1Δ::KanMX6*	This study
Mz74d	*h-/h- pat-114/pat1-114 isp3Δ::KanMX6/isp3Δ::KanMX6*	This study
Mz64d	*h-/h- pat-114/pat1-114 rho3Δ::KanMX6/rho3Δ::KanMX6*	This study
Mz88d	*h-/h- pat-114/pat1-114 isp3-HA$_3$::KanMX6/isp3-HA$_3$::KanMX6*	This study
Mz68d	*h-/h- pat-114/pat1-114 rho3-HA$_3$::KanMX6/rho3-HA$_3$::KanMX6*	This study
Mz89d	*h-/h- pat-114/pat1-114 rho3-HA$_3$::KanMX6/rho3-HA$_3$::KanMX6 erf2Δ::NatMX6/erf2Δ::NatMX6*	This study
Mz129d	*h-/h- pat1-114/pat1-114 nmt41:erf2::KanMX6/nmt41:erf2::KanMX6 rho3-HA$_3$::KanMX6/rho3-HA$_3$::KanMX6*	This study
Mz189d	*h-/h- pat1-114/pat1-114 erf2$^+$/erf2Δ::ura4$^+$ rho3-HA$_3$::KanMX6/rho3-HA$_3$::KanMX6 ura4-D18/ura4-D18*	This study
Mz197d	*h-/h- pat1-114/pat1-114 nmt1:erf2::KanMX6/nmt1:erf2::KanMX6 nmt1:erf4::KanMX6/nmt1:erf4::KanMX6 rho3-HA$_3$::KanMX6/ rho3-HA$_3$::KanMX6*	This study

*Strain was obtained from the Yeast Genetic Resource Center of Japan, supported by the National Bioresource Project (YGRC/NBRP).

Strain construction and growth conditions. Standard media and methods were used[145, 146]. All experiments were carried out in minimal medium (EMM) and minimal medium plus supplements (EMM4S) for prototrophic and auxotrophic strains respectively at 25 °C unless otherwise noted. When applicable, strains were generated by tetrad dissection and validated by marker segregation or PCR. Deletion strains, strains expressing *erf2-HA$_3$, isp3-HA$_3$,* and those expressing *erf2* and *erf4* from *nmt* promoters were constructed by PCR integration[147]. For Rho3, the HA_3-tag sequence was inserted in-frame 42 bp upstream of its termination codon by PCR integration. Functional rescue in *erf2*Δ cells was performed using the pDUAL plasmid (RIKEN BRC, Japan) expressing *YFP-FLAG-His$_6$-erf2* under the *nmt41* promoter, which was linearized and integrated into the *leu1* locus. The Quikchange XL II kit (Stratagene) was used for site-directed mutagenesis of the *erf2 DHHC* motif. Homozygous diploids were obtained by incubating midlog cultures of haploid cells with 20 μg/ml Carbendazim (Sigma) for 4.5 hours at 25 °C and screening colonies on YES + phloxin B plates.

Synchronized Pat1-driven meiosis. Pat1-driven meiosis in diploid *pat1-114/pat1-114* cells was carried out as described[135]. Midlog cultures grown in EMM, which contains 0.5% NH_4Cl, were filter-washed three times with nitrogen-free minimal medium (EMM-N) using the Microfil filtration system (Millipore), and resuspended in EMM-N for 14 hours at 25 °C. Meiosis was induced by shifting the cultures to 34 °C in the presence of 0.05% NH_4Cl. t=0 is defined as the time of the temperature shift.

erf2 and/or erf4 overexpression from thiamine-repressible nmt promoters. Cultures were grown to midlog in EMM plus 10 mg/mL thiamine at 25 °C. *erf2* and/or *erf4* expression from *nmt* promoters was induced by filter-washing the cells three times with EMM as described above. The cells were resuspended in EMM and growth was maintained at 25 °C. The cultures were diluted with EMM approximately every 12 hours for the duration of each experiment to keep OD_{595} <0.6 and in the presence of nutrients. t=0 is defined as the time of thiamine removal.

Flow cytometry. DNA content was analyzed by flow cytometry using ethanol-fixed and propidium iodide-stained cells (2 μg/mL propidium iodide in 50 mM sodium citrate) on a BD FACS Calibur and analyzed using FlowJo software.

Cell size measurements and DNA staining. For cell size measurements, live cells were stained with Blankophor (MP Biomedicals). For DNA staining, ethanol-fixed cells were stained with DAPI. Images were acquired in Metamorph (MDS Analytical Technologies) using an Axioplan 2 microscope (Carl Zeiss) and a CoolSNAP HQ camera (Roper Scientific). Cell size measurements were obtained using the Pointpicker plug-in of Image J (National Institute of Health).

I*mmunofluorescence microscopy.* Cells were fixed at the indicated time points in 3.7% formaldehyde for 30 minutes at 25 ºC, washed three times in PEM (100 mM Pipes, 1 mM EGTA, 1 mM $MgSO_4$ pH 6.9), and digested with 0.25 mg/mL zymolyase in PEMS (PEM

+ 1.2 M Sorbitol) for 20 min at 37 ºC. Cells were then permeabilized by treatment with PEMS + 1% Triton X-100 for 30 s, after which they were recovered in PEMBAL (PEM with 1% BSA, 0.1% NaN_3, 100 mM lysine hydrochloride) for incubation with α-HA antibody (12CA5, mouse monoclonal) at 1:1000 dilution overnight at room temperature. After three washes in PEMBAL, samples were incubated with Alexa 568-conjugated anti-mouse secondary antibody (Invitrogen) at 1:2000 dilution for 3 hours in the dark at room temperature. Cells were then washed with PEMBAL and PBS. For imaging, cells were stained with 2 µg/mL DAPI to visualize nuclei. Microscopic images were acquired in Metamorph (MDS Analytical Technologies) using a 63x objective on an Axioplan 2 (Carl Zeiss, Inc.) epifluorescence microscope and a CoolSNAP HQ camera (Roper Scientific), with the same exposure settings for all images.

Quantitative RT-PCR. Total RNA was extracted using acidic phenol, DNase I-treated, and purified with the RNeasy kit (Qiagen). RNA concentration was quantified and its integrity was determined by agarose gel electrophoresis. cDNA was synthesized using random hexamers and the SuperScriptIII First Strand Synthesis SuperMix (Invitrogen). Relative quantification of cDNA was carried out in triplicate for each independent experiment using qPCR MasterMix Plus for SYBR Green (Applied Biosystems) on an ABI 7900 Real-Time PCR system. Primers used for quantitative PCR are listed in Supplementary Table 2. Standard curves were generated using least six 2-fold serial dilutions of a control sample and values within the linear exponential phase were used to calculate relative concentrations after normalization to the endogenous actin controls.

Oligonucleotide primers used in quantitative RT-PCR.

Gene	ID	Left	Right
actin	SPBC32H8.12c	CGAACGTGAAATTGTTCGTG	GGAGGAAGATTGAGCAGCAG
mde5	SPAC25H1.09	TTGCCGGACATTGATACAGA	CCGTCGATTTTGAACTGCTT
erf2	SPBC3H7.09	CTTTTTGGCTCTGGCATCAT	AATTCCTGGATCAGCAGTCG
erf4	SPAC3F10.07c	CGCAATATGGGGTTTTTGAG	GGCAGAGGGAAGTGTTCGTA
pfa3	SPBC2F12.15c	TGCCATCACCAAAACTTTCA	TCATTCCAACAGCAAAAGCA
pfa5	SPBC691.01	GGTGATTTACCATGGGATCG	GAAGCGGCAAAATCCAATTA
swf1	SPBC13G1.07	TCCATACTCCGCCTTGGTTA	CCCAGTTCCCCTTCACTTTT
akr1	SPAC2F7.10	TTAGCCGCTAGTCAGGGAGA	AATGCAGTTGCTCCACCTTC

Metabolic labeling and preparation of cell lysates. Cells were labeled with 10 μM of alk-16 (20-50 mM DMSO stock) for 15 min, washed once with PBS prior to liquid nitrogen freezing and storage at -80 °C. For inhibitor experiments, cells were preincubated for 30 min with either 200 μg/mL CHX or 200 μM 2BP, which were maintained in the cultures during alk-16 labeling. Competition experiments were carried out with various palmitate concentrations in the cultures during metabolic labeling. To prepare cell lysates, Brij lysis buffer (1% (v/v) Brij-97, 150 mM NaCl, 50 mM triethanolamine pH 7.4, 5× concentration of Roche EDTA-free protease inhibitor cocktail, 10 mM PMSF) and acid-washed glass beads (Sigma) were added to the frozen yeast cell pellets, which were lysed (3 x 20 s) using the Fastprep homogenizer (Thermo Scientific) at 4 min intervals to avoid overheating. Lysates were spun at 1,000 g for 5 min to remove cellular debris. Typical lysate protein concentrations of 5-10 mg/mL were obtained, as quantified using the BCA assay (Pierce).

Immunoprecipitations and CuAAC. For analyses of whole cell lysates, 50 μg of protein was diluted with Brij lysis buffer to a final volume of 44.5 μL, to which 5.5 μL of freshly mixed CuAAC reagents were added. The CuAAC reagents consisted of 1 μL az-Rho (5 mM stock solution in DMSO), 1 μL tris(2-carboxyethyl)phosphine hydrochloride (TCEP) (50 mM freshly prepared stock solution in deionized water), 2.5 μL tris[(1-benzyl-1*H*-1,2,3-triazol-4-yl)methyl]amine (TBTA) (2 mM stock solution in 1:4 DMSO:t-butanol) and 1 μL $CuSO_4 \cdot 5H_2O$ (50 mM freshly prepared stock solution in deionized water). After 1 hour at room temperature, proteins were methanol-chloroform precipitated to remove excess CuAAC reagents. The protein pellets were air-dried and resuspended in SDS buffer (4% (w/v) SDS, 150 mM NaCl, 50 mM triethanolamine pH 7.4) by sonication before SDS-PAGE. For Ras1 and HA immunoprecipitations, 1-3 mg of cell lysate was added to 4 μg anti-Ras antibody (Ras10, Millipore) with 25 μL Protein A agarose (Roche) or to 15 μL of anti-HA antibody–conjugated agarose (3F10, Roche) respectively. After 2 hours incubation with rocking at 4 °C, the beads were washed three times with ice-cold RIPA buffer (1% (v/v) Triton X-100, 1% (w/v) sodium deoxycholate, 0.1% (w/v) SDS, 50 mM triethanolamine pH 7.4, 150 mM NaCl). The washed beads were resuspended in 20 μL of PBS and 2.25 μL freshly-mixed CuAAC reagents described above. The beads were then washed three times with ice-cold RIPA buffer prior to boiling in SDS buffer for SDS-PAGE.

In-gel fluorescence scanning and Western blots. Fluorescence gels were visualized on a Typhoon 9400 variable mode imager (GE Healthcare) at excitation 532 nm/emission 580 nm. For Western blotting, proteins separated by SDS-PAGE were transferred to nitrocellulose membranes and probed with the following antibodies: anti-Ras (Ras10, Millipore), anti-tubulin (Tat1, gift from Keith Gull) and anti-HA (3F10, Roche). To avoid visualizing the light chain band in anti-Ras1 immunoblots of Ras1 immunopurifications, an Fc-specific anti-mouse-HRP secondary antibody (A2544, Sigma) was used. Blots were developed using the enhanced chemiluminescence kit (GE Healthcare). Images were processed using Image J.

Affinity enrichment and mass spectrometry. CuAAC reagents (az-azo-biotin) were added to 10 mg cell lysate at the same concentrations described above. Proteins were methanol-precipitated and resulting air-dried protein pellets were resuspended in 1 mL SDS buffer containing 10 mM EDTA by sonication. The mixture was diluted 1:3 with Brij lysis buffer and incubated with 100 μL of washed streptavidin agarose resin (Pierce) for 1 hour on a nutating mixer at room temperature. The beads were then washed once with 0.2% (w/v) SDS in PBS, three times with PBS and twice with 250 mM ammonium bicarbonate (ABC). Beads were resuspended in 500 μL 8 M urea, and reactive cysteines were alkylated by addition of 25 μL 200 mM TCEP and 25 μL 400 mM iodoacetamide for 30 min. The beads were washed twice with 50 mM ABC. Two sequential elutions of proteins from the resin were performed by incubating the beads with 250 μL of 25 mM sodium dithionite in 50 mM ABC with 0.1% (w/v) SDS for 30 min each. Proteins were

concentrated using YM-10 Centricons (Millipore), dried in a speed vac and separated by SDS-PAGE. Upon staining with Coomassie blue, each lane was cut into 10 slices for trypsin digestion and peptide extraction. Extracted peptides were dried and resuspended in 0.1% (v/v) trifluoroacetic acid for mass spectrometry identification. Acquired MS/MS spectra were analyzed using the Sequest search engine to identify proteins from the primary sequence database obtained from the *S. pombe* GeneDB. Exported Sequest results were analyzed using Scaffold (Proteome Software).

CHAPTER 4

A FISSION YEAST MODEL FOR PALMITOYLATION-MEDIATED REGULATION OF SIGNAL TRANSDUCTION

Introduction

In *S. pombe*, meiosis is part of a highly coordinated sexual differentiation process that is triggered by nutrient depletion. This important switch from the mitotic cell cycle to meiosis involves striking changes global gene expression[135, 136] and is governed by master regulator Mei2, an RNA binding protein (Fig. 4.1a). Mei2 binds to meiRNA, forming a dot structure that sequesters Mmi1 and enables stable expression of meiosis-specific transcripts critical for meiosis I[148]. Although the molecular functions of Mei2 in initiating and orchestrating the meiotic program are not fully elucidated, it is apparent that Mei2 is the master regulator that integrates extracellular cues (stress, nutrients and pheromones), primarily through transcription factor Ste11, and drives the meiosis (Fig. 4.1b). Mei2 function is tightly regulated by the Pat1 kinase, which phosphorylates and inactivates Mei2, preventing meiotic entry during the mitotic cell cycle[149]. Together, the Pat1-Mei2 system constitute the core mitosis-meiosis switch in fission yeast. Thermal inactivation of Pat1 in cells carrying the temperature sensitive *pat1-114* allele or even weak expression of a constitutively active Mei2 ($Mei2^{SATA}$) is sufficient to induce ectopic meiosis and sporulation regardless of nutritional cues and ploidy of the cells[137-139, 149]. Under physiological conditions, however, complete inactivation of Pat1 and meiotic induction strictly requires the stoichiometric inhibitor Mei3, which is only expressed in

heterozygous diploids formed after successful conjugation[150-152]. Working in concert, these key cellular factors integrate environmental cues and control cellular commitment to meiosis.

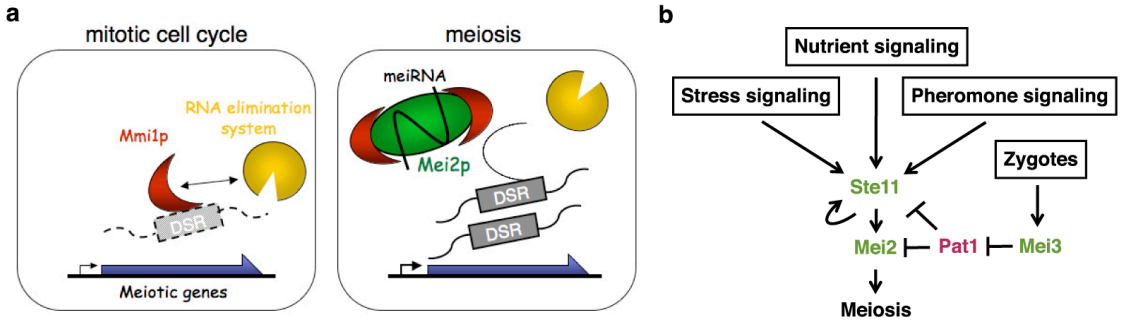

Figure 4.1 | Key cellular factors underlying the mitotic-meiotic decision in *S. pombe*. a, RNA-binding protein Mei2 is a critical regulator of meiotic initiation and progression. A number of meiosis-specific transcripts carry DSR (determinant of selective removal) regions, which renders them eliminated during the mitotic cell cycle by Mmi1. During meiotic prophase, Mei2, together with meiRNA, sequesters Mmi1, so that meiosis-specific transcripts become free from Mmi1-dependent elimination and be expressed. Adapted from Harigaya et al.[148] **b,** Key regulators integrate different signal transduction pathways (boxes) to regulate the initiation of meiosis. Green: positive regulators. Red: negative regulators.

In the previous chapter, I demonstrated that rheostatic control of Rho3 palmitoylation by varying levels of the Erf2-Erf4 PAT is a major determinant of meiotic commitment in *S. pombe*. In this chapter, I seek to determine where Erf2-Erf4 fit in the regulatory network of the meiotic program. Epistasis analysis revealed genetic interactions between *erf2*, *erf4* and the key regulators of meiotic commitment (Fig. 4.1b) as well as the components of the stress-activated protein kinase (SAPK) pathway. Consistent with this, various stress response defects were observed for *erf2*Δ and *erf4*Δ cells, which were associated with changes in global palmitoylation profiles. Taken

together, these results, though somewhat preliminary, suggest an intriguing role of the Erf2-Erf4 PAT in coordinating cellular response to stress and sexual differentiation. Given the homology between components of the S. *pombe* and mammalian MAPK/ SAPK pathways, if validated, this system offers a powerful tool to study palmitoylation-mediated regulation of signal transduction for diverse stimuli.

Results

pat1-114 provides a sensitized genetic background for Erf2-induced meiosis

In normal meiosis, heterozygous diploid zygotes formed after successful conjugation express Mei3, which inactivates Pat1 and leads to activation of Ste11 and Mei2, which in turn drives meiotic entry (Fig. 4.2a, box). As described in Chapter 3, overproduction of the Erf2-Erf4 PAT is sufficient to trigger a meiotic phenotype in otherwise proliferating cells. I further determined that induction of this meiotic phenotype requires canonical meiotic regulators, specifically Ste11 and Mei2, but not Mei3 (Fig. 4.2a). The latter is not unexpected since *mei3* expression is restricted to heterozygous zygotes whereas Erf2-Erf4 overproduction is sufficient to induce meiosis in haploid and homozygous diploid cells. This also indicates that the Erf2-induced meiotic phenotype is not a result of unscheduled *mei3* expression. Curiously, a routine control experiment revealed that the meiotic phenotype observed with Erf2-Erf4 overproduction is only apparent in the *pat1-114* but not *pat1*$^{+}$ genetic background (Fig. 4.2b). Since lower Pat1 kinase activity has been reported for *pat1-114* cells even at permissive temperature[153], I hypothesized that high Erf2-Erf4 activity induces the meiotic phenotype in these sensitized cells by activating the Ste11-Mei2 pathway or inactivating Pat1 via a Mei3-independent mechanism.

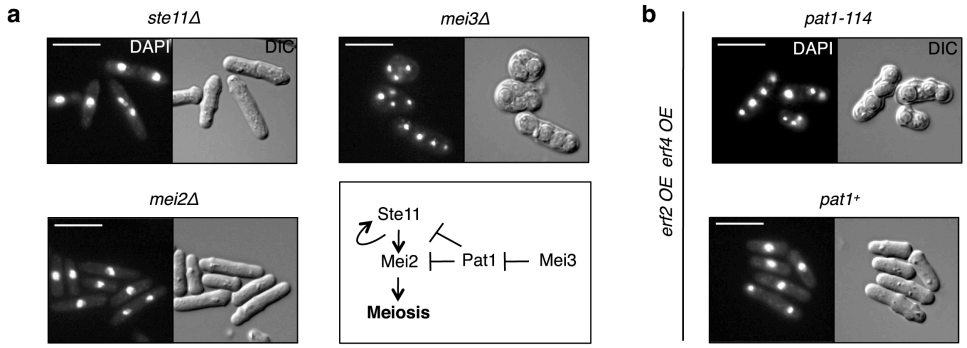

Figure 4.2 | Erf2-Erf4 function in meiotic control is revealed in *pat1-114* cells. DAPI (left) and DIC (right) images of haploid cells 96 h after *erf2* and *erf4* co-overexpression. Cells were maintained in the presence of nutrients at permissive temperature. Scale bars, 10 μm. **a,** Epistasis analysis revealed that canonical meiotic regulators Ste11 and Mei2, but not Mei3, are required for Erf2-Erf4 induced meiosis in *pat1-114* cells. Cellular factors involved in the *S. pombe* mitosis-meiotic switch are indicated in the box. In normal meiosis, Mei3 inactivation of Pat1 leads to activation of Ste11 and Mei2, which drives meiotic entry. Activation and inhibition are represented by arrows and crossing bars, respectively. **b,** Erf2-Erf4 induced meiosis is observed in *pat1-114* but not *pat1*$^{+}$ cells.

Erf2-induced meiosis requires the stress-activated protein kinase (SAPK) pathway

To test this, I determined the epistatic relationship of Erf2-Erf4 overproduction to a number of mutants constructed in the *pat1-114* genetic background, focusing on the genes in major pathways involved in the commitment to sexual differentiation in fission yeast. These include the cAMP, the pheromone signaling MAPK and the SAPK pathways (Fig. 4.3b). Erf2-Erf4 was overproduced in haploid strains with deletions of different components in each signaling pathway. Cells lacking components of the nutrient-sensing cAMP pathway (*rst2*) or pheromone signaling pathway (*ras1* and *spk1*) exhibited the meiotic phenotype upon Erf2-Erf4 overproduction (Fig. 4.3a). In contrast, deletion of kinases in the SAPK pathway, *wis1* and *sty1*, suppressed the meiotic phenotype (Fig. 4.3a). Deletion of a specific Sty1 effector, *atf1*, but not other Sty1 substrates (*srk1* and

smk2), also suppressed the meiotic phenotype (Fig. 4.3a). Given that Atf1 is required for *ste11* expression, these observations suggest that Erf2-Erf4 induces the meiotic phenotype by activating Ste11-Mei2 via the Wis1-Sty1-Atf1 SAPK pathway (Fig. 4.3b). Such activation is perhaps sufficient to overcome the Pat1-mediated meiotic repression in *pat1-114* cells, in which the Pat1 kinase is not fully active even at permissive temperature.

Genetic interactions between *erf2*, *erf4* and core components of the SAPK pathway raises the possibility that Erf2-Erf4, in addition to their roles in meiotic commitment, may also be important in controlling cellular response to environmental stresses (Fig. 4.3b). Interestingly, both Sty1 and Atf1 are involved in both sexual differentiation as well as stress response in fission yeast, suggesting coordination between both processes[154]. Is Erf2-Erf4 also involved in general stress response? In the rest of this chapter, I present a series of preliminary observations to support the role of the Erf2-Erf4 PAT in the stress response pathway.

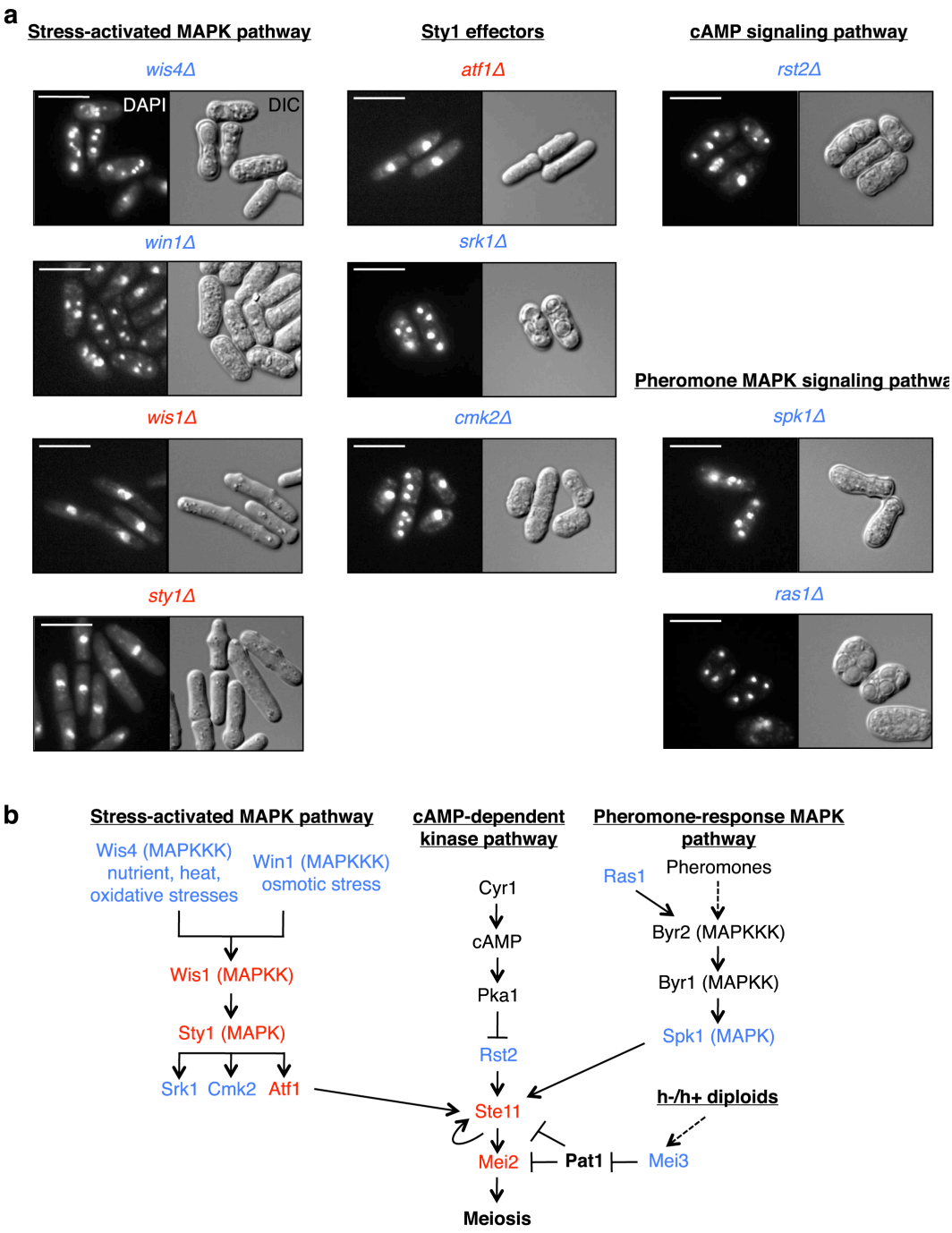

Figure 4.3 | Epistasis analysis reveals that Erf2-induced meiosis requires the SAPK pathway. a, DAPI (left) and DIC (right) images of haploid cells 96 h after *erf2* and *erf4* co-overexpression. Cells were maintained in the presence of nutrients at permissive temperature. Scale bars, 10 μm. **b,** Signaling pathways involved in the commitment to sexual differentiation in fission yeast. Red, gene products are required for Erf2-induced meiosis. Blue, gene products are not required for Erf2-induced meiosis. Activation and inhibition are represented by arrows and crossing bars, respectively.

erf2*Δ *cells are inviable at high temperatures

First, *erf2*Δ and *erf4*Δ cells are inviable at 36 °C (Fig. 4.4). Notably, no significant growth defects was observed at 34 °C, the restrictive temperature for inactivating Pat1 in the synchronous meiosis experiments described in the Chapter 3, suggesting that this growth defect at high temperatures does not contribute to the meiotic delay of e*rf2*Δ cells. In contrast, deletion of the other PATs does not affect growth at higher temperatures, indicating a specific role of the Erf2-Erf4 PAT in maintaining cell viability at elevated temperatures.

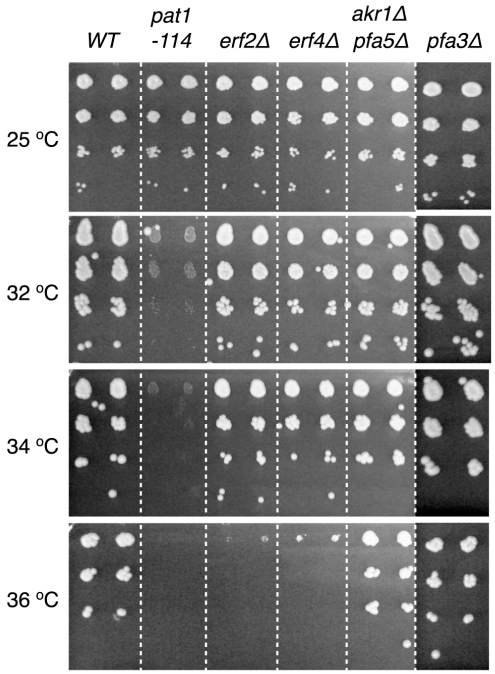

Figure 4.4 | *erf2*Δ and *erf4*Δ cells are temperature sensitive. Serial 10-fold dilutions of exponentially growing cultures of the indicated strains, normalized to the same OD, were spotted on YE4S plates and incubated for 4 days at the indicated temperatures. The *pat1-114* strain was used as a positive control for temperature sensitivity. The deletions were made in a *pat1*$^{+}$ wild type background.

***erf2*Δ cells are delayed in G1 arrest during nitrogen starvation**

Second, *erf2*Δ cells are delayed in their nitrogen starvation response. When homothallic fission yeast cells are subjected to depravation of a nitrogen source, they arrest at G1 of the cell cycle prior to mating and sporulation. Mutants deficient in sty1 or atf1 deficient in G1 arrest and sterile[154, 155]. Compared to wild type cells, *erf2*Δ cells arrest much less efficiently at G1 and arrest in these cells takes a longer time, as observed by the relative sizes of the 1C peak 8 h after nitrogen depletion (Fig. 4.5a). This inefficient G1 arrest in *erf2*Δ cells is accompanied by the appearance of misshapened cells with abnormally thick septa (Fig. 4.5a).

To determine whether Erf2 PAT activity has an impact on the global protein palmitoylation during nitrogen starvation, I profiled palmitoylated proteins by in-gel fluorescence at different times after transfer to a nitrogen-free medium. In wild type cells, palmitoylation of at least two distinct substrates between 25-37 kDa was maintained for 7-8 h after nitrogen removal despite large-scale protein degradation as observed by Coomassie staining of the gel (Fig. 4.5b). On the other hand, in *erf2*Δ cells, palmitoylation of these substrates were only sustained for 3-4 h after nitrogen removal (Fig. 4.5b). It would be interesting to determine what these Erf2 substrates are and how they contribute to G1 arrest in response to nitrogen depletion.

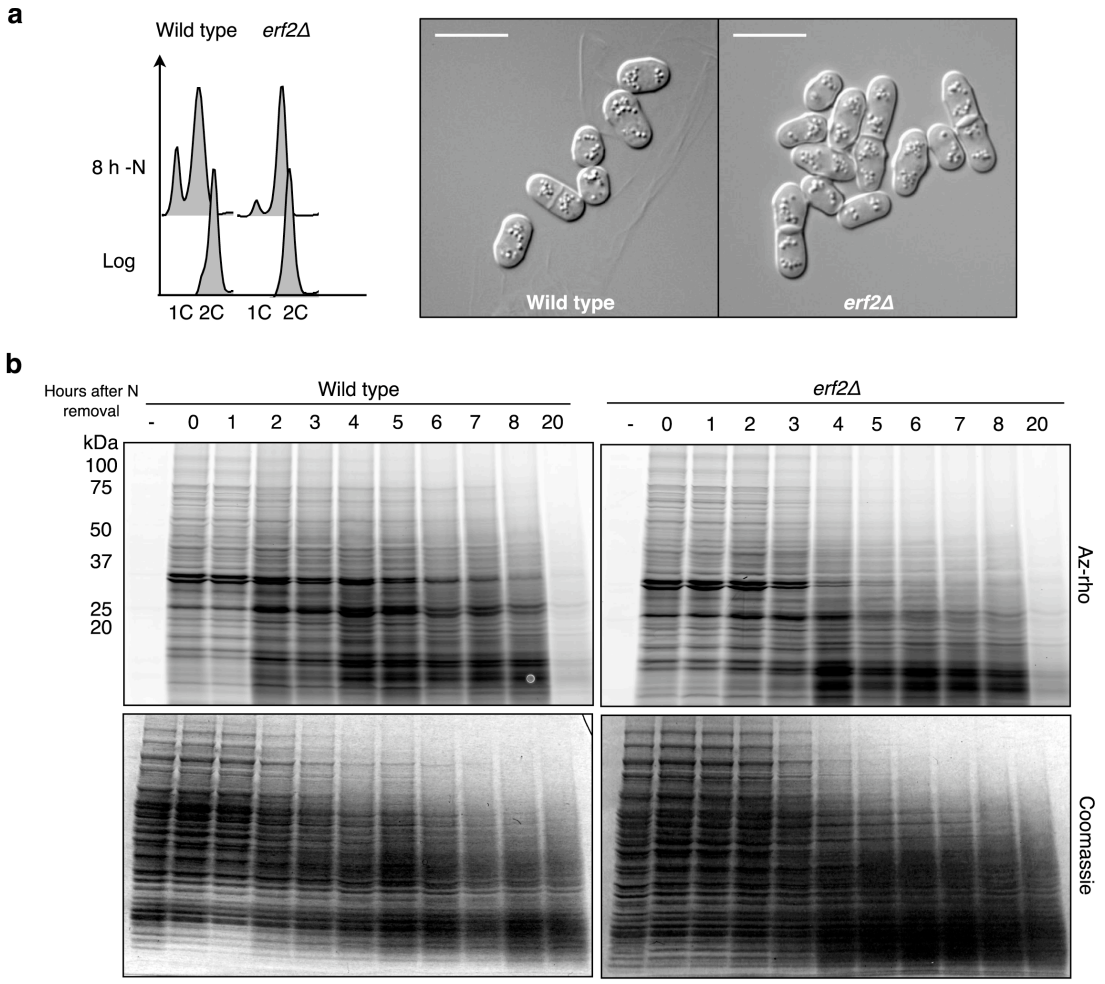

Figure 4.5 | *erf2*Δ cells are defective in G1 arrest in response to nitrogen starvation. a, Exponentially growing cells were filter-washed and transferred to nitrogen-free medium for the indicated times. Right panel: DNA content analysis of indicated cells pre- and 8 h post- nitrogen removal. Left panels: DIC images of the indicated cells 8 h after nitrogen removal. Scale bars, 10 μm. **b,** Alk-16 fluorescence profiles of palmitoylated substrates of indicated strains at different times after nitrogen removal (top panels) and Coomassie staining of the gels (bottom panels). (-): DMSO controls.

To investigate whether *erf2*Δ cells can sense nutritional cues, I performed the following nutritional shift experiment. It was previously reported that cells shifted from a good nitrogen source (glutamate) to a poor nitrogen source (proline) are advanced into mitosis, which is observed as a transient increase in the proportion of dividing cells and a reduced cell length at division[156]. It is evident that *erf2*Δ cells, like wild type cells, are able to sense and respond to the nutritional glutamate-proline downshift by advancing mitotic onset, which leads to a peak in the percentage of dividing cells about 1 h after nutritional shift and a reduced cell size at division (Fig. 4.6). These results demonstrate that the delay in G1 arrest upon nitrogen starvation in *erf2*Δ cells was not due to their inability to sense nutritional cues.

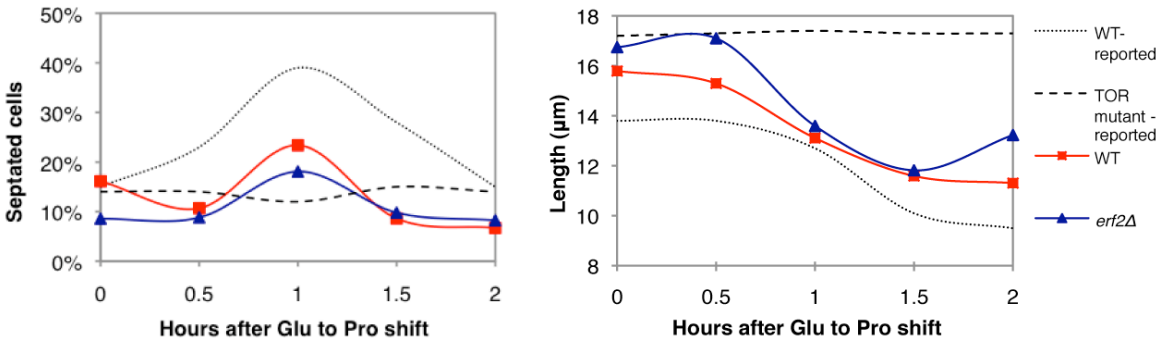

Figure 4.6 | *erf2*Δ cells respond to nutrient shifts. Exponentially growing cultures in glutamate-containing medium were shifted to proline-containing medium at t=0 h. At the indicated times after the shift, cells were stained with blankophor. The percentage of septated cells (left panel, n≥200) and cell length at division (right panel, n=20) were determined by counting and measuring blankophor-stained cells. Previously reported values for wild type cells and a TOR mutant that is unable to respond to nutritional shift are also included[156]. Although the trend holds, discrepancies between the two studies may be due to different growth temperatures (25 °C vs 32 °C) and the use of synchronous vs asynchronous cultures.

***erf2*Δ cells exhibit morphological defects during recovery from stationary phase**

Third, *erf2*Δ and *erf4*Δ cells exhibit are defective in growth recovery from stationary phase. Upon growth to saturation, fission yeast cells exit the mitotic cycle and enter stationary phase, accumulating in G1 or G2 depending on whether they are deprived of nitrogen or carbon, respectively[157]. Because of the growth medium used, when haploid cells are grown to high densities, glucose is usually limiting and cells accumulate in G2[157]. When the starved cultures were reinoculated into fresh medium, wild type cells exit stationary phase and resume normal cell division (Fig. 4.7a). In contrast, morphological defects were observed in *erf2*Δ and *erf4*Δ cells after dilution into fresh medium. These include the appearance of misshapened and multiseptated cells as well as excessive deposition of cell wall material and abnormally thick septa (Fig. 4.7a). The heterogeneity of these cells can be observed by the spread of data points on the forward/ side scatter plots compared to wild type (Fig. 4.7d). The failure by the multiseptated cells to complete cytokinesis is also reflected in the DNA content analysis, where a 4C peak is observed for *erf2*Δ cells (Fig. 4.7c). Interestingly, this phenotype is transient and resolves over time as the cells resume normal growth but can be observed if the culture is again starved and refed (Fig. 4.7b), suggesting that these defects in *erf2*Δ and *erf4*Δ cells are restricted to the initial recovery period from stationary phase.

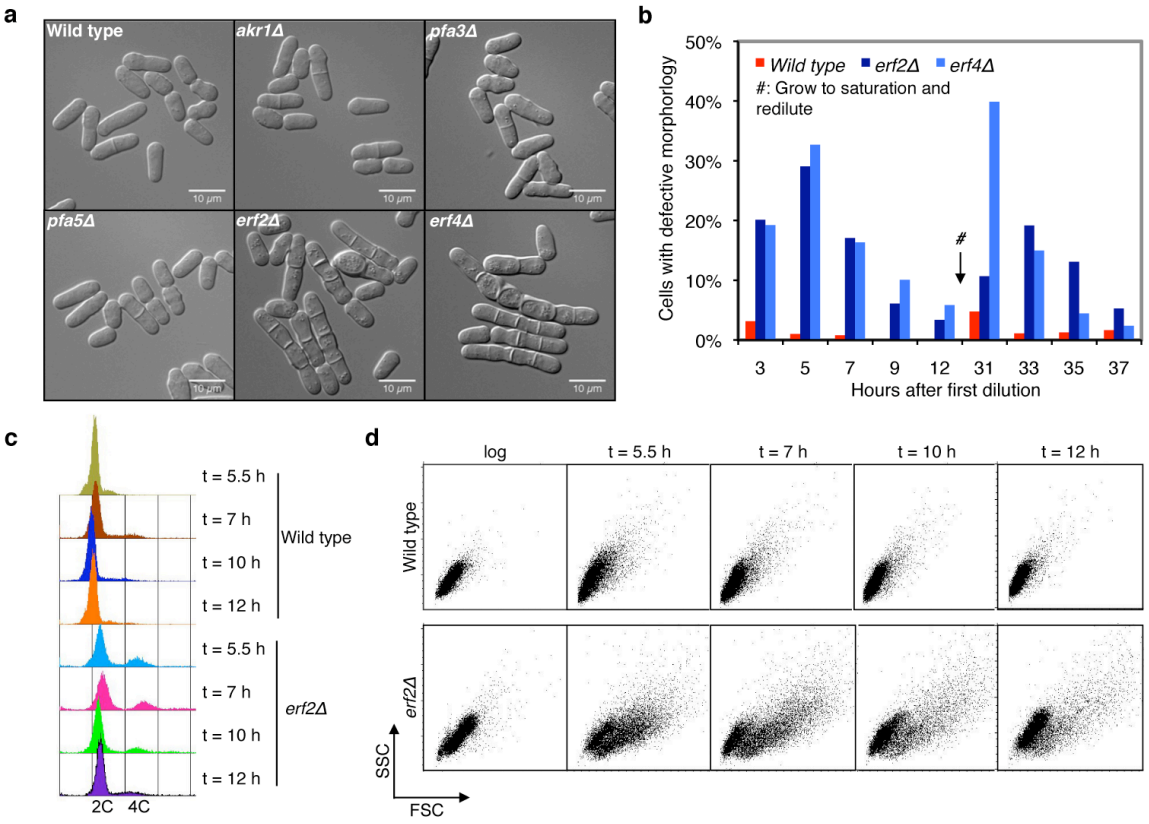

Figure 4.7 | *erf2*Δ cells exhibit morphological defects during recovery from starvation at high cell density. Cultures at OD_{595} ~3 were incubated at 32 °C for 16 h prior to dilution into fresh medium. Indicated times refer to the time after starved cultures were diluted into fresh medium. **a,** DIC images of indicated strains 5.5 h after dilution of starved cultures into fresh medium. Scale bars, 10 μm. **b,** Percentage of cells with defective morphology (misshapened, multiseptated, excessive cell wall material) for indicated strains (n=200). #: cultures were grown to high density and then rediluted into fresh medium. **c,** DNA content analysis of indicated strains. **d,** Forward (FSC) and side (SSC) scatter plots of the indicated strains.

To determine whether Erf2 PAT activity has an impact on the global protein palmitoylation during recovery from stationary phase, I profiled palmitoylated proteins by in-gel fluorescence at different time points after dilution of the starved cultures into fresh medium. In wild type cells, there is a striking and reproducible increase in protein palmitoylation 1 h after refeeding the cultures (Fig. 4.8a). Interestingly, this increase in global protein palmitoylation, which is absent in *erf2*Δ cells (Fig. 4.8a), occurs before the appearance of the multiseptated *erf2*Δ cells as observed by the appearance of the 4C peak by flow cytometry analysis (Fig. 4.8b). It would be interesting to determine how these modified substrates contribute to recovery from stationary phase and if they are the same substrates that mediates the nitrogen starvation response.

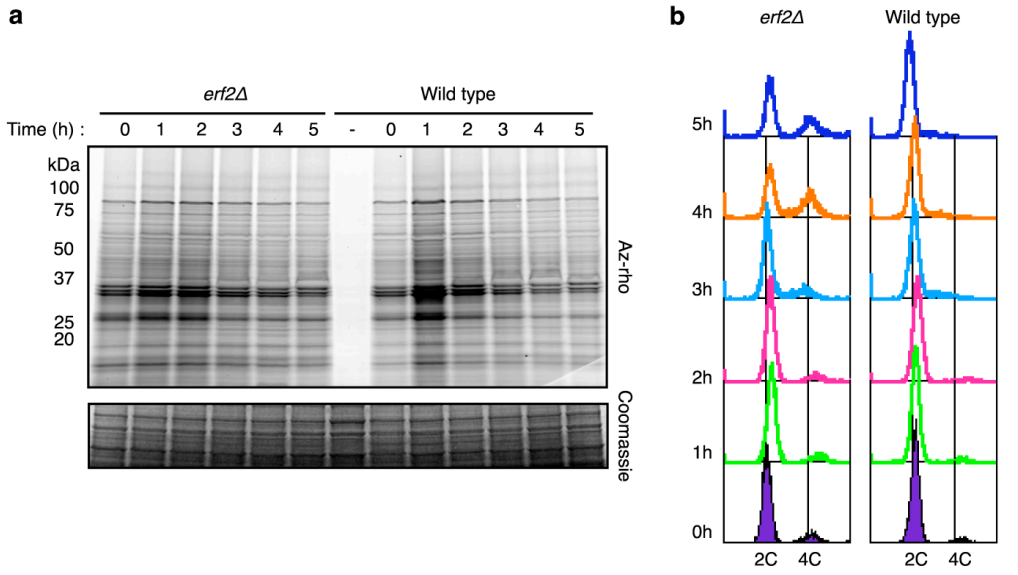

Figure 4.8 | Different palmitoylation profile of *erf2*Δ cells during recovery from starvation at high cell density. Cultures at OD_{595} ~3 were incubated at 32 °C for 16 h prior to dilution into fresh medium. Indicated times refer to the time after starved cultures were diluted into fresh medium. **a,** Alk-16 fluorescence profiles of palmitoylated substrates of indicated strains (top panels) and Coomassie staining of the gels (bottom panels). (-): DMSO controls. **b,** DNA content analysis of the indicated strains.

Summary and Discussion

In this chapter, I showed genetic interactions between *erf2*, *erf4* and important regulators of meiotic commitment as well as the components of the SAPK pathway. Together with the abnormal stress responses observed in *erf2*Δ and *erf4*Δ cells, these preliminary results suggest potential role(s) of the Erf2-Erf4 PAT in coordinating cellular response to stress and sexual differentiation.

In *S. pombe*, the SAPK pathway mediates a variety of cellular responses to heat, oxidative, nutritional, osmotic and UV stresses, controlling the initiation of sexual differentiation/mating and stationary phase survival as well as resistance to drugs and heavy metals. Sty1 is the core MAPK module in the SAPK pathway. Sty1 is activated by the Wis1 MAPKK[158, 159], which in turn is activated by MAPKKK's Wis4 and Win1[160-164] (Fig. 4.9a). Atf1 is a target transcription factor downstream of Sty1 and directs stress-specific gene expression[155, 165]. Consistent with Sty1 and its targets playing critical roles in general stress response, inactivation of *sty1* or *atf1* results in cells that are hypersensitive and fail to respond appropriately to a variety of stresses, including the inability to grow at high temperatures, survive stationary phase growth and arrest cell cycle in G1 upon nitrogen depletion[154, 155]. Similar phenotypes observed in *erf2*Δ cells suggest role(s) for Erf2 and protein palmitoylation in regulating the general stress response. This is further suggested by the altered global palmitoylation profiles in *erf2*Δ cells under these conditions. It would be interesting to identify the Erf2 substrates involved in these stress responses and determine how palmitoylation regulates their function. Nonetheless, more work will have to be done to validate the function of the

Erf2-Erf4 PAT in the general stress response and if it has a direct or indirect regulatory role on the SAPK pathway and meiotic commitment (Fig 4.9a).

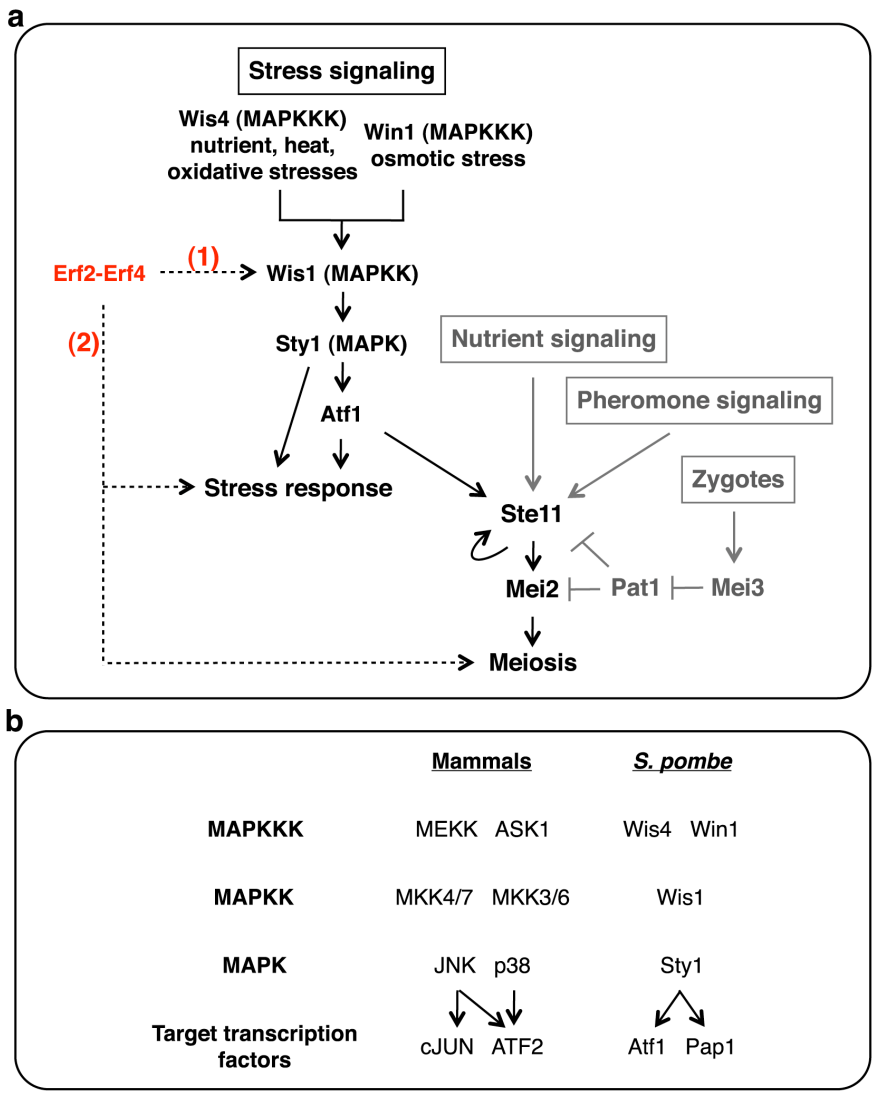

Figure 4.9 | A fission yeast model for palmitoylation-mediated regulation of signal transduction. a, A model for the role(s) of the Erf2-Erf4 PAT in coordinating cellular response to stress and sexual differentiation. Pathways indicated by dashed lines are conceptual and speculative. Activation and inhibition are represented by arrows and crossing bars, respectively. **b,** Homology between mammalian and *S. pombe* SAPK pathways.

Given the homology between components of the S. *pombe* and mammalian SAPK pathways, if validated, the system described above offers a powerful tool to study palmitoylation-mediated regulation of signal transduction. Besides structural homology between the SAPKs and transcription factors, the SAPK cascades in fission yeast and mammals are similarly regulated and control the activity of transcriptional factors that determine biological responses to various stresses (Fig. 4.9b). In mammals, the SAPK pathways are activated by environmental stimuli similar to *S. pombe* and are involved in apoptosis, DNA repair, cellular proliferation and differentiation[166]. Stress signals are delivered to the SAPKs by small GTPases of the Ras and Rho (Rac, Rho, Cdc42) families, some of which are known to be reversibly palmitoylated[11, 167]. Ras, for example, is proposed to signal through distinct MAPK/SAPK pathways from different membrane compartments[19, 26, 168], which is in turn regulated by palmitoylation[22, 24]. Nonetheless, evidence for differential signal outputs from each compartment is limited and largely confined to overexpression studies of molecules re-targeted to ectopic compartments. Therefore, this fission yeast system, in which a specific PAT function is coupled to a conserved signaling pathway, provides a tractable model to uncover the role of protein palmitoylation in generating spatial complexity of signaling networks in a physiological context.

Materials and Methods

Genotype of S. pombe strains used.

Strain	Genotype	Source
PN1	*h-*	Nurse lab
PN2283	*h- pat1-114*	Nurse lab
Mz53	*h- erf2Δ::NatMX6*	This study
Mz166	*h- erf4Δ::KanMX6*	This study
Mz126	*h- akr1Δ::KanMX6*	This study
Mz120	*h- pfa5Δ::KanMX6*	This study
Mz254	*h- akr1Δ::KanMX6 pfa5Δ::KanMX6*	This study
Mz364	*h- pfa3Δ::KanMX6 ade6-M216*	This study
Mz476	*h- pat1-114 nmt1:erf2::KanMX6 nmt1:erf4::KanMX6 rho3-HA$_3$::KanMX6*	This study
Mz518	*h- nmt1:erf2::KanMX6 nmt1:erf4::KanMX6 rho3-HA$_3$::KanMX6*	This study
Mz531	*h- pat1-114 nmt1:erf2::KanMX6 nmt1:erf4::KanMX6 mei2Δ::natMX6 ura4-D18*	This study
Mz626	*h- pat1-114 nmt1:erf2::KanMX6 nmt1:erf4::KanMX6 mei3Δ::ura4$^+$ ura4-D18*	This study
Mz630	*h- pat1-114 nmt1:erf2::KanMX6 nmt1:erf4::KanMX6 ste11Δ::ura4$^+$ ura4-D18*	This study
Mz632	*h- pat1-114 nmt1:erf2::KanMX6 nmt1:erf4::KanMX6 atf1Δ::ura4$^+$ ura4-D18*	This study
Mz564	*h- pat1-114 nmt1:erf2::KanMX6 nmt1:erf4::KanMX6 spk1Δ::ura4$^+$ ura4-D18*	This study
Mz551	*h- pat1-114 nmt1:erf2::KanMX6 nmt1:erf4::KanMX6 sty1Δ::ura4$^+$ ura4-D18*	This study
Mz571	*h- pat1-114 nmt1:erf2::KanMX6 nmt1:erf4::KanMX6 wis1Δ::ura4$^+$ ura4-D18*	This study
Mz624	*h- pat1-114 nmt1:erf2::KanMX6 nmt1:erf4::KanMX6 wis4Δ::ura4$^+$ ura4-D18*	This study
Mz644	*h- pat1-114 nmt1:erf2::KanMX6 nmt1:erf4::KanMX6 win1Δ::ura4$^+$ ura4-D18*	This study
Mz572	*h- pat1-114 nmt1:erf2::KanMX6 nmt1:erf4::KanMX6 rst2Δ::ura4$^+$ ura4-D18*	This study
Mz627	*h- pat1-114 nmt1:erf2::KanMX6 nmt1:erf4::KanMX6 srk1Δ::ura4$^+$ ura4-D18*	This study
Mz628	*h- pat1-114 nmt1:erf2::KanMX6 nmt1:erf4::KanMX6 cmk2Δ::ura4$^+$ ura4-D18*	This study

Strain construction and growth conditions. Standard media and methods were used[145, 146]. Strains used in this study are listed in Supplementary Table 1. All experiments were carried out in minimal medium (EMM) and minimal medium plus supplements (EMM4S) for prototrophic and auxotrophic strains respectively at 32 °C unless otherwise noted. When applicable, strains were generated by tetrad dissection and validated by marker segregation or PCR. Deletion strains and those expressing *erf2* and *erf4* from *nmt* promoters were constructed by PCR integration[147].

Epistasis analysis. Cultures were grown to midlog in EMM plus 10 mg/mL thiamine at 25 °C. *erf2* and/or *erf4* expression from *nmt* promoters was induced by filter-washing the cells three times with EMM as described above. The cells were resuspended in EMM and growth was maintained at 25 °C since these strains are constructed in a *pat1-114* background. The cultures were diluted with EMM approximately every 12 hours for the duration of each experiment to keep OD_{595} <0.6 and in the presence of nutrients. t=0 is defined as the time of thiamine removal. At t=96 h, cells were harvested and ethanol-fixed prior to DAPI staining and imaging.

Nitrogen starvation. Cultures were grown to midlog in EMM at 32 °C. Nitrogen was removed by filter-washing the cells three times with nitrogen-free EMM (EMM-N) and resuspending the cells in EMM-N. Cultures were then returned to 32 °C.

Glutamate to proline nutritional shift. These experiments were conducted as reported[156] with the exception that the cells were grown at 32 °C rather than 25 °C. Cultures were grown to midlog in EMM plus 1 mg/mL glutamate at 32 °C. Nutritional shift to a poorer nitrogen source was performed by filter-washing the cells three times with EMM plus 1.15 mg/mL proline. The cells were resuspened in EMM+proline and returned to growth at 32 °C.

Recovery from high cell density starvation. Starter cultures at OD_{595} ~3 in EMM were incubated for 16 h at 32 °C prior to dilution into fresh EMM at t=0. Indicated times refer to the time after starved cultures were diluted into fresh medium. Most analyses were performed at 5.5 h after dilution into fresh medium, when morphological defects were observed for a large proportion of *erf2Δ* cells.

Flow cytometry. DNA content was analyzed by flow cytometry using ethanol-fixed and propidium iodide-stained cells (2 μg/mL propidium iodide in 50 mM sodium citrate) on a BD FACS Calibur and analyzed using CellQuest software (BD).

Cell size measurements and cellular staining. For cell size measurements, live cells were stained with Blankophor (MP Biomedicals). For DNA staining, ethanol-fixed cells were stained with DAPI. Images were acquired in Metamorph (MDS Analytical Technologies) using an Axioplan 2 microscope (Carl Zeiss) and a CoolSNAP HQ camera (Roper Scientific). Cell size measurements were obtained using the Pointpicker plug-in of Image J (National Institute of Health).

Metabolic labeling and preparation of cell lysates. Cells were labeled with 10 μM of alk-16 (20-50 mM DMSO stock) for 15 min, washed once with PBS prior to liquid nitrogen freezing and storage at -80 °C. To prepare cell lysates, Brij lysis buffer (1% (v/v) Brij-97, 150 mM NaCl, 50 mM triethanolamine pH 7.4, 5× concentration of Roche EDTA-free protease inhibitor cocktail, 10 mM PMSF) and acid-washed glass beads (Sigma) were added to the frozen yeast cell pellets, which were lysed (3 x 20 s) using the Fastprep homogenizer (Thermo Scientific) at 4 min intervals to avoid overheating. Lysates were spun at 1,000 g for 5 min to remove cellular debris. Typical lysate protein concentrations of 5-10 mg/mL were obtained, as quantified using the BCA assay (Pierce).

CuAAC. For analyses of whole cell lysates, 50 μg of protein was diluted with Brij lysis buffer to a final volume of 44.5 μL, to which 5.5 μL of freshly mixed CuAAC reagents were added. The CuAAC reagents consisted of 1 μL az-Rho (5 mM stock solution in DMSO), 1 μL tris(2-carboxyethyl)phosphine hydrochloride (TCEP) (50 mM freshly prepared stock solution in deionized water), 2.5 μL tris[(1-benzyl-1*H*-1,2,3-triazol-4-yl)methyl]amine (TBTA) (2 mM stock solution in 1:4 DMSO:t-butanol) and 1 μL $CuSO_4 \cdot 5H_2O$ (50 mM freshly prepared stock solution in deionized water). After 1 hour at room temperature, proteins were methanol-chloroform precipitated to remove excess CuAAC reagents. The protein pellets were air-dried and resuspended in SDS buffer (4% (w/v) SDS, 150 mM NaCl, 50 mM triethanolamine pH 7.4) by sonication before SDS-PAGE.

In-gel fluorescence scanning. Fluorescence gels were visualized on a Typhoon 9400 variable mode imager (GE Healthcare) at excitation 532 nm/emission 580 nm. After fluorescence scanning, gels were stained with Coomassie Blue for determination of protein load. Images were processed using Image J.

CHAPTER 5

GENERAL DISCUSSION

This thesis describes the development and application of chemical approaches to study the function and regulation of protein *S*-palmitoylation, a uniquely reversible lipid modification that primarily serves as an important membrane targeting mechanisms in eukaryotes. Using fatty acid chemical reporters, combined with bioorthogonal labeling conditions involving Cu^{I}-catalyzed azide-alkyne cycloaddition, I was able to specifically and robustly detect lipid modified proteins by fluorescence. I further extended this method to allow fluorescent detection of two distinct protein modifications on proteins of interest and showed that this tandem imaging method can be used to efficiently monitor dynamic palmitoylation in cells. These protocols are currently used by most members of the lab on a routine basis as well as by multiple labs that we have collaborated with for studying various protein modifications. Combining chemical and genetic approaches in fission yeast, I showed that quantitative control of an acyltransferase complex during meiosis results in differential activity on cognate substrates and shaping of the palmitoylome, which is an important determinant for commitment to this major transitional event in *S. pombe*. Based on this study, I propose that rheostatic control of acyltransferase activity provides an important mechanism for regulating global protein palmitoylation and that this may have significant impacts on major developmental transitions.

Fission yeast is a relevant and complementary model for palmitoylation studies

The genetically amendable fission yeast *S. pombe*, combined with the use of chemical strategies that we have developed, is a relevant and complementary model for understanding basic control mechanisms and function of protein palmitoylation. Its simple PAT network facilitates dissection of the regulation and functional contribution of individual PATs. Interestingly, Swf1 is required for cell viability[134], and if validated to be a bona fide PAT, would be the first report of an essential DHHC-PAT. Initial efforts to make a conditional mutant by replacing the endogenous *swf1* promoter with thiamine-repressible *nmt* promoters failed, suggesting that regulated *swf1* expression is perhaps key to its function in maintaining cellular viability. Why is *swf1* essential? In budding yeast, SWF1 palmitoylates SNAREs required for membrane fusion[12, 45] and by homology, the putative SNARE substrates of Swf1 in fission yeast, Psy1 and Syb1 , are essential for cell viability[134, 169, 170]. Hence, it is likely Swf1 mediates essential cellular processes such as membrane trafficking and fusion. It will be interesting to study the function of Swf1 by means of temperature-sensitive or conditional switch-off alleles.

Although this thesis focuses on the palmitoylating machinery, some of the preliminary experiments that I have conducted indicates that *S. pombe* would also be a good system to study the depalmitoylation machinery. The fact that palmitate turns over faster on Ras1 than the protein argues for the existence of protein thioesterase(s). Disruption of the only Apt1 thioesterase homolog in fission yeast did not affect cell viability, cell growth at high temperature and stationary phase, mating efficiency, steady state Ras1 palmitoylation or global protein palmitoylation by in-gel fluorescence. It

remains to be determined if the palmitate half-lives of Ras1 and other palmitoylated substrates are different in wild type and *apt1*Δ cells. As discussed in Chapter 1, it is still unclear if APT1 and related isoforms are the main depalmitoylating enzymes or if there are potentially more enzymes to be uncovered. By homology to APT1 and inhibitor studies[14, 52, 84], it is likely that depalmitoylating enzymes are serine thioesterases. Given that there are hundreds of serine/cysteine hydrolases encoded in the mammalian genome, it is more practical to systematically screen candidate enzymes for the ability to depalmitoylate proteins in fission yeast.

PAT levels matter: shaping palmitoylomes by rheostatic control of PAT activity

Evidence for regulation of palmitoylating and depalmitoylating enzymes are limited and although individual PATs and APT1 have multiple substrates[12, 65, 77, 82], studies tend to focus on a single enzyme:substrate pair. For example, It would be interesting to determine if the activity-sensitive translocation of DHHC2 affects palmitoylation of other neuronal substrates besides PSD95 and if that contributes to modulation of synaptic activity[51]. Our study in fission yeast, where we identified and monitored three cognate Erf2-Erf4 substrates in vegetative and meiotic cells, offers a different perspective. We showed that physiological control of Erf2-Erf4 activity levels underlie the differential modification of its cognate substrates in distinct cellular states, suggesting that rheostatic control of single or multiple PAT activities is a basic mechanism by which cells shape their palmitoylomes. It raises the possibility that a single PAT can have different functions and regulate different cellular processes depending on its levels. We further showed that PAT level-dependent changes in palmitoylomes are important for cellular events such as

meiotic commitment in fission yeast. This highlights the importance of studying PATs and palmitoylomes in physiologically relevant contexts and provides a possible explanation for the extensive biochemical and functional overlap between the PATs in cellular studies involving non-physiological enzyme and substrate concentrations[68, 69].

Because of technical difficulties, it remains to be determined how levels of a PAT affect its substrate specificity. As previously discussed, one possibility is a difference in "specificity constant" (k_{cat}/K_M) and this is supported by the discovery of specificity determinants on both the PATs and their substrates that dictate enzyme-substrate interactions[66, 67]. If this were the case, one would predict higher k_{cat}/K_M for substrates that require lower PAT levels for effective palmitoylation and vice versa. I am currently investigating the possibility of recognition domains on the substrates by first swapping Rho3 and Ras1 palmitoylation motifs and asking if this affects the PAT level-dependence of each substrate. Another possibility is that depalmitoylating thioesterases or competing cellular factors target certain substrates more efficiently[40, 84, 86, 87]. This can be addressed by comparing the palmitate turnover on the different Erf2 substrates. Alternatively, level-dependent changes in PAT localization might alter substrate availability. For example, DHHC2 translocates to post-synaptic membranes upon neuronal stimulation and mediates increased palmitoylation and synaptic targeting of PSD95[51], implicating PAT compartmentalization as a means to control activity-induced palmitoylomes. In our study, however, subcellular localization is unlikely to account for the difference in Ras1 and Rho3 palmitoylation since both proteins are localized to the same compartments in vegetative cells[28, 144]. These proposed mechanisms are not mutually exclusive since

mobilization of PATs might be interpreted as an increase in local PAT concentration, which might then increase protein palmitoylation by mass action or by titration of competing cellular factors.

Conservation of specific PAT:substrate pairs

I showed that the Erf2 PAT in fission yeast, can have different substrate preferences and that specific PAT-substrate pairs are needed for efficient palmitate transfer, which is consistent with studies in mammals and budding yeast[12, 65]. Notably, the Erf2-Erf4:Ras1 PAT:substrate pairing in fission yeast is reminiscent of the ERF2-ERF4:RAS1/RAS2 and DHHC9-GCP16:H-/N-Ras pairs in budding yeast and human, respectively[58, 59]. Given that humans and yeast diverged about 1 billion years ago while *S. pombe* and *S. cerevisae* diverged 300-400 million years ago, this suggests an evolutionary selection for specific cognate PAT:substrate pairs, which would be unlikely if PATs have extensive overlapping substrate preferences and were able to freely substitute for each other. Interestingly, the Erf2-Erf4:Rho3 pair in fission yeast is also found in budding yeast[12], raising the possibility that DHHC9-GCP16 might also modify Rho GTPases in mammals. This is further suggested by the large number of mammalian Rho GTPases with cysteines close to the N- or C- terminus, which serve as potential palmitoylation sites (Fig. 5.1). If DHHC9-GCP16 indeed does palmitoylate Rho proteins, it would be interesting to determine if, like Erf2-Erf4, it can differentially modify Ras and Rho proteins.

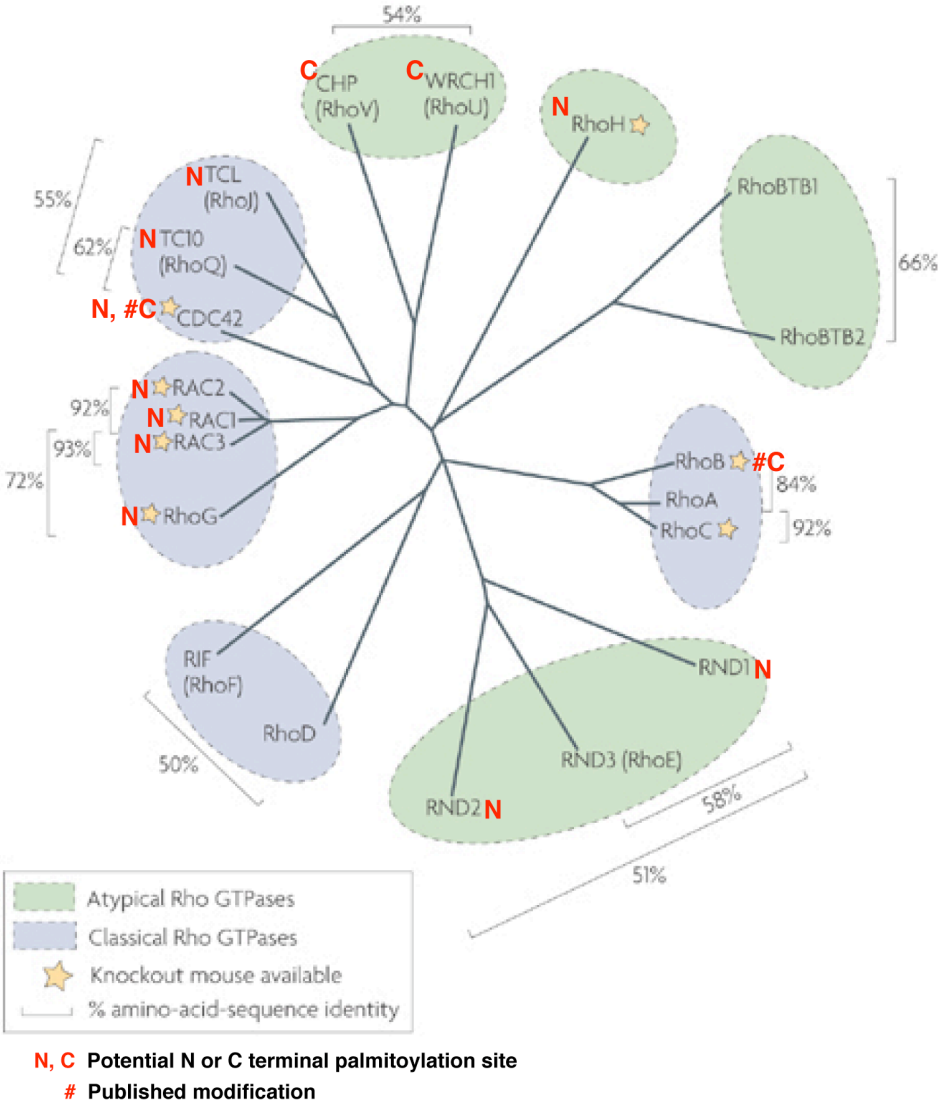

Figure 5.1 | Mammalian Rho GTPases. An unrooted phylogentic tree that is based on the ClustlW alignment of the amino-acid sequences of the 20 Rho GTPase proteins. The tree demonstrates the relationship between the different family members. EMBOSS pairwise alignment was used to calculate the percentage of amino-acid-sequence identity within subfamilies. High sequence similarity is found between proteins within the Rac and Rho subfamilies, whereas the other subfamilies are much less similar. Adapted from Heasman et al.[171]

Role of protein palmitoylation in other developmental transitions

The highly conserved Ras and Rho GTPases are essential for cellular differentiation and development in mammals[171]. Conservation of PAT function and specific PAT:substrate pairs between yeasts and humans suggests regulatory roles of palmitoylation in major developmental transitions in metazoa. This is supported by expression profiling experiments in flies and humans in which transcript levels of specific PATs vary widely across tissues[70, 71]. Neuronal differentiation signals were found to induce the PAT degradation via the ubiquitin-proteosome pathway[74]. In addition, PAT mutation and misregulation is associated with a variety of developmental defects as well as cancers in humans (summarized in Table 1.2). It will be interesting to determine if the control of PAT levels and regulation of palmitoylomes are important for cellular development and disease.

Rho3 coordinates regulation of membrane trafficking and polarized exocytosis

We demonstrated that both the actin nucleating formin For3 and exocyst subunit Exo70, but not the clathrin-adaptor Apm1, is required for the essential role of Rho3 in Erf2-induced meiosis. A recent study proposed that polarized exocytosis in fission yeast, rather than being a linear event of actin-dependent long-range vesicle transport followed by exocyst-dependent vesicle tethering at the PM[172], can be independently mediated by either pathway[173]. Physical and/or genetic interactions between Rho3 and For3 as well as different subunits of the exocyst complex indicates that Rho3 regulates and potentially coordinates these actin-dependent and exocyst-dependent secretory pathways[143, 144] (Fig.

5.2a). Interestingly, Rho3 is localized to the cell periphery as well as endomembranes (Golgi/endosome), raising the possibility that Rho3 signaling, like Ras1, may be compartmentalized. This is supported by studies showing that Rho3 colocalizes with For3 at the cell periphery[143, 144] and with Apm1 at endomembranes[174]. Physical interactions between Rho3 and For3 as well as Apm1 were validated biochemically[144, 174]. Spatial compartmentalization may explain how Rho3 can control multiple pathways including golgi/endosome trafficking, cytoskeletal organization and polarized exocytosis[143, 144, 174] (Fig. 5.2b). This can be tested by artificially targeting Rho3 to different compartments and measuring signaling outputs from each pathway biochemically and phenotypically.

How does Rho3 palmitoylation regulate meiotic commitment? If the compartmentalized signaling model is correct, one would expect factors that regulate the cellular distribution of Rho3 to affect its function. These factors include Cdc42 and exocyst localization[143, 144] and, as shown here, Erf2-mediated palmitoylation. I am currently constructing strains that express palmitoylation-deficient Rho3 to confirm this. The role of Rho3 palmitoylation may then be tested by looking at trafficking of known cycling substrates (e.g. vesicular SNAREs), secretion of acid phosphatase as well as endocytosis and vacuole sizes (FM4-64, membrane markers) in cells expressing wild type and palmitoylation-deficient Rho3. Delivery of cytoplasmic vesicles to discrete plasma-membrane domains is critical for establishing and maintaining cell polarity, neurite differentiation and regulated exocytosis. Anastasia and co-workers showed that blocking membrane traffic causes a mitotic checkpoint, suggesting a link between mitotic entry and membrane growth in budding yeast[175]. If Rho3 palmitoylation affects membrane

trafficking, signals that are coupled to membrane growth may explain how Rho3 regulates meiotic entry in fission yeast. These signals may be increased concentration of receptors and effectors at the plasma membrane or simply non-specific stress signaling as a result of defective membrane trafficking or cytoskeleton organization. The identity of these signals are unknown (Fig. 5.2b).

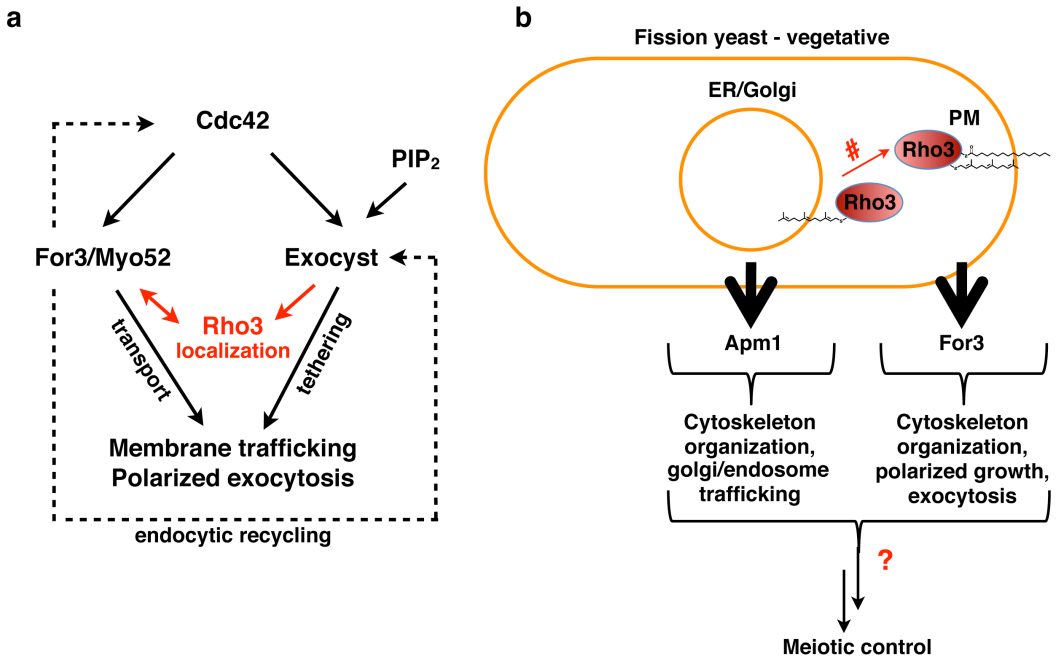

Figure 5.2 | Model for coordination of membrane trafficking and polarized exocytosis by Rho3 in *S. pombe*. a, Rho3 may coordinate parallel actin-dependent and exocyst-dependent secretory pathways. Cdc42 sets up cell polarity and regulates two parallel morphogenetic modules for polarized cell growth, the formin-dependent actin cable module and the exocyst module, contributing to transport and tethering of exocytic vesicles, respectively. The exocyst is also controlled by PIP_2 levels at the plasma membrane. Actin patches, and thus endocytosis, may contribute to maintaining polarized localization of Cdc42 and the exocyst. An effector of Rho3, For3 binds to both active forms of Cdc42 and Rho3. Rho3 localization is dependent on the exocyst but not vice versa. **b,** Speculative model of compartmentalized Rho3 signaling. # depicts the different factors such as cytoskeleton, exocyst function and palmitoylation may affect Rho3 distribution, which in turn affect its function by signaling though different effectors. How these different signals are integrated and contribute to meiotic entry are not known. PM: plasma membrane.

Multiple Erf2-Erf4 functions

Although I chose to focus on meiosis for my thesis, Erf2-Erf4 function is implicated in multiple cellular processes including stress response, mating, meiosis and sporulation. This raises an important question - how does a single PAT selectively control and coordinate these different pathways? This may be achieved via different substrates and we showed here that substrates of the same PAT can be differentially modified simply by changing PAT activity levels. It will be worthwhile to catalog the different Erf2 substrates that are modified during each of the cellular events and determine if their palmitoylation states affect coordination of these temporally separated processes: stress response ➔ mating ➔ meiosis ➔ sporulation.

As shown by others and in our study, palmitoylation is not an all-or-nothing process and the steady state palmitoylation levels of a specific substrate can vary over a large range. While I have focused on the high and low palmitoylation levels of Rho3 in meiotic and vegetative cells respectively, it remains to be seen if intermediate Rho3 palmitoylation has a function in the different cellular processes. In the case of PSD95, whose palmitoylation has been shown to affect synaptic clustering and signaling strength[39, 51, 176-178], one expects a positive correlation between synaptic strength and the levels of steady state PSD95 palmitoylation.

Model organisms and technical advances are important for new discoveries

Technical difficulties in palmitoyl enzymology and detection/analysis hindered palmitoylation studies for more than 30 years since the initial discovery of the

modification[179]. In the last decade, the use of model organisms and technical advances in the detection and analysis of palmitoylation have propelled this emerging field (Fig. 5.1).

Yeast genetics have proven fruitful in landmark discovery of the PATs as the main palmitoylating enzymes[57, 58, 63] when biochemical attempts to purify them were complicated by the instability of these enzymes once they are extracted from membranes[180, 181]. The budding yeast model has been and continues to be instrumental in our understanding of PAT specificity[12, 66, 69] and mechanism of palmitate transfer[61, 62].

The advent of the acyl-biotin exchange protocol as well as bioorthogonal chemical reporters described in this thesis enabled identification of palmitoylomes, greatly expanding the scope of the modification and providing unprecedented insights into the cellular function of palmitoylation. Furthermore, these two approaches allowed robust non-radioactive detection of palmitoylated proteins expressed at endogenous levels, reducing experimental times and enabling faster testing of hypotheses.

Advanced microscopy techniques, in combination with semi-synthetic lipopeptides, offer unprecedented insights into the dynamics of protein palmitoylation. Photo-activation/bleaching of fluorescent palmitoylated proteins estimate protein-bound palmitate to turnover in milliseconds or seconds[22, 24], which is consistent with rapid physiological responses that can occur on the seconds time scale. This is in contrast to biochemical pulse-chase experiments, which yield palmitate half-life measurements in the order of minutes or hours potentially due to rapid recycling of the labeled fatty acid analogs. Use of semi-synthetic proteins irreversibly linked to palmitate definitively showed the importance of the reversibility of the modification and how palmitate cycling

contributes to cellular distribution of modified proteins[22]. More recently, the design of a specific APT inhibitor, Palmostatin B[83, 84], potentially allows rapid temporal control of depalmitoylation activity and further dissection of the palmitoylation kinetics in cells.

Together, these technical advances are beginning to reveal mechanistic and functional insights into the effect dynamic palmitoylation exerts on physiology and disease but tool development will continue to be critical for progress in the field. For example, there is still a need for specific PAT inhibitors since most existing palmitoylation inhibitors such as 2-bromopalmitate have pleiotropic effects on lipid metabolism[128]. On a similar note, development of activity-based probes that selectively react with active PATs or thioesterases will not only allow one to profile the functional states of these enzymes in normal and disease models (Fig. 5.3a), but also aid in the development of specific inhibitors. In addition, solving the structures of PATs will invaluable towards understanding the mechanism of palmitate transfer to substrates and origin of substrate selectivity as well as greatly facilitate the design of selective activity-based probes and inhibitors. Understanding what dictates enzyme:substrate specificity will further help development of approaches that allows control of the palmitoylation state of specific proteins of interest. For instance, one can imagine engineering specificity determinants that can be appended onto a PAT and a protein of interest such that the latter will only be modified when this orthogonal PAT is expressed. Last but not least, given the evidence for interactions between different PTMs, palmitoylation should not be studied in isolation but in conjunction with other modifications, especially phosphorylation and other cysteine modifications.

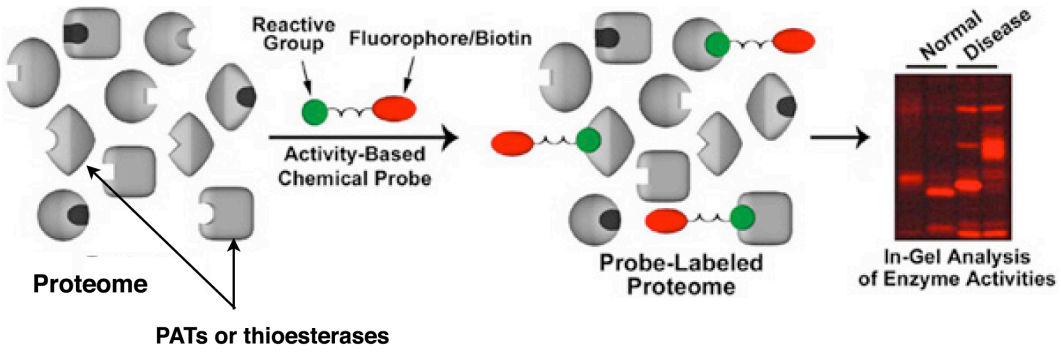

Figure 5.3 | Activity-based probes for palmitoylation studies. Activity-based probes (selective chemically reactive group with a detection/affinity handle) that specifically react with active PATs or thioesterases enable the profiling of functional states of the enzymes in normal and disease models. Figure adapted from the Cravatt lab (Scripps) website.

Concluding remarks

In conclusion, we have developed chemical strategies to efficiently detect and identify palmitoylated proteins in mammalian systems and by applying them in an alternative *S. pombe* model, uncovered a mechanism by which PATs regulate global protein palmitoylation as well as important cellular events such as meiosis. Our study also highlights the importance of studying the regulation and function of protein palmitoylation in physiologically relevant contexts. This is perhaps best demonstrated by a series of studies in neurons, which collectively showed that neuronal activity-driven regulation of PAT localization and protein nitrosylation modulates protein palmitoylation, which in turn modulates neuronal morphogenesis, receptor clustering and synaptic strength[39, 40, 51, 65, 177, 178]. In this thesis, we introduced a genetically tractable system with relatively simple enzymatic machinery and substrate "catalog" that is valuable towards understanding basic principles and control mechanisms of protein palmitoylation in a

physiological context. This work exemplifies how chemical strategies may be used in the fission yeast system to study the PAT-mediated regulation of palmitoylation and the associated effects on cellular physiology. In the process, new questions about multiple PAT functions, differential substrate specificity and potential regulatory roles of palmitoylation are generated, which can be systematically tested using this system. The next few years represent a challenging and exciting time that promises to reveal fundamental insights into protein palmitoylation, which one hopes may one day lead to novel therapeutic strategies to control diverse physiological processes.

APPENDIX 1 - Proteomics data (Pages 134-146)

Identified proteins	Accession Number	MW (kDa)	Vegetative WT (spectral counts)		Meiotic WT (spectral counts)			Meiotic *erf2Δ* (spectral counts)	
			DMSO	alk-16	DMSO	alk-16	Net counts	DMSO	alk-16
Isp3	**SPAC1F8.05**	**20**	**3**	**2**	**30**	**99**	**69**	**8**	**4**
P-type ATPase	SPAC6C3.06c	117	0	7	0	14	14	9	9
Vps13b	SPBC16C6.02c	339	4	3	0	11	11	4	4
Rho3	**SPAC23C4.08**	**23**	**0**	**2**	**0**	**11**	**11**	**0**	**0**
Sir2	SPBC16D10.07c	53	4	7	0	8	8	0	0
Noc1	SPAC4F10.09c	98	2	4	0	8	8	0	3
Rad24	SPAC8E11.02c	30	7	10	0	6	6	0	3
Cid11	SPBC1685.06	55	4	6	0	6	6	0	0
Dcr1	SPCC188.13c	158	3	0	0	6	6	0	3
Pre5	SPAC6G10.04c	30	0	0	0	6	6	0	0
Gpd1	SPBC215.05	42	0	2	0	6	6	2	3
Hxk1	SPAC24H6.04	54	0	2	0	6	6	0	2
Sak1	SPAC3G9.14	86	3	0	0	5	5	0	2
Ferric-chelate reductase	SPBC947.05c	65	2	2	0	5	5	2	2
Ucp8	SPBC83.01	98	0	0	0	5	5	0	0
Mss1	SPAC222.05c	55	0	0	0	5	5	0	0
Pli1	SPAC1687.05	81	0	0	0	5	5	0	0
Non classical export pathway protein	SPBC1685.13	20	0	0	0	5	5	0	0
Top1	SPBC1703.14c	94	0	0	0	5	5	0	2

Identified proteins	Accession Number	MW (kDa)	Vegetative WT (spectral counts)		Meiotic WT (spectral counts)			Meiotic *erf2Δ* (spectral counts)	
Alpha,alpha-trehalose-phosphate synthase	SPACUNK4.16c	107	0	0	0	5	5	0	2
UPF0061 family protein	SPAC20G4.05c	64	0	0	0	5	5	0	2
Nep1	SPBC17D11.01	47	0	2	0	5	5	0	0
Adf1	SPAC20G4.06c	16	0	2	0	5	5	0	0
Trk1	SPAC3F10.02c	96	0	4	4	9	5	2	0
Rpl14	SPAC1805.13	15	9	16	0	4	4	0	0
Uso1	SPAC29E6.03c	122	4	6	0	4	4	0	0
Oxa101	SPAC9G1.04	42	3	0	0	4	4	0	2
Spt8	SPBC14C8.17c	58	3	2	0	4	4	0	0
Hrp3	SPAC3G6.01	159	3	4	0	4	4	4	6
Cytoskeletal protein binding protein Sla1 family	SPAC16E8.01	155	2	0	0	4	4	0	0
Membrane transporter	SPAC3H1.06c	64	2	0	0	4	4	0	0
Ptc4	SPAC4A8.03c	44	2	2	0	4	4	0	0
Rhp54	SPAC15A10.03c	97	2	2	0	4	4	0	2
Rpl22	SPAC11E3.15	13	2	2	0	4	4	0	2
NAD/NADH kinase	SPAC3H5.11	45	2	3	0	4	4	2	3
Sir1	SPAC10F6.01c	164	2	3	0	4	4	0	0
Vps4	SPAC2G11.06	48	0	0	0	4	4	2	0
Klp8	SPAC144.14	57	0	0	0	4	4	2	0
Coq3	SPCC162.05	30	0	0	0	4	4	2	0
Lhs1	SPAC1F5.06	95	0	0	0	4	4	2	2

Identified proteins	Accession Number	MW (kDa)	Vegetative WT (spectral counts)		Meiotic WT (spectral counts)			Meiotic *erf2Δ* (spectral counts)	
Rsc7	SPCC1281.05	44	0	0	0	4	4	0	0
cdc23	SPBC1347.10	67	0	0	0	4	4	0	0
DuF1740 family protein	SPBC20F10.05	113	0	0	0	4	4	0	0
Conserved fungal protein	SPCPB16A4.02c	38	0	0	0	4	4	0	0
Grx3	SPCC1450.06c	18	0	0	0	4	4	0	0
Suc22	SPBC25D12.04	45	0	0	0	4	4	0	0
Ght5	SPCC1235.14	60	0	0	0	4	4	0	0
FAD-dependent amino acid oxidase	SPAC6G10.06	42	0	0	0	4	4	0	0
Rrp6	SPAC1F3.01	90	0	0	0	4	4	0	0
Htb1	SPCC622.09	14	0	0	0	4	4	0	0
zf-CCHC type zinc finger protein	SPAC683.02c	25	0	0	0	4	4	0	0
Ptc2	SPCC1223.11	41	0	0	0	4	4	0	0
ATP-dependent RNA helicase, eIF4A related	SPAC1F5.10	45	0	0	0	4	4	0	0
Rds1	SPAC343.12	44	0	0	0	4	4	0	0
Shf1	SPAC22F8.12c	19	0	0	0	4	4	0	2
Aif1	SPAC26F1.14c	62	0	0	0	4	4	0	2
Ppp1	SPBC19F5.05c	69	0	0	0	4	4	0	2
Mrpl32	SPBC1604.13c	12	0	0	0	4	4	0	2
Rpn2	SPBC17D11.07c	107	0	2	0	4	4	4	2
Ubp22	SPCC188.08c	129	0	2	0	4	4	4	3
Pga2	SPBC27.01c	16	0	2	0	4	4	3	2

Identified proteins	Accession Number	MW (kDa)	Vegetative WT (spectral counts)		Meiotic WT (spectral counts)			Meiotic *erf2Δ* (spectral counts)	
Arh1	SPBC3B8.01c	53	0	2	0	4	4	3	3
Spt5	SPAC23C4.19	109	0	2	0	4	4	2	0
Conserved eukaryotic protein	SPAC1687.04	57	0	2	0	4	4	0	0
Sequence orphan	SPBC405.02c	50	0	2	0	4	4	0	0
Str2	SPCC61.01c	66	0	2	0	4	4	0	2
transcription factor, zf-fungal binuclear cluster type	SPAC1399.05c	61	3	3	0	3	3	0	0
RNA binding protein	SPAC4G8.03c	88	2	2	0	3	3	0	0
Dbp9	SPCC1494.06c	67	2	2	0	3	3	0	0
guanyl-nucleotide exchange factor	SPAC11E3.11c	106	0	0	0	3	3	3	3
Mcm3	SPCC1682.02c	97	0	0	0	3	3	3	4
Pig-F	SPCC1450.15	57	0	0	0	3	3	2	2
Ubiquitin-protein ligase E3	SPBC947.10	77	0	0	0	3	3	2	2
Yop1	SPCC830.08c	21	0	0	0	3	3	2	2
Sequence orphan	SPAC821.03c	54	0	0	0	3	3	2	3
Sequence orphan	SPAC13G7.09c	16	0	0	0	3	3	0	0
AAA family ATPase, unknown biological role	SPBC947.01	72	0	0	0	3	3	0	0
Sec6	SPCC1235.10c	83	0	0	0	3	3	0	0
Ulp1	SPBC19G7.09	65	0	0	0	3	3	0	0
Apl4	SPCP1E11.06	96	0	0	0	3	3	0	0

Identified proteins	Accession Number	MW (kDa)	Vegetative WT (spectral counts)		Meiotic WT (spectral counts)			Meiotic *erf2Δ* (spectral counts)	
D123 family	SPAP27G11.03	37	0	0	0	3	3	0	0
Hst4	SPAC1783.04c	47	0	0	0	3	3	0	0
Pinin homolog	SPAC26F1.02	23	0	0	0	3	3	0	0
CorA family magnesium ion transporter	SPAC17A2.14	71	0	0	0	3	3	0	0
Aspartate kinase	SPBC19F5.04	57	0	0	0	3	3	0	0
Fumarate lyase superfamily	SPBC8E4.05c	50	0	0	0	3	3	0	0
Transcription factor	SPAPB1A11.04c	79	0	0	0	3	3	0	0
tRNA nucleotidyltransferase	SPAC1093.04c	58	0	0	0	3	3	0	0
WD repeat protein, human WDR55 family	SPAC1A6.02	40	0	0	0	3	3	0	0
Biotin-protein ligase	SPBC30D10.07c	71	0	0	0	3	3	0	0
Transcription factor	SPBC19C7.10	48	0	0	0	3	3	0	0
Ctf1	SPBC3B9.11c	40	0	0	0	3	3	0	0
Sec15	SPCC1183.01	91	0	0	0	3	3	0	0
Nak1	SPBC17F3.02	71	0	0	0	3	3	0	0
Rpt6	SPBC23G7.12c	45	0	0	0	3	3	0	0
Nucleoporin Nup157/170	SPAC890.06	148	0	0	0	3	3	0	0
Mitochondrial citrate transporter	SPAC19G12.05	32	0	0	0	3	3	0	0
Amidase	SPAC869.01	65	0	0	0	3	3	0	0
Uve1	SPBC19C7.09c	69	0	0	0	3	3	0	0
Leu3	SPBC3E7.16c	64	0	0	0	3	3	0	0

Identified proteins	Accession Number	MW (kDa)	Vegetative WT (spectral counts)		Meiotic WT (spectral counts)			Meiotic *erf2Δ* (spectral counts)	
Adaptin	SPAC1F3.05	57	0	0	0	3	3	0	0
Ubp6	SPAC6G9.08	52	0	0	0	3	3	0	0
ZIP zinc transporter 1	SPAP8A3.03	50	0	0	0	3	3	0	0
Taf1	SPAC1002.04c	23	0	0	0	3	3	0	0
Phx1	SPAC32A11.03c	104	0	0	0	3	3	0	0
Pex7	SPAC17D4.01	35	0	0	0	3	3	0	0
Gln1	SPAC23H4.06	40	0	0	0	3	3	0	0
Ptr6	SPAC13F5.02c	45	0	0	0	3	3	0	0
Ubi1	SPAC11G7.04	15	0	0	0	3	3	0	0
Las1-like protein	SPBC16C6.12c	54	0	0	0	3	3	0	0
Gpi18	SPAC18B11.05	49	0	0	0	3	3	0	0
AMP-activated protein kinase beta subunit	SPCC1919.03c	33	0	0	0	3	3	0	0
Cbs2	SPAC1556.08c	37	0	0	0	3	3	0	0
Sdh3	SPCC330.12c	20	0	0	0	3	3	0	0
DUF726 family protein	SPAC607.08c	64	0	0	3	6	3	0	3
Sti1	SPCC645.14c	66	0	2	2	5	3	3	3
Pmc2	SPAC2F7.04	51	3	4	0	2	2	0	0
Rps21	SPBC18E5.06	10	3	5	0	2	2	0	0
Lsk1	SPAC2F3.15	67	2	2	0	2	2	0	0
Swi2	SPAC1142.03c	82	2	2	0	2	2	0	0
Dbp3	SPBC17D1.06	64	2	2	0	2	2	0	0
PQ loop protein	SPAC2E12.03c	32	2	3	0	2	2	3	5

Identified proteins	Accession Number	MW (kDa)	Vegetative WT (spectral counts)		Meiotic WT (spectral counts)			Meiotic *erf2Δ* (spectral counts)	
Ypt3	SPAC18G6.03	24	2	3	0	2	2	0	0
TRP-like ion channel	SPCC663.14c	77	0	0	0	2	2	2	2
Irs1	SPBC8D2.06	123	0	0	0	2	2	2	3
Lsd90	SPBC16E9.16c	82	0	0	0	2	2	2	3
Pdt1	SPAC27F1.08	58	0	0	0	2	2	2	3
alpha-1,2-mannosyltransferase	SPBC16H5.09c	44	0	0	0	2	2	2	3
Rec11	SPCC4E9.01c	107	0	0	0	2	2	0	0
Conserved fungal protein	SPCC1494.08c	31	0	0	0	2	2	0	0
Nat10	SPAC20G8.09c	116	0	0	0	2	2	0	0
Abp2	SPBC1861.02	60	0	0	0	2	2	0	0
Sid4	SPBC244.01c	74	0	0	0	2	2	0	0
Aminotransferase class-III, unknown specificty	SPAC27F1.05c	53	0	0	0	2	2	0	0
Mfh1	SPAC9.05	97	0	0	0	2	2	0	0
Conserved fungal protein	SPAC2F3.14c	38	0	0	0	2	2	0	0
Glc9	SPAC17A5.09c	35	0	0	0	2	2	0	0
Sequence orphan	SPBC2G2.14	60	0	0	0	2	2	0	0
Atp23	SPCC320.12	22	0	0	0	2	2	0	0
Spermidine family transporter	SPBC36.03c	59	0	0	0	2	2	0	0
Mug100	SPBC16E9.07	36	0	0	0	2	2	0	0

Identified proteins	Accession Number	MW (kDa)	Vegetative WT (spectral counts)		Meiotic WT (spectral counts)			Meiotic *erf2Δ* (spectral counts)	
DUF1716 family protein	SPAC1952.06c	65	0	0	0	2	2	0	0
Ltv1	SPAC3F10.17	44	0	0	0	2	2	0	0
Arg7	SPBC1773.14	52	0	0	0	2	2	0	0
Cmk1	SPACUNK12.02c	38	0	0	0	2	2	0	0
Mitochondrial tRNA	SPAC12B10.08c	52	0	0	0	2	2	0	0
Ran GTP-binding protein	SPAC31A2.10	51	0	0	0	2	2	0	0
Acetyl-CoA hydrolase	SPAC1952.09c	58	0	0	0	2	2	0	0
C2 domain protein	SPCC962.01	156	0	0	0	2	2	0	0
Transcription factor	SPAC105.03c	81	0	0	0	2	2	0	0
Arrestin/ PY protein 1	SPAC31A2.12	66	0	0	0	2	2	0	0
Tht1	SPAC13C5.03	63	0	0	0	2	2	0	0
Sbh1	SPBC2G2.03c	10	0	0	0	2	2	0	0
Nap1	SPCC364.06	44	0	0	0	2	2	0	0
Sequence orphan	SPAC7D4.13c	36	0	0	0	2	2	0	0
Ark1	SPCC320.13c	41	0	0	0	2	2	0	0
Svf1	SPCC584.11c	43	0	0	0	2	2	0	0
LEA domain protein	SPAC23C4.05c	50	0	0	0	2	2	0	0
Short chain dehydrogenase	SPAC19A8.06	45	0	0	0	2	2	0	0
TLDc domain protein 2	SPBC21.02	59	0	0	0	2	2	0	0

Identified proteins	Accession Number	MW (kDa)	Vegetative WT (spectral counts)		Meiotic WT (spectral counts)			Meiotic *erf2Δ* (spectral counts)	
NADPH-dependent diflavin oxidoreductase	SPAC1296.06	64	0	0	0	2	2	0	0
Gma12	SPCC736.04c	43	0	0	0	2	2	0	0
Rsv2	SPBC1105.14	69	0	0	0	2	2	0	0
Pgp1	SPCC1259.10	46	0	0	0	2	2	0	0
Mep33	SPBC28F2.02	33	0	0	0	2	2	0	0
Rft1	SPBC887.19	60	0	0	0	2	2	0	0
Mitochondrial m-AAA protease	SPBC543.09	85	0	0	0	2	2	0	0
Hta2	SPAC19G12.06c	14	0	0	0	2	2	0	0
Rae1	SPBC16A3.05c	39	0	0	0	2	2	0	0
Hhp1	SPBC3H7.15	42	0	0	0	2	2	0	0
Wee1	SPCC18B5.03	96	0	0	0	2	2	0	0
Pfs2	SPAC12G12.14c	58	0	0	0	2	2	0	0
Cytoskeletal signaling protein	SPAC637.13c	56	0	0	0	2	2	0	0
Mcp2	SPCC1682.08c	79	0	0	0	2	2	0	0
Mug73	SPCC31H12.02c	35	0	0	0	2	2	0	0
Mbx1	SPBC19G7.06	51	0	0	0	2	2	0	0
Apc11	SPAC343.03	11	0	0	0	2	2	0	0
Nudix family hydrolase	SPAC14C4.10c	38	0	0	0	2	2	0	0
DUF544 family protein	SPAC12G12.11c	42	0	0	0	2	2	0	0

Identified proteins	Accession Number	MW (kDa)	Vegetative WT (spectral counts)		Meiotic WT (spectral counts)			Meiotic *erf2Δ* (spectral counts)	
Ppk29	SPBC557.04	96	0	0	0	2	2	0	0
Rfc2	SPAC23D3.02	38	0	0	0	2	2	0	0
Sgf29	SPBC1921.07c	28	0	0	0	2	2	0	0
Nicotinic acid plasma membrane transporter	SPAC1002.16c	55	0	0	0	2	2	0	0
Peptidase	SPCC1259.02c	92	0	0	0	2	2	0	0
Steriod dehydrogenase	SPAC7D4.09c	32	0	0	0	2	2	0	0
Rhp18	SPBC1734.06	43	0	0	0	2	2	0	0
Membrane transporter	SPCC965.13	60	0	0	0	2	2	0	0
RINT1 family protein	SPBC691.02c	79	0	0	0	2	2	0	0
Rad17	SPAC14C4.13	69	0	0	0	2	2	0	0
Ura3	SPAC57A10.12c	48	0	0	0	2	2	0	0
Fun1	SPCC18.18c	56	0	0	0	2	2	0	0
Erv41	SPBC2G5.04c	38	0	0	0	2	2	0	0
Sce3	SPBC18H10.04c	43	0	0	0	2	2	0	0
IMP 5'-nucleotidase	SPBC30D10.03c	46	0	0	0	2	2	0	0
Rax2	SPAC6F6.06c	128	0	0	0	2	2	0	0
CTNS domain protein	SPAC4C5.03	34	0	0	0	2	2	0	0
Nup120	SPBC3B9.16c	130	0	0	0	2	2	0	0
Asa1	SPAC1006.02	41	0	0	0	2	2	0	0

Identified proteins	Accession Number	MW (kDa)	Vegetative WT (spectral counts)		Meiotic WT (spectral counts)			Meiotic *erf2Δ* (spectral counts)	
Sequence orphan	SPAC24C9.04	14	0	0	0	2	2	0	0
Spp2	SPBC17D11.06	53	0	0	0	2	2	0	0
Clr2	SPAC1B3.17	62	0	0	0	2	2	0	0
Tea1	SPCC1223.06	127	0	0	0	2	2	0	0
Sequence orphan	SPAC17A2.07c	20	0	0	0	2	2	0	0
Nab2	SPAC14C4.06c	34	0	0	0	2	2	0	0
Conserved protein	SPAC6G9.01c	10	0	0	0	2	2	0	0
Ubiquitin-protein ligase E3	SPBC16G5.03	31	0	0	0	2	2	0	0
Atp6	SPMIT.07	28	0	0	0	2	2	0	0
Histone acetyltransferase complex subunit	SPAC25H1.06	47	0	0	0	2	2	0	0
SRR1 family protein	SPBC14C8.13	29	0	0	0	2	2	0	0
Sgf11	SPAC57A10.14	13	0	0	0	2	2	0	0
Atf31	SPAC22F3.02	24	0	0	0	2	2	0	0
Swd1	SPAC23H3.05c	45	0	0	0	2	2	0	0
Short chain dehydrogenase	SPAC977.08	26	0	0	0	2	2	0	0
Eng2	SPAC23D3.10c	78	0	0	0	2	2	0	0
Swd1	SPBC354.02c	53	0	0	0	2	2	0	0
Mis16	SPCC1672.10	48	0	0	0	2	2	0	0

Identified proteins	Accession Number	MW (kDa)	Vegetative WT (spectral counts)		Meiotic WT (spectral counts)			Meiotic *erf2Δ* (spectral counts)	
Membrane transporter	SPCC417.10	57	0	0	0	2	2	0	0
Psy1	SPCC825.03c	33	0	0	0	2	2	0	0
Moc3	SPAC821.07c	55	0	0	0	2	2	0	0
RNA-binding protein, G-patch type	SPAC2G11.04	33	0	0	0	2	2	0	0
Cwf20	SPCC4B3.14	33	0	0	0	2	2	0	0
Mug117	SPCC645.11c	22	0	0	0	2	2	0	0
DUF1000 family protein	SPBP35G2.02	23	0	0	0	2	2	0	0
Mitochondrial ribosomal protein subunit L9	SPCC777.17c	12	0	0	0	2	2	0	0
ORMDL family protein	SPBC119.09c	21	0	0	0	2	2	0	0
Tif212	SPAC32A11.04c	36	0	0	0	2	2	0	0
Mdm10	SPAC17H9.17c	42	0	0	0	2	2	0	0
tRNA specific adenosine deaminase	SPBC16A3.06	44	0	0	0	2	2	0	0
Hem2	SPAC1805.06c	36	0	0	0	2	2	0	0
Imidazoleglycerol-phosphate synthase	SPAC222.08c	26	0	0	0	2	2	0	0
Diacylglycerol cholinephosphotranferase/ diacylglycerol ethanolaminesphotranferase	SPAC22A12.10	44	0	0	0	2	2	0	0
Metal dependent phosphohydrolase	SPCC4G3.17	23	0	0	0	2	2	0	0

Identified proteins	Accession Number	MW (kDa)	Vegetative WT (spectral counts)		Meiotic WT (spectral counts)			Meiotic *erf2Δ* (spectral counts)	
Gpi12	SPAPB2B4.01c	28	0	0	0	2	2	0	0
tspO homolog	SPBC725.10	18	0	0	0	2	2	0	0
Btn1	SPAC607.09c	44	0	0	0	2	2	0	0
Sequence orphan	SPBPB21E7.05	15	0	0	0	2	2	0	0
Amino acid permease, unknown 15	SPCC74.04	60	0	0	0	2	2	0	0
Rng3	SPCC613.04c	84	0	0	2	4	2	0	0

REFERENCES

1. Magee, A.I. & Courtneidge, S.A. Two classes of fatty acid acylated proteins exist in eukaryotic cells. *The EMBO journal* **4**, 1137-1144 (1985).

2. Magee, A.I., Gutierrez, L., McKay, I.A., Marshall, C.J. & Hall, A. Dynamic fatty acylation of p21N-ras. *The EMBO journal* **6**, 3353-3357 (1987).

3. Liang, X. *et al.* Heterogeneous fatty acylation of Src family kinases with polyunsaturated fatty acids regulates raft localization and signal transduction. *The Journal of biological chemistry* **276**, 30987-30994 (2001).

4. Liang, X., Lu, Y., Neubert, T.A. & Resh, M.D. Mass spectrometric analysis of GAP-43/ neuromodulin reveals the presence of a variety of fatty acylated species. *The Journal of biological chemistry* **277**, 33032-33040 (2002).

5. Liang, X., Lu, Y., Wilkes, M., Neubert, T.A. & Resh, M.D. The N-terminal SH4 region of the Src family kinase Fyn is modified by methylation and heterogeneous fatty acylation: role in membrane targeting, cell adhesion, and spreading. *The Journal of biological chemistry* **279**, 8133-8139 (2004).

6. Inoue, T. *et al.* Activation of canonical Wnt pathway promotes proliferation of retinal stem cells derived from adult mouse ciliary margin. *Stem Cells* **24**, 95-104 (2006).

7. Zhai, L., Chaturvedi, D. & Cumberledge, S. Drosophila wnt-1 undergoes a hydrophobic modification and is targeted to lipid rafts, a process that requires porcupine. *The Journal of biological chemistry* **279**, 33220-33227 (2004).

8. Chamoun, Z. *et al.* Skinny hedgehog, an acyltransferase required for palmitoylation and activity of the hedgehog signal. *Science* **293**, 2080-2084 (2001).

9. Chen, M.H., Li, Y.J., Kawakami, T., Xu, S.M. & Chuang, P.T. Palmitoylation is required for the production of a soluble multimeric Hedgehog protein complex and long-range signaling in vertebrates. *Genes & development* **18**, 641-659 (2004).

10. Zhang, J. *et al.* Identification of CKAP4/p63 as a major substrate of the palmitoyl acyltransferase DHHC2, a putative tumor suppressor, using a novel proteomics method. *Molecular & cellular proteomics : MCP* **7**, 1378-1388 (2008).

11. Kang, R. *et al.* Neural palmitoyl-proteomics reveals dynamic synaptic palmitoylation. *Nature* **456**, 904-909 (2008).

12. Roth, A.F. *et al.* Global analysis of protein palmitoylation in yeast. *Cell* **125**, 1003-1013 (2006).

13. Martin, B.R. & Cravatt, B.F. Large-scale profiling of protein palmitoylation in mammalian cells. *Nature methods* **6**, 135-138 (2009).

14. Martin, B.R., Wang, C., Adibekian, A., Tully, S.E. & Cravatt, B.F. Global profiling of dynamic protein palmitoylation. *Nature methods* **9**, 84-89 (2012).

15. Wilson, J.P., Raghavan, A.S., Yang, Y.Y., Charron, G. & Hang, H.C. Proteomic analysis of fatty-acylated proteins in mammalian cells with chemical reporters reveals S-acylation of histone H3 variants. *Molecular & cellular proteomics : MCP* **10**, M110 001198 (2011).

16. Yount, J.S. *et al.* Palmitoylome profiling reveals S-palmitoylation-dependent antiviral activity of IFITM3. *Nature chemical biology* **6**, 610-614 (2010).

17. Emmer, B.T. *et al.* Global analysis of protein palmitoylation in African trypanosomes. *Eukaryotic cell* **10**, 455-463 (2011).

18. Yang, W., Di Vizio, D., Kirchner, M., Steen, H. & Freeman, M.R. Proteome scale characterization of human S-acylated proteins in lipid raft-enriched and non-raft membranes. *Molecular & cellular proteomics : MCP* **9**, 54-70 (2010).

19. Karnoub, A.E. & Weinberg, R.A. Ras oncogenes: split personalities. *Nature reviews. Molecular cell biology* **9**, 517-531 (2008).

20. Hancock, J.F., Magee, A.I., Childs, J.E. & Marshall, C.J. All ras proteins are polyisoprenylated but only some are palmitoylated. *Cell* **57**, 1167-1177 (1989).

21. Gutierrez, L., Magee, A.I., Marshall, C.J. & Hancock, J.F. Post-translational processing of p21ras is two-step and involves carboxyl-methylation and carboxy-terminal proteolysis. *The EMBO journal* **8**, 1093-1098 (1989).

22. Rocks, O. *et al.* An acylation cycle regulates localization and activity of palmitoylated Ras isoforms. *Science* **307**, 1746-1752 (2005).

23. Shahinian, S. & Silvius, J.R. Doubly-lipid-modified protein sequence motifs exhibit long-lived anchorage to lipid bilayer membranes. *Biochemistry* **34**, 3813-3822 (1995).

24. Goodwin, J.S. *et al.* Depalmitoylated Ras traffics to and from the Golgi complex via a nonvesicular pathway. *The Journal of cell biology* **170**, 261-272 (2005).

25. Kanaani, J., Patterson, G., Schaufele, F., Lippincott-Schwartz, J. & Baekkeskov, S. A palmitoylation cycle dynamically regulates partitioning of the GABA-synthesizing enzyme GAD65 between ER-Golgi and post-Golgi membranes. *Journal of cell science* **121**, 437-449 (2008).

26. Chiu, V.K. *et al.* Ras signalling on the endoplasmic reticulum and the Golgi. *Nature cell biology* **4**, 343-350 (2002).

27. Papadaki, P., Pizon, V., Onken, B. & Chang, E.C. Two ras pathways in fission yeast are differentially regulated by two ras guanine nucleotide exchange factors. *Molecular and cellular biology* **22**, 4598-4606 (2002).

28. Onken, B., Wiener, H., Philips, M.R. & Chang, E.C. Compartmentalized signaling of Ras in fission yeast. *Proceedings of the National Academy of Sciences of the United States of America* **103**, 9045-9050 (2006).

29. Lingwood, D. & Simons, K. Lipid rafts as a membrane-organizing principle. *Science* **327**, 46-50 (2010).

30. Webb, Y., Hermida-Matsumoto, L. & Resh, M.D. Inhibition of protein palmitoylation, raft localization, and T cell signaling by 2-bromopalmitate and polyunsaturated fatty acids. *The Journal of biological chemistry* **275**, 261-270 (2000).

31. Zhang, W., Trible, R.P. & Samelson, L.E. LAT palmitoylation: its essential role in membrane microdomain targeting and tyrosine phosphorylation during T cell activation. *Immunity* **9**, 239-246 (1998).

32. Hundt, M. *et al.* Impaired activation and localization of LAT in anergic T cells as a consequence of a selective palmitoylation defect. *Immunity* **24**, 513-522 (2006).

33. Li, Q.J. *et al.* CD4 enhances T cell sensitivity to antigen by coordinating Lck accumulation at the immunological synapse. *Nature immunology* **5**, 791-799 (2004).

34. Balamuth, F., Brogdon, J.L. & Bottomly, K. CD4 raft association and signaling regulate molecular clustering at the immunological synapse site. *J Immunol* **172**, 5887-5892 (2004).

35. Arcaro, A. *et al.* Essential role of CD8 palmitoylation in CD8 coreceptor function. *J Immunol* **165**, 2068-2076 (2000).

36. Hawash, I.Y. *et al.* The oxygen-substituted palmitic acid analogue, 13-oxypalmitic acid, inhibits Lck localization to lipid rafts and T cell signaling. *Biochimica et biophysica acta* **1589**, 140-150 (2002).

37. Otahal, P. *et al.* A new type of membrane raft-like microdomains and their possible involvement in TCR signaling. *J Immunol* **184**, 3689-3696 (2010).

38. Kabouridis, P.S., Magee, A.I. & Ley, S.C. S-acylation of LCK protein tyrosine kinase is essential for its signalling function in T lymphocytes. *The EMBO journal* **16**, 4983-4998 (1997).

39. El-Husseini Ael, D. *et al.* Synaptic strength regulated by palmitate cycling on PSD-95. *Cell* **108**, 849-863 (2002).

40. Ho, G.P. *et al.* S-nitrosylation and S-palmitoylation reciprocally regulate synaptic targeting of PSD-95. *Neuron* **71**, 131-141 (2011).

41. Fukata, Y. & Fukata, M. Protein palmitoylation in neuronal development and synaptic plasticity. *Nature reviews. Neuroscience* **11**, 161-175 (2010).

42. Resh, M.D. Palmitoylation of ligands, receptors, and intracellular signaling molecules. *Science's STKE : signal transduction knowledge environment* **2006**, re14 (2006).

43. Cao, Y. & Huang, Y. Palmitoylation regulates GDP/GTP exchange of G protein by affecting the GTP-binding activity of Goalpha. *The international journal of biochemistry & cell biology* **37**, 637-644 (2005).

44. Yang, S., Zhang, L. & Huang, Y. Membrane association and conformational change of palmitoylated G(o)alpha. *FEBS letters* **498**, 76-81 (2001).

45. Valdez-Taubas, J. & Pelham, H. Swf1-dependent palmitoylation of the SNARE Tlg1 prevents its ubiquitination and degradation. *The EMBO journal* **24**, 2524-2532 (2005).

46. Maeda, A. *et al.* Palmitoylation stabilizes unliganded rod opsin. *Proceedings of the National Academy of Sciences of the United States of America* **107**, 8428-8433 (2010).

47. Gao, Z., Ni, Y., Szabo, G. & Linden, J. Palmitoylation of the recombinant human A1 adenosine receptor: enhanced proteolysis of palmitoylation-deficient mutant receptors. *The Biochemical journal* **342 (Pt 2)**, 387-395 (1999).

48. Percherancier, Y. *et al.* Palmitoylation-dependent control of degradation, life span, and membrane expression of the CCR5 receptor. *The Journal of biological chemistry* **276**, 31936-31944 (2001).

49. Abrami, L., Leppla, S.H. & van der Goot, F.G. Receptor palmitoylation and ubiquitination regulate anthrax toxin endocytosis. *The Journal of cell biology* **172**, 309-320 (2006).

50. Yanai, A. *et al.* Palmitoylation of huntingtin by HIP14 is essential for its trafficking and function. *Nature neuroscience* **9**, 824-831 (2006).

51. Noritake, J. *et al.* Mobile DHHC palmitoylating enzyme mediates activity-sensitive synaptic targeting of PSD-95. *The Journal of cell biology* **186**, 147-160 (2009).

52. Zhang, M.M., Tsou, L.K., Charron, G., Raghavan, A.S. & Hang, H.C. Tandem fluorescence imaging of dynamic S-acylation and protein turnover. *Proceedings of the National Academy of Sciences of the United States of America* **107**, 8627-8632 (2010).

53. Mouillac, B., Caron, M., Bonin, H., Dennis, M. & Bouvier, M. Agonist-modulated palmitoylation of beta 2-adrenergic receptor in Sf9 cells. *The Journal of biological chemistry* **267**, 21733-21737 (1992).

54. Wedegaertner, P.B. & Bourne, H.R. Activation and depalmitoylation of Gs alpha. *Cell* **77**, 1063-1070 (1994).

55. Degtyarev, M.Y., Spiegel, A.M. & Jones, T.L. Increased palmitoylation of the Gs protein alpha subunit after activation by the beta-adrenergic receptor or cholera toxin. *The Journal of biological chemistry* **268**, 23769-23772 (1993).

56. Mundy, D.I. & Warren, G. Mitosis and inhibition of intracellular transport stimulate palmitoylation of a 62-kD protein. *The Journal of cell biology* **116**, 135-146 (1992).

57. Roth, A.F., Feng, Y., Chen, L. & Davis, N.G. The yeast DHHC cysteine-rich domain protein Akr1p is a palmitoyl transferase. *The Journal of cell biology* **159**, 23-28 (2002).

58. Lobo, S., Greentree, W.K., Linder, M.E. & Deschenes, R.J. Identification of a Ras palmitoyltransferase in Saccharomyces cerevisiae. *The Journal of biological chemistry* **277**, 41268-41273 (2002).

59. Swarthout, J.T. *et al.* DHHC9 and GCP16 constitute a human protein fatty acyltransferase with specificity for H- and N-Ras. *The Journal of biological chemistry* **280**, 31141-31148 (2005).

60. Politis, E.G., Roth, A.F. & Davis, N.G. Transmembrane topology of the protein palmitoyl transferase Akr1. *The Journal of biological chemistry* **280**, 10156-10163 (2005).

61. Jennings, B.C. & Linder, M.E. DHHC Protein S-Acyltransferases Use Similar Ping-Pong Kinetic Mechanisms but Display Different Acyl-CoA Specificities. *The Journal of biological chemistry* **287**, 7236-7245 (2012).

62. Mitchell, D.A., Mitchell, G., Ling, Y., Budde, C. & Deschenes, R.J. Mutational analysis of Saccharomyces cerevisiae Erf2 reveals a two-step reaction mechanism for protein palmitoylation by DHHC enzymes. *The Journal of biological chemistry* **285**, 38104-38114 (2010).

63. Bartels, D.J., Mitchell, D.A., Dong, X. & Deschenes, R.J. Erf2, a novel gene product that affects the localization and palmitoylation of Ras2 in Saccharomyces cerevisiae. *Molecular and cellular biology* **19**, 6775-6787 (1999).

64. Young, F.B., Butland, S.L., Sanders, S.S., Sutton, L.M. & Hayden, M.R. Putting proteins in their place: Palmitoylation in Huntington disease and other neuropsychiatric diseases. *Progress in neurobiology* (2011).

65. Fukata, M., Fukata, Y., Adesnik, H., Nicoll, R.A. & Bredt, D.S. Identification of PSD-95 palmitoylating enzymes. *Neuron* **44**, 987-996 (2004).

66. Nadolski, M.J. & Linder, M.E. Molecular recognition of the palmitoylation substrate Vac8 by its palmitoyltransferase Pfa3. *The Journal of biological chemistry* **284**, 17720-17730 (2009).

67. Huang, K. *et al.* Neuronal palmitoyl acyl transferases exhibit distinct substrate specificity. *FASEB journal : official publication of the Federation of American Societies for Experimental Biology* **23**, 2605-2615 (2009).

68. Rocks, O. *et al.* The palmitoylation machinery is a spatially organizing system for peripheral membrane proteins. *Cell* **141**, 458-471 (2010).

69. Hou, H., John Peter, A.T., Meiringer, C., Subramanian, K. & Ungermann, C. Analysis of DHHC acyltransferases implies overlapping substrate specificity and a two-step reaction mechanism. *Traffic* **10**, 1061-1073 (2009).

70. Bannan, B.A. *et al.* The Drosophila protein palmitoylome: characterizing palmitoyl-thioesterases and DHHC palmitoyl-transferases. *Fly* **2**, 198-214 (2008).

71. Ohno, Y., Kihara, A., Sano, T. & Igarashi, Y. Intracellular localization and tissue-specific distribution of human and yeast DHHC cysteine-rich domain-containing proteins. *Biochimica et biophysica acta* **1761**, 474-483 (2006).

72. Gorleku, O.A., Barns, A.M., Prescott, G.R., Greaves, J. & Chamberlain, L.H. Endoplasmic reticulum localization of DHHC palmitoyltransferases mediated by lysine-based sorting signals. *The Journal of biological chemistry* **286**, 39573-39584 (2011).

73. Greaves, J., Carmichael, J.A. & Chamberlain, L.H. The palmitoyl transferase DHHC2 targets a dynamic membrane cycling pathway: regulation by a C-terminal domain. *Molecular biology of the cell* **22**, 1887-1895 (2011).

74. Li, Y., Martin, B.R., Cravatt, B.F. & Hofmann, S.L. DHHC5 protein palmitoylates flotillin-2 and is rapidly degraded on induction of neuronal differentiation in cultured cells. *The Journal of biological chemistry* **287**, 523-530 (2012).

75. Huang, K. *et al.* Wild-type HTT modulates the enzymatic activity of the neuronal palmitoyl transferase HIP14. *Human molecular genetics* **20**, 3356-3365 (2011).

76. Camp, L.A. & Hofmann, S.L. Purification and properties of a palmitoyl-protein thioesterase that cleaves palmitate from H-Ras. *The Journal of biological chemistry* **268**, 22566-22574 (1993).

77. Duncan, J.A. & Gilman, A.G. A cytoplasmic acyl-protein thioesterase that removes palmitate from G protein alpha subunits and p21(RAS). *The Journal of biological chemistry* **273**, 15830-15837 (1998).

78. Duncan, J.A. & Gilman, A.G. Characterization of Saccharomyces cerevisiae acyl-protein thioesterase 1, the enzyme responsible for G protein alpha subunit deacylation in vivo. *The Journal of biological chemistry* **277**, 31740-31752 (2002).

79. Verkruyse, L.A. & Hofmann, S.L. Lysosomal targeting of palmitoyl-protein thioesterase. *The Journal of biological chemistry* **271**, 15831-15836 (1996).

80. Heinonen, O. *et al.* Expression of palmitoyl protein thioesterase in neurons. *Molecular genetics and metabolism* **69**, 123-129 (2000).

81. Kim, S.J. *et al.* Palmitoyl protein thioesterase-1 deficiency impairs synaptic vesicle recycling at nerve terminals, contributing to neuropathology in humans and mice. *The Journal of clinical investigation* **118**, 3075-3086 (2008).

82. Yeh, D.C., Duncan, J.A., Yamashita, S. & Michel, T. Depalmitoylation of endothelial nitric-oxide synthase by acyl-protein thioesterase 1 is potentiated by Ca(2+)-calmodulin. *The Journal of biological chemistry* **274**, 33148-33154 (1999).

83. Rusch, M. *et al.* Identification of Acyl Protein Thioesterases 1 and 2 as the Cellular Targets of the Ras-Signaling Modulators Palmostatin B and M. *Angew Chem Int Ed Engl* (2011).

84. Dekker, F.J. *et al.* Small-molecule inhibition of APT1 affects Ras localization and signaling. *Nature chemical biology* **6**, 449-456 (2010).

85. Tomatis, V.M., Trenchi, A., Gomez, G.A. & Daniotti, J.L. Acyl-protein thioesterase 2 catalyzes the deacylation of peripheral membrane-associated GAP-43. *PloS one* **5**, e15045 (2010).

86. Siegel, G. *et al.* A functional screen implicates microRNA-138-dependent regulation of the depalmitoylation enzyme APT1 in dendritic spine morphogenesis. *Nature cell biology* **11**, 705-716 (2009).

87. Ahearn, I.M. *et al.* FKBP12 binds to acylated H-ras and promotes depalmitoylation. *Molecular cell* **41**, 173-185 (2011).

88. Tian, L. *et al.* Palmitoylation gates phosphorylation-dependent regulation of BK potassium channels. *Proceedings of the National Academy of Sciences of the United States of America* **105**, 21006-21011 (2008).

89. Jeffries, O., Tian, L., McClafferty, H. & Shipston, M.J. An electrostatic switch controls palmitoylation of the large conductance voltage- and calcium-activated potassium (BK) channel. *The Journal of biological chemistry* **287**, 1468-1477 (2012).

90. Moffett, S., Mouillac, B., Bonin, H. & Bouvier, M. Altered phosphorylation and desensitization patterns of a human beta 2-adrenergic receptor lacking the palmitoylated Cys341. *The EMBO journal* **12**, 349-356 (1993).

91. Lin, D.T. *et al.* Regulation of AMPA receptor extrasynaptic insertion by 4.1N, phosphorylation and palmitoylation. *Nature neuroscience* **12**, 879-887 (2009).

92. Bredt, D.S. Endogenous nitric oxide synthesis: biological functions and pathophysiology. *Free radical research* **31**, 577-596 (1999).

93. Towler, D.A. *et al.* Purification and characterization of yeast myristoyl CoA:protein N-myristoyltransferase. *Proceedings of the National Academy of Sciences of the United States of America* **84**, 2708-2712 (1987).

94. Zha, J., Weiler, S., Oh, K.J., Wei, M.C. & Korsmeyer, S.J. Posttranslational N-myristoylation of BID as a molecular switch for targeting mitochondria and apoptosis. *Science* **290**, 1761-1765 (2000).

95. Ntwasa, M., Aapies, S., Schiffmann, D.A. & Gay, N.J. Drosophila embryos lacking N-myristoyltransferase have multiple developmental defects. *Experimental cell research* **262**, 134-144 (2001).

96. Duronio, R.J., Towler, D.A., Heuckeroth, R.O. & Gordon, J.I. Disruption of the yeast N-myristoyl transferase gene causes recessive lethality. *Science* **243**, 796-800 (1989).

97. Resh, M.D. Targeting protein lipidation in disease. *Trends in molecular medicine* **18**, 206-214 (2012).

98. Tang, C. *et al.* Entropic switch regulates myristate exposure in the HIV-1 matrix protein. *Proceedings of the National Academy of Sciences of the United States of America* **101**, 517-522 (2004).

99. Tanaka, T., Ames, J.B., Harvey, T.S., Stryer, L. & Ikura, M. Sequestration of the membrane-targeting myristoyl group of recoverin in the calcium-free state. *Nature* **376**, 444-447 (1995).

100. Ames, J.B. *et al.* Molecular mechanics of calcium-myristoyl switches. *Nature* **389**, 198-202 (1997).

101. Goldberg, J. Structural basis for activation of ARF GTPase: mechanisms of guanine nucleotide exchange and GTP-myristoyl switching. *Cell* **95**, 237-248 (1998).

102. Nagar, B. *et al.* Structural basis for the autoinhibition of c-Abl tyrosine kinase. *Cell* **112**, 859-871 (2003).

103. Peseckis, S.M., Deichaite, I. & Resh, M.D. Iodinated fatty acids as probes for myristate processing and function. Incorporation into pp60v-src. *The Journal of biological chemistry* **268**, 5107-5114 (1993).

104. Drisdel, R.C. & Green, W.N. Labeling and quantifying sites of protein palmitoylation. *BioTechniques* **36**, 276-285 (2004).

105. Hang, H.C. *et al.* Chemical probes for the rapid detection of Fatty-acylated proteins in Mammalian cells. *Journal of the American Chemical Society* **129**, 2744-2745 (2007).

106. Anderson, N.L. & Anderson, N.G. The human plasma proteome: history, character, and diagnostic prospects. *Molecular & cellular proteomics : MCP* **1**, 845-867 (2002).

107. Ghaemmaghami, S. *et al.* Global analysis of protein expression in yeast. *Nature* **425**, 737-741 (2003).

108. Beck, M. *et al.* The quantitative proteome of a human cell line. *Molecular systems biology* **7**, 549 (2011).

109. Paige, L.A., Nadler, M.J., Harrison, M.L., Cassady, J.M. & Geahlen, R.L. Reversible palmitoylation of the protein-tyrosine kinase p56lck. *The Journal of biological chemistry* **268**, 8669-8674 (1993).

110. Koegl, M., Zlatkine, P., Ley, S.C., Courtneidge, S.A. & Magee, A.I. Palmitoylation of multiple Src-family kinases at a homologous N-terminal motif. *The Biochemical journal* **303 (Pt 3)**, 749-753 (1994).

111. Agard, N.J., Baskin, J.M., Prescher, J.A., Lo, A. & Bertozzi, C.R. A comparative study of bioorthogonal reactions with azides. *ACS chemical biology* **1**, 644-648 (2006).

112. Speers, A.E. & Cravatt, B.F. Profiling enzyme activities in vivo using click chemistry methods. *Chemistry & biology* **11**, 535-546 (2004).

113. Alland, L., Peseckis, S.M., Atherton, R.E., Berthiaume, L. & Resh, M.D. Dual myristylation and palmitylation of Src family member p59fyn affects subcellular localization. *The Journal of biological chemistry* **269**, 16701-16705 (1994).

114. Tsou, L.K., Zhang, M.M. & Hang, H.C. Clickable fluorescent dyes for multimodal bioorthogonal imaging. *Organic & biomolecular chemistry* **7**, 5055-5058 (2009).

115. Shenoy-Scaria, A.M., Gauen, L.K., Kwong, J., Shaw, A.S. & Lublin, D.M. Palmitylation of an amino-terminal cysteine motif of protein tyrosine kinases p56lck and p59fyn mediates interaction with glycosyl-phosphatidylinositol-anchored proteins. *Molecular and cellular biology* **13**, 6385-6392 (1993).

116. Abraham, N., Miceli, M.C., Parnes, J.R. & Veillette, A. Enhancement of T-cell responsiveness by the lymphocyte-specific tyrosine protein kinase p56lck. *Nature* **350**, 62-66 (1991).

117. Beatty, K.E. & Tirrell, D.A. Two-color labeling of temporally defined protein populations in mammalian cells. *Bioorganic & medicinal chemistry letters* **18**, 5995-5999 (2008).

118. Baskin, J.M. *et al.* Copper-free click chemistry for dynamic in vivo imaging. *Proceedings of the National Academy of Sciences of the United States of America* **104**, 16793-16797 (2007).

119. Laughlin, S.T., Baskin, J.M., Amacher, S.L. & Bertozzi, C.R. In vivo imaging of membrane-associated glycans in developing zebrafish. *Science* **320**, 664-667 (2008).

120. Kele, P., Mezo, G., Achatz, D. & Wolfbeis, O.S. Dual labeling of biomolecules by using click chemistry: a sequential approach. *Angew Chem Int Ed Engl* **48**, 344-347 (2009).

121. Wolven, A., Okamura, H., Rosenblatt, Y. & Resh, M.D. Palmitoylation of p59fyn is reversible and sufficient for plasma membrane association. *Molecular biology of the cell* **8**, 1159-1173 (1997).

122. Yurchak, L.K. & Sefton, B.M. Palmitoylation of either Cys-3 or Cys-5 is required for the biological activity of the Lck tyrosine protein kinase. *Molecular and cellular biology* **15**, 6914-6922 (1995).

123. Kosugi, A. *et al.* A pivotal role of cysteine 3 of Lck tyrosine kinase for localization to glycolipid-enriched microdomains and T cell activation. *Immunology letters* **76**, 133-138 (2001).

124. Secrist, J.P., Burns, L.A., Karnitz, L., Koretzky, G.A. & Abraham, R.T. Stimulatory effects of the protein tyrosine phosphatase inhibitor, pervanadate, on T-cell activation events. *The Journal of biological chemistry* **268**, 5886-5893 (1993).

125. Qanbar, R. & Bouvier, M. Determination of protein-bound palmitate turnover rates using a three-compartment model that formally incorporates [3H]palmitate recycling. *Biochemistry* **43**, 12275-12288 (2004).

126. Das, A.K. *et al.* Structural basis for the insensitivity of a serine enzyme (palmitoyl-protein thioesterase) to phenylmethylsulfonyl fluoride. *The Journal of biological chemistry* **275**, 23847-23851 (2000).

127. Jennings, B.C. *et al.* 2-Bromopalmitate and 2-(2-hydroxy-5-nitro-benzylidene)-benzo[b]thiophen-3-one inhibit DHHC-mediated palmitoylation in vitro. *Journal of lipid research* **50**, 233-242 (2009).

128. Coleman, R.A., Rao, P., Fogelsong, R.J. & Bardes, E.S. 2-Bromopalmitoyl-CoA and 2-bromopalmitate: promiscuous inhibitors of membrane-bound enzymes. *Biochimica et biophysica acta* **1125**, 203-209 (1992).

129. Beatty, K.E. *et al.* Fluorescence visualization of newly synthesized proteins in mammalian cells. *Angew Chem Int Ed Engl* **45**, 7364-7367 (2006).

130. Hinz, F.I., Dieterich, D.C., Tirrell, D.A. & Schuman, E.M. Non-canonical amino acid labeling in vivo to visualize and affinity purify newly synthesized proteins in larval zebrafish. *ACS chemical neuroscience* **3**, 40-49 (2012).

131. Baker, T.L., Zheng, H., Walker, J., Coloff, J.L. & Buss, J.E. Distinct rates of palmitate turnover on membrane-bound cellular and oncogenic H-ras. *The Journal of biological chemistry* **278**, 19292-19300 (2003).

132. Sletten, E.M. & Bertozzi, C.R. Bioorthogonal chemistry: fishing for selectivity in a sea of functionality. *Angew Chem Int Ed Engl* **48**, 6974-6998 (2009).

133. Mitchell, D.A., Vasudevan, A., Linder, M.E. & Deschenes, R.J. Protein palmitoylation by a family of DHHC protein S-acyltransferases. *Journal of lipid research* **47**, 1118-1127 (2006).

134. Kim, D.U. *et al.* Analysis of a genome-wide set of gene deletions in the fission yeast Schizosaccharomyces pombe. *Nature biotechnology* **28**, 617-623 (2010).

135. Mata, J., Lyne, R., Burns, G. & Bahler, J. The transcriptional program of meiosis and sporulation in fission yeast. *Nature genetics* **32**, 143-147 (2002).

136. Wilhelm, B.T. *et al.* Dynamic repertoire of a eukaryotic transcriptome surveyed at single-nucleotide resolution. *Nature* **453**, 1239-1243 (2008).

137. Iino, Y. & Yamamoto, M. Negative control for the initiation of meiosis in Schizosaccharomyces pombe. *Proceedings of the National Academy of Sciences of the United States of America* **82**, 2447-2451 (1985).

138. Beach, D., Rodgers, L. & Gould, J. ran1+ controls the transition from mitotic division to meiosis in fission yeast. *Current genetics* **10**, 297-311 (1985).

139. Nurse, P. Mutants of the fission yeast Schizosaccharomyces pombe which alter the shift between cell proliferation and sporulation. *Mol. & Gen. Genet.* **198**, 497-502 (1985).

140. Charron, G. *et al.* Robust fluorescent detection of protein fatty-acylation with chemical reporters. *Journal of the American Chemical Society* **131**, 4967-4975 (2009).

141. Dudler, T. & Gelb, M.H. Palmitoylation of Ha-Ras facilitates membrane binding, activation of downstream effectors, and meiotic maturation in Xenopus oocytes. *The Journal of biological chemistry* **271**, 11541-11547 (1996).

142. Shimoda, C. Existence of a major spore wall protein (23K) in the fission yeast Schizosaccharomyces pombe: a possible sporulation-specific protein. *Archives of microbiology* **136**, 26-27 (1983).

143. Wang, H., Tang, X. & Balasubramanian, M.K. Rho3p regulates cell separation by modulating exocyst function in Schizosaccharomyces pombe. *Genetics* **164**, 1323-1331 (2003).

144. Nakano, K. *et al.* The small GTPase Rho3 and the diaphanous/formin For3 function in polarized cell growth in fission yeast. *Journal of cell science* **115**, 4629-4639 (2002).

145. Moreno, S., Klar, A. & Nurse, P. Molecular genetic analysis of fission yeast Schizosaccharomyces pombe. *Methods in enzymology* **194**, 795-823 (1991).

146. Hayles, J. & Nurse, P. Genetics of the fission yeast Schizosaccharomyces pombe. *Annual review of genetics* **26**, 373-402 (1992).

147. Bahler, J. *et al.* Heterologous modules for efficient and versatile PCR-based gene targeting in Schizosaccharomyces pombe. *Yeast* **14**, 943-951 (1998).

148. Harigaya, Y. *et al.* Selective elimination of messenger RNA prevents an incidence of untimely meiosis. *Nature* **442**, 45-50 (2006).

149. Watanabe, Y., Shinozaki-Yabana, S., Chikashige, Y., Hiraoka, Y. & Yamamoto, M. Phosphorylation of RNA-binding protein controls cell cycle switch from mitotic to meiotic in fission yeast. *Nature* **386**, 187-190 (1997).

150. McLeod, M. & Beach, D. A specific inhibitor of the ran1+ protein kinase regulates entry into meiosis in Schizosaccharomyces pombe. *Nature* **332**, 509-514 (1988).

151. Li, P. & McLeod, M. Molecular mimicry in development: identification of ste11+ as a substrate and mei3+ as a pseudosubstrate inhibitor of ran1+ kinase. *Cell* **87**, 869-880 (1996).

152. Van Heeckeren, W.J., Dorris, D.R. & Struhl, K. The mating-type proteins of fission yeast induce meiosis by directly activating mei3 transcription. *Molecular and cellular biology* **18**, 7317-7326 (1998).

153. Davey, J. & Nielsen, O. Mutations in cyr1 and pat1 reveal pheromone-induced G1 arrest in the fission yeast Schizosaccharomyces pombe. *Current genetics* **26**, 105-112 (1994).

154. Shiozaki, K. & Russell, P. Conjugation, meiosis, and the osmotic stress response are regulated by Spc1 kinase through Atf1 transcription factor in fission yeast. *Genes & development* **10**, 2276-2288 (1996).

155. Takeda, T. *et al.* Schizosaccharomyces pombe atf1+ encodes a transcription factor required for sexual development and entry into stationary phase. *The EMBO journal* **14**, 6193-6208 (1995).

156. Petersen, J. & Nurse, P. TOR signalling regulates mitotic commitment through the stress MAP kinase pathway and the Polo and Cdc2 kinases. *Nature cell biology* **9**, 1263-1272 (2007).

157. Costello, G., Rogers, L. & Beach, D. Fission yeast enters the stationary phase G0 state from either mitotic G1 or G2. *Current genetics* **11**, 119-125 (1986).

158. Millar, J.B., Buck, V. & Wilkinson, M.G. Pyp1 and Pyp2 PTPases dephosphorylate an osmosensing MAP kinase controlling cell size at division in fission yeast. *Genes & development* **9**, 2117-2130 (1995).

159. Shiozaki, K. & Russell, P. Counteractive roles of protein phosphatase 2C (PP2C) and a MAP kinase kinase homolog in the osmoregulation of fission yeast. *The EMBO journal* **14**, 492-502 (1995).

160. Shieh, J.C., Wilkinson, M.G. & Millar, J.B. The Win1 mitotic regulator is a component of the fission yeast stress-activated Sty1 MAPK pathway. *Molecular biology of the cell* **9**, 311-322 (1998).

161. Shieh, J.C. *et al.* The Mcs4 response regulator coordinately controls the stress-activated Wak1-Wis1-Sty1 MAP kinase pathway and fission yeast cell cycle. *Genes & development* **11**, 1008-1022 (1997).

162. Shiozaki, K., Shiozaki, M. & Russell, P. Mcs4 mitotic catastrophe suppressor regulates the fission yeast cell cycle through the Wik1-Wis1-Spc1 kinase cascade. *Molecular biology of the cell* **8**, 409-419 (1997).

163. Samejima, I., Mackie, S. & Fantes, P.A. Multiple modes of activation of the stress-responsive MAP kinase pathway in fission yeast. *The EMBO journal* **16**, 6162-6170 (1997).

164. Samejima, I., Mackie, S., Warbrick, E., Weisman, R. & Fantes, P.A. The fission yeast mitotic regulator win1+ encodes an MAP kinase kinase kinase that phosphorylates and activates Wis1 MAP kinase kinase in response to high osmolarity. *Molecular biology of the cell* **9**, 2325-2335 (1998).

165. Wilkinson, M.G. *et al.* The Atf1 transcription factor is a target for the Sty1 stress-activated MAP kinase pathway in fission yeast. *Genes & development* **10**, 2289-2301 (1996).

166. Chang, L. & Karin, M. Mammalian MAP kinase signalling cascades. *Nature* **410**, 37-40 (2001).

167. Adamson, P., Marshall, C.J., Hall, A. & Tilbrook, P.A. Post-translational modifications of p21rho proteins. *The Journal of biological chemistry* **267**, 20033-20038 (1992).

168. Chang, E.C. & Philips, M.R. Spatial segregation of Ras signaling: new evidence from fission yeast. *Cell Cycle* **5**, 1936-1939 (2006).

169. Nakamura, T., Nakamura-Kubo, M., Hirata, A. & Shimoda, C. The Schizosaccharomyces pombe spo3+ gene is required for assembly of the forespore membrane and genetically interacts with psy1(+)-encoding syntaxin-like protein. *Molecular biology of the cell* **12**, 3955-3972 (2001).

170. Edamatsu, M. & Toyoshima, Y.Y. Fission yeast synaptobrevin is involved in cytokinesis and cell elongation. *Biochemical and biophysical research communications* **301**, 641-645 (2003).

171. Heasman, S.J. & Ridley, A.J. Mammalian Rho GTPases: new insights into their functions from in vivo studies. *Nature reviews. Molecular cell biology* **9**, 690-701 (2008).

172. Pruyne, D., Legesse-Miller, A., Gao, L., Dong, Y. & Bretscher, A. Mechanisms of polarized growth and organelle segregation in yeast. *Annual review of cell and developmental biology* **20**, 559-591 (2004).

173. Bendezu, F.O. & Martin, S.G. Actin cables and the exocyst form two independent morphogenesis pathways in the fission yeast. *Molecular biology of the cell* **22**, 44-53 (2011).

174. Kita, A. *et al.* Role of the Small GTPase Rho3 in Golgi/Endosome trafficking through functional interaction with adaptin in Fission Yeast. *PloS one* **6**, e16842 (2011).

175. Anastasia, S.D. *et al.* A link between mitotic entry and membrane growth suggests a novel model for cell size control. *The Journal of cell biology* **197**, 89-104 (2012).

176. El-Husseini, A.E., Schnell, E., Chetkovich, D.M., Nicoll, R.A. & Bredt, D.S. PSD-95 involvement in maturation of excitatory synapses. *Science* **290**, 1364-1368 (2000).

177. Craven, S.E., El-Husseini, A.E. & Bredt, D.S. Synaptic targeting of the postsynaptic density protein PSD-95 mediated by lipid and protein motifs. *Neuron* **22**, 497-509 (1999).

178. El-Husseini, A.E. *et al.* Dual palmitoylation of PSD-95 mediates its vesiculotubular sorting, postsynaptic targeting, and ion channel clustering. *The Journal of cell biology* **148**, 159-172 (2000).

179. Schmidt, M.F. & Schlesinger, M.J. Fatty acid binding to vesicular stomatitis virus glycoprotein: a new type of post-translational modification of the viral glycoprotein. *Cell* **17**, 813-819 (1979).

180. Dunphy, J.T., Greentree, W.K., Manahan, C.L. & Linder, M.E. G-protein palmitoyltransferase activity is enriched in plasma membranes. *The Journal of biological chemistry* **271**, 7154-7159 (1996).

181. Berthiaume, L. & Resh, M.D. Biochemical characterization of a palmitoyl acyltransferase activity that palmitoylates myristoylated proteins. *The Journal of biological chemistry* **270**, 22399-22405 (1995).

182. Wedegaertner, P.B., Chu, D.H., Wilson, P.T., Levis, M.J. & Bourne, H.R. Palmitoylation is required for signaling functions and membrane attachment of Gq alpha and Gs alpha. *The Journal of biological chemistry* **268**, 25001-25008 (1993).

183. Skene, J.H. & Virag, I. Posttranslational membrane attachment and dynamic fatty acylation of a neuronal growth cone protein, GAP-43. *The Journal of cell biology* **108**, 613-624 (1989).

184. Takemoto-Kimura, S. *et al.* Regulation of dendritogenesis via a lipid-raft-associated Ca2+/calmodulin-dependent protein kinase CLICK-III/CaMKIgamma. *Neuron* **54**, 755-770 (2007).

185. O'Brien, P.J. & Zatz, M. Acylation of bovine rhodopsin by [3H]palmitic acid. *The Journal of biological chemistry* **259**, 5054-5057 (1984).

186. Yang, X. *et al.* Palmitoylation supports assembly and function of integrin-tetraspanin complexes. *The Journal of cell biology* **167**, 1231-1240 (2004).

187. Chakrabandhu, K. *et al.* Palmitoylation is required for efficient Fas cell death signaling. *The EMBO journal* **26**, 209-220 (2007).

188. Heindel, U., Schmidt, M.F. & Veit, M. Palmitoylation sites and processing of synaptotagmin I, the putative calcium sensor for neurosecretion. *FEBS letters* **544**, 57-62 (2003).

189. Chamberlain, L.H. & Burgoyne, R.D. The cysteine-string domain of the secretory vesicle cysteine-string protein is required for membrane targeting. *The Biochemical journal* **335 (Pt 2)**, 205-209 (1998).

190. Singaraja, R.R. *et al.* HIP14, a novel ankyrin domain-containing protein, links huntingtin to intracellular trafficking and endocytosis. *Human molecular genetics* **11**, 2815-2828 (2002).

191. Saleem, A.N. *et al.* Mice with alopecia, osteoporosis, and systemic amyloidosis due to mutation in Zdhhc13, a gene coding for palmitoyl acyltransferase. *PLoS genetics* **6**, e1000985 (2010).

192. Mizumaru, C. *et al.* Suppression of APP-containing vesicle trafficking and production of beta-amyloid by AID/DHHC-12 protein. *Journal of neurochemistry* **111**, 1213-1224 (2009).

193. Mukai, J. *et al.* Evidence that the gene encoding ZDHHC8 contributes to the risk of schizophrenia. *Nature genetics* **36**, 725-731 (2004).

194. Raymond, F.L. *et al.* Mutations in ZDHHC9, which encodes a palmitoyltransferase of NRAS and HRAS, cause X-linked mental retardation associated with a Marfanoid habitus. *American journal of human genetics* **80**, 982-987 (2007).

195. Mill, P. *et al.* Palmitoylation regulates epidermal homeostasis and hair follicle differentiation. *PLoS genetics* **5**, e1000748 (2009).

196. Qin, L.X. Chromosomal aberrations related to metastasis of human solid tumors. *World journal of gastroenterology : WJG* **8**, 769-776 (2002).

197. Nakase, Y., Hirata, A., Shimoda, C. & Nakamura, T. Ectopic overproduction of a sporulation-specific transcription factor induces assembly of prespore-like membranous compartments in vegetative cells of fission yeast. *Genetics* **183**, 1195-1199 (2009).

198. Kang, J.U., Koo, S.H., Kwon, K.C., Park, J.W. & Kim, J.M. Gain at chromosomal region 5p15.33, containing TERT, is the most frequent genetic event in early stages of non-small cell lung cancer. *Cancer genetics and cytogenetics* **182**, 1-11 (2008).

199. Draper, J.M. & Smith, C.D. DHHC20: a human palmitoyl acyltransferase that causes cellular transformation. *Molecular membrane biology* **27**, 123-136 (2010).

200. Ducker, C.E., Stettler, E.M., French, K.J., Upson, J.J. & Smith, C.D. Huntingtin interacting protein 14 is an oncogenic human protein: palmitoyl acyltransferase. *Oncogene* **23**, 9230-9237 (2004).

201. Mansilla, F. *et al.* Differential expression of DHHC9 in microsatellite stable and instable human colorectal cancer subgroups. *British journal of cancer* **96**, 1896-1903 (2007).

202. Yamamoto, Y. *et al.* Gain of 5p15.33 is associated with progression of bladder cancer. *Oncology* **72**, 132-138 (2007).

203. Oyama, T. *et al.* Isolation of a novel gene on 8p21.3-22 whose expression is reduced significantly in human colorectal cancers with liver metastasis. *Genes, chromosomes & cancer* **29**, 9-15 (2000).

204. Mayer, T.C., Kleiman, N.J. & Green, M.C. Depilated (dep), a mutant gene that affects the coat of the mouse and acts in the epidermis. *Genetics* **84**, 59-65 (1976).

205. Mansouri, M.R. *et al.* Loss of ZDHHC15 expression in a woman with a balanced translocation t(X;15)(q13.3;cen) and severe mental retardation. *European journal of human genetics : EJHG* **13**, 970-977 (2005).

206. Mukai, J. *et al.* Palmitoylation-dependent neurodevelopmental deficits in a mouse model of 22q11 microdeletion. *Nature neuroscience* **11**, 1302-1310 (2008).

207. Liu, H. *et al.* Genetic variation in the 22q11 locus and susceptibility to schizophrenia. *Proceedings of the National Academy of Sciences of the United States of America* **99**, 16859-16864 (2002).

208. Singaraja, R.R. *et al.* Altered palmitoylation and neuropathological deficits in mice lacking HIP14. *Human molecular genetics* **20**, 3899-3909 (2011).

209. Huang, K. *et al.* Huntingtin-interacting protein HIP14 is a palmitoyl transferase involved in palmitoylation and trafficking of multiple neuronal proteins. *Neuron* **44**, 977-986 (2004).

210. Schweizer, A., Rohrer, J. & Kornfeld, S. Determination of the structural requirements for palmitoylation of p63. *The Journal of biological chemistry* **270**, 9638-9644 (1995).

211. Hess, D.T., Slater, T.M., Wilson, M.C. & Skene, J.H. The 25 kDa synaptosomal-associated protein SNAP-25 is the major methionine-rich polypeptide in rapid axonal transport and a major substrate for palmitoylation in adult CNS. *The Journal of neuroscience : the official journal of the Society for Neuroscience* **12**, 4634-4641 (1992).

212. DeSouza, S., Fu, J., States, B.A. & Ziff, E.B. Differential palmitoylation directs the AMPA receptor-binding protein ABP to spines or to intracellular clusters. *The Journal of neuroscience : the official journal of the Society for Neuroscience* **22**, 3493-3503 (2002).

213. Topinka, J.R. & Bredt, D.S. N-terminal palmitoylation of PSD-95 regulates association with cell membranes and interaction with K+ channel Kv1.4. *Neuron* **20**, 125-134 (1998).

214. Yang, X. *et al.* Palmitoylation of tetraspanin proteins: modulation of CD151 lateral interactions, subcellular distribution, and integrin-dependent cell morphology. *Molecular biology of the cell* **13**, 767-781 (2002).

215. Hayashi, T., Rumbaugh, G. & Huganir, R.L. Differential regulation of AMPA receptor subunit trafficking by palmitoylation of two distinct sites. *Neuron* **47**, 709-723 (2005).

216. O'Dowd, B.F., Hnatowich, M., Caron, M.G., Lefkowitz, R.J. & Bouvier, M. Palmitoylation of the human beta 2-adrenergic receptor. Mutation of Cys341 in the carboxyl tail leads to an uncoupled nonpalmitoylated form of the receptor. *The Journal of biological chemistry* **264**, 7564-7569 (1989).

217. Di Paolo, G. *et al.* Targeting of SCG10 to the area of the Golgi complex is mediated by its NH2-terminal region. *The Journal of biological chemistry* **272**, 5175-5182 (1997).

218. Liu, J., Garcia-Cardena, G. & Sessa, W.C. Biosynthesis and palmitoylation of endothelial nitric oxide synthase: mutagenesis of palmitoylation sites, cysteines-15 and/or -26, argues against depalmitoylation-induced translocation of the enzyme. *Biochemistry* **34**, 12333-12340 (1995).

219. Linder, M.E. *et al.* Lipid modifications of G proteins: alpha subunits are palmitoylated. *Proceedings of the National Academy of Sciences of the United States of America* **90**, 3675-3679 (1993).